Investigating the potential of load and power control on a VAWT through active pitch control in 2D

B.M. de Korte

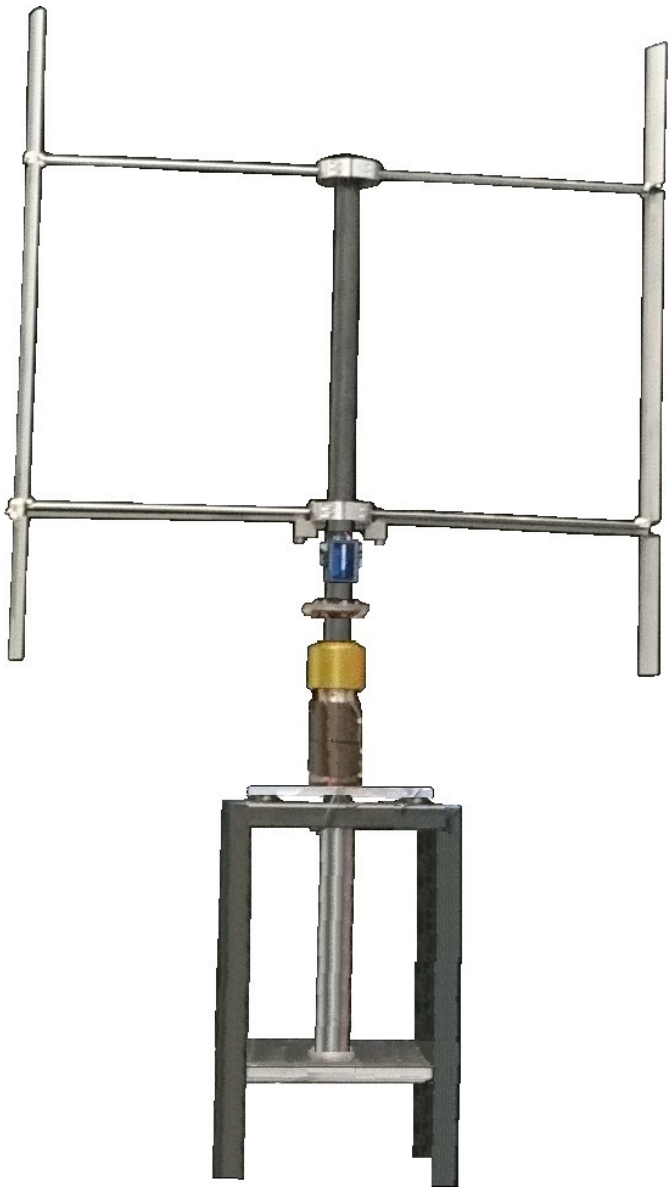

TU Delft Delft University of Technology

Investigating the potential of load and power control on a VAWT through active pitch control in 2D

by

B.M. de Korte

to obtain the degree of Master of Science
at the Delft University of Technology,
to be defended publicly on Wednesday June 5th 2019 at time 09:00.

Student number:	1514059	
Thesis committee:	Dr. ir. C. J. Simão Ferreira,	TU Delft, Chair committee, Supervisor
	Dr. ir. A. Viré,	TU Delft
	Dr. ir. A. H. van Zuijlen,	TU Delft
	Msc. C. P. LeBlanc	TU Delft, Ph.D candidate, Supervisor

An electronic version of this thesis is available at `http://repository.tudelft.nl/`.

TU Delft Delft University of Technology

Abstract

Vertical axis wind turbines hold the potential of being the superior turbine for offshore applications, due to their inherent structural layout. Offshore applications could benefit from load control on both integral and instantaneous level. Within this thesis influence of thrust vectoring, controlling the magnitude and direction of the thrust vector with respect to the freestream, is investigated through pitch actuation. The H-type Darrieus VAWT is modeled in $2D$ through the actuator cylinder model with the Mod-Lin correction included.

The increased emphasis on the integrated force component normal to the freestream requires a redefinition of thrust, where C_T is the summation of all normalized load vectors. This thrust vector can be decomposed to streamwise thrust coefficient, C_{T_x}, and a streamnormal component, C_{T_y}, and a new definition: the thrust angle, being the inclination angle of the thrust vector with the freestream.

The VAWT is modeled in two representations; one that represents the TU Delft H-Darrieus VAWT windtunnel model with independent variable blade pitch, called PitchVAWT, and one through directly prescribing the surface loading. The PitchVAWT is assumed to have no pitch rate limit and always avoids (dynamic) stall.

The turbine representation with prescribed surface loading has been analyzed over a range of thrust angles from 0° up to 75°. Thrust vectors within this range are evaluated for streamwise thrust coefficients up to 0.9. The absence of tangential loading causes the relation between streamwise thrust and power extraction to be nearly invariant with the thrust angle. Analysis of surface loading through peak amplitude and average amplitude are required to show variation in performance with thrust vectoring.

The PitchVAWT is analyzed over a similar range of thrust vectors, to allow comparison between the two turbine representations. The PitchVAWT is also analyzed on minimal value of thrust and streamwise thrust against power generation to observe potential variation between these methods and which could be more beneficial. Furthermore, the PitchVAWT is evaluated on its limits to deflect the thrust angle, in positive and negative directions, for specified value of power generation to obtain the $2D$ relation between these two parameters.

PitchVAWT has shown, in $2D$, to be capable to attain power generation over a large range of thrust angles with minor losses and greatly exceeds the most optimal performance of a yawed HAWT as described by Dahlberg and Montgomerie.[11] Three dimensional computations on the VAWT will have to determine what remains of this advantage in performance over the HAWT.

Acknowledgements

The finalization of this report truly marks the end of an era for me. Over the years at the university I've had the freedom to explore further interests and hobbies, go traveling and learn valuable life lessons. This all took a toll on the progress of my studies, but it has been a great personal enrichment. The current report is the finalization of my education at the TU Delft in aerospace engineering and obtaining the title of master of science. Finishing a university grade education is never a solo achievement and therefore there are a few people I want to give the recognition that they deserve for aiding me on this journey.

I would like to thank Dr. Carlos Simão Ferreira for the opportunity to graduate on this interesting topic. Your lectures on 'Rotorwake Aerodynamics' sparked my interest on wind energy and in particular vertical axis wind turbines. The advice and guidance have been an essential part in keeping this graduation project on the right track, for which I am grateful. Further appreciation goes out to Bruce LeBLanc, for the aid in upholding the quality of my investigation and reporting at any day of the week.

A special thanks goes out to my parents for the constant support on all fronts, without you none of this would have been possible in the first place.

The final word of appreciation goes out to my girlfriend Selma, for the motivational support and for her alleged code-whispering abilities that removed bugs when simply re-executing the code.

In the entire English language there are no combinations of three words better than "I love you".

Except for...

"Assume ideal gas"
"Assume incompressible flow"
"Friction is negligible"
"Steady state operation"

Delft, The Netherlands — B.M. de Korte
February, 2019

Contents

List of Figures

List of Tables

Nomenclature

Latin symbols

a	Induction factor
B	Number of blades
c	Chord length
C	Correction factor in weighting functions
C_d	Drag coefficient
C_n	Coefficient of load normal to the cylinder surface
C_l	Lift coefficient
C_T	Thrust coefficient, summation of all dimensionless force vectors
C_{T_x}	Component of the thrust coefficient parallel to free stream
C_{T_y}	Component of the thrust coefficient normal to free stream
$C_{T_{x,lim}}$	Limiting streamwise thrust coefficient during load optimization
C_t	Coefficient of load tangential to the cylinder surface
C_P	Coefficient of power generation
C_{P_i}	Coefficient of power extraction
$C_{p_{ideal}}$	Coefficient of power extraction in literature, see also C_{P_i}
$C_{P_{max}}$	Largest value of power coefficient obtained
$C_{P_{subset}}$	Set of power coefficients for which computations are performed
D	Drag force of a blade
D_w	Drag force of a blade as experienced by the flow
F_n	Load normal to the cylinder surface
F_{res}	Resultant aerodynamic force on blade
F_{res_w}	Resultant aerodynamic force on blade as experienced by the flow
F_t	Load tangential to the cylinder surface
f	Scaling factor for control point coordinates
i	Index in matrices
j	Index in matrices
k_a	Induction factor based correction
K	Weighting function
L	Lift force on a blade
L_w	Lift force on a blade as experienced by the flow
N	Number of control points on the cylinder surface
P	Power generation
P_0	Power generation under 0 yaw angle
R	Radius of the rotor
Re_c	Chord based Reynolds number
$R_{w,x}$	Rotor influence coefficients on velocity field in 'x' direction
$R_{w,y}$	Rotor influence coefficients on velocity field in 'y' direction
Q_n	Non-dimensional load normal to the cylinder surface
$Q_{n_{lim}}$	Maximum value of Q_n applied at a control point
Q_t	Non-dimensional load tangential to the cylinder surface

V_n	Velocity normal to cylinder surface
V_t	Velocity tangential to cylinder surface
V_{rel}	Relative velocity experienced by the blade
V_x	Velocity in 'x' direction
V_y	Velocity in 'y' direction
V_∞	Free stream velocity
w_x	Perturbation velocities in 'x' direction
w_y	Perturbation velocities in 'y' direction
x	Cartesian coordinate
x	Variable exponential in HAWT power law
x_0	Initial value of optimization vector
y	Cartesian coordinate

Greek symbols

α	Angle of attack
$\alpha_{x,0}$	Initial angle of attack distribution for optimization function
α_{ss}	Angle of attack at static stall
Δ	Step size
ε	Angle between lift force and resultant force
θ	Rotor angular (azimuthal) position
θ_p	Pitch angle
λ	Tip speed ratio
ρ	Fluid density
ϕ_y	HAWT yaw angle
φ	Inflow angle
φ_{max}	Largest inflow angle over all control points
Ψ	Thrust angle
ω	Angular velocity

Abreviations

ACM	Actuator Cylinder Model
BL	Boundary Layer
HAWT	Horizontal Axis Wind Turbine
PitchVAWT	Wind tunnel test model
TSR	Tip Speed Ratio
VATT	Vertical Axis Tidal Turbine
VAWT	Vertical Axis Wind Turbine
VG	Vortex Generator

Chapter 1

Introduction

The global energy consumption is increasing annually and government actions are being taken to reduce the polluting energy generators and increase the prevalence of renewable energy on the overall power generation. Europe is enforcing quota on renewable energy, where wind energy is expected to be a serious contributor to meet these requirements and is thereby stimulating the market to increase development and research. The European waters hold a surplus of potential energy compared to the European usage of energy,[16] but harnessing this energy will be challenging.

The transport of electricity from generator to user experiences losses from the wiring that increases with the length of transportation, making it beneficial to position power generators, including wind turbines, near their users. The application of offshore turbines comes at the benefit of having lower surface roughness of the water and no obstacles that would both impact the freestream. Furthermore there are no noise regulations on offshore locations in place. The limitations on land and the limited availability of land near populated regions raise the interest further of exploring the possibilities of offshore turbines.[48]

Some of the downsides to offshore applications are related to difficulties of installation and maintenance, but also include a harsher environment, related to waves and currents, and often saline conditions. Estimations of the cost of energy dating from 2008 declared that cost of energy of offshore turbines was almost twice as high as those of land based turbines,[48] but offshore regions hold large energy potential near populated areas.[1]

The application of horizontal axis wind turbines (HAWT) in wind farms requires significant separation between turbines to mitigate the impact of adjacent turbine wakes. To enhance the energy extraction potential of HAWTs, larger turbines are built that can access greater wind resources due to the higher altitudes.[10] The scale up of HAWTs has limitations, since the blade fatigue life is affected by gravitational loading. HAWT blade weight is reported to scale cubically with blade length and can be a restricting factor for the blades to achieve 10^8 cycles of their lifetime safely.[47]

The vertical axis wind turbine (VAWT) is more easily scalable than the HAWT, as its not affected by cyclic gravitational loading on a level surface. Lift driven VAWTs have the potential to be superior in wind farm applications, since the spacing of HAWTs is approximately ten diameters, while it has been reported that VAWTs can be spaced 4 diameters apart at which they lose less than 5% of the undisturbed power generation. The associated power generation per unit land/water of the VAWT can be noticeably more than for the HAWT.[10] The VAWTs inherent unsteady nature makes the turbine less sensitive to unsteady inflow than its horizontal axis counterpart,[38] as the VAWT appears to harness more wind energy in highly turbulent environments than the HAWT.[39] Furthermore, the VAWT benefits from a lower center of gravity than the HAWT, since the gearbox and generator can be positioned at or even below sea level for floating applications that benefits production costs and adds an ease of maintenance.[48]

Contrary to the HAWT, the VAWT is characterized by inherent unsteady aerodynamics. As an example, the fixed, zero pitch Darrieus VAWT is taken, where geometric angle of attack and inflow angle are equal. This VAWT experiences varying angles of attack over a full revolution. The magnitude of the geometrical angles of attack is determined mainly through the tip speed ratio and easily exceeds the static stall angle for small tip speed ratios. The difference between the angle of attack and geometric angle of attack is caused through flow curvature that adds an artificial angle of attack which is dependent on the chord-to-radius ratio.[35] Below TSR$= 1$ the geometrical angle of attack can reach values up to nearly $180°$, which is responsible for the fixed pitch VAWT's inherent self-starting difficulty. The performance of the fixed pitch VAWT in low tip speed ratios might be enhanced by altering the offset pitch angle for a fixed pitch application, but will mainly enhance upwind performance at the cost of downwind performance or vice versa. The influence of varying the fixed pitch offset was investigated by Ferreira and Scheurich[43] for TSRs where the angle of attack remained below the static stall angle and showed that the variation in performance is mainly on the instantaneous parameters with minor variations on the integral parameters such as thrust and power generation.

The VAWT is more capable of extracting energy in highly turbulent conditions than the HAWT, but under steady conditions it is not. This comparison is slightly misleading as HAWT development has advanced further and these turbines often include flaps, pitch control, vortex generators or other methods of circulation control to enhance the overall performance, while these are not yet standard included on the lift driven Darrieus VAWTs. VAWTs are capable of extracting more energy from the flow due to their three dimensional actuation plane, but this requires circulation control to achieve. Circulation control on the VAWT is not limited to high-lift devices, but also includes methods that can reduce lift and/or expand the angle of attack range of attached flow of the unaugmented fixed pitch VAWT's blade.

The implementation of circulation control could contribute more to the increment of power generation than fixed pitch offset and might do so at lower corresponding thrust values. Circulation control can range from static features added to the blade up to (re)active flow control mechanisms. The static features are considered passive flow control devices and these include vortex generators, surface roughness and zigzag tape. Vortex generators (VG) create vortices that reenergize the boundary layer (BL) by mixing high momentum flow from outside the BL with the boundary layer flow that has been slowed due to viscous effects. VGs have shown to increase power generation for HAWTs by increasing the angle of attack range of attached flow, particularly on the inboard region of the rotor.[18] The VAWT does not have a region of the blade that performs lesser to the rest of the blade like the inboard part of the HAWT does, which would result in the implementation of VGs on a VAWT to raise the performance on the lower TSRs, but should also reduce peak performance through the increased drag.

Active circulation control also comes in a variety of forms, which include: plasma actuators, flap/slat actuation, pitch control, applying blowing/suction and others. Plasma actuation in the form of dielectric barrier discharge consists of two electrodes of which one is positioned in the flow and one beneath the dielectric material. The two electrodes are supplied with an AC current that, when above its threshold, ionizes the airflow, making it a plasma. The ionized air creates a body force on the surrounding air while the plasma is in the electric field created by the electrodes. The work of Corke[8] has shown a potential increase in the static stall angle by 7° to $\alpha_{ss} = 22^\circ$ by applying leading edge plasma actuators under $Re_c = 0.217 \cdot 10^6$. The extension of the angle of attack region of attached flow through plasma actuators could benefit the performance of the VAWT, especially below the peak tip speed ratio.

Flap actuation is applied as a method increasing lift coefficient, mostly on airplanes. The augmentation of lift through flaps can be extended on VAWTs as well, which was investigated by Xiao et al.[50] who applied oscillating flaps on a vertical axis tidal turbine (VATT). The different medium of the flow of a VATT causes the parameters to vary differently, but the results showed that the performance can be increased through flap actuation. Ertem et al.[15] focused on applying active flap control on a VAWT and demonstrated the gain in power extraction through an inviscid load idealization representing the wing and flap. The ability of raising power extraction on a VAWT through flap actuation has been demonstrated, but so far there has not been any work, as far as the author is aware, on flap actuation's ability to extend the attached flow region for VAWT's operating at low TSRs.

Application of slot blowing has been evaluated by Sasson and Greenblatt,[41] who investigated the potential power gain over a wide range of tip speed ratios. The slot through which air is injected into the flow around the blade is positioned at the leading edge and calculations were performed on single sided blowing and double sided blowing. Results show that, through the injection of air at the leading edge, the gross power is increased over the entire operational range at sufficient injection of momentum. The turbine is able to generate energy at lower TSR than the reference turbine and the gain in gross energy is even more for the double

sided blowing. The adjustment to net power generation shows that slot blowing is only effective at TSRs below the base turbine's peak tip speed ratio, but can have a strong impact on the overall performance of a VAWT.

Pitch control has been investigated by many, but mainly through surface loading only in search of the theoretical maximum of power extraction. Madsen et al.[30] showed that by applying constant load forms on the actuator cylinder model, the Betz limit can be exceeded if the azimuthal regions of constant loading are large enough. They further stated that one should remain cautious on applying constant load forms over large azimuthal regions, as these would cause large flow gradients that will increase the numerical uncertainties of the model.

Pitch control has also been investigated for enhancing the start-up potential by applying a passive pitching mechanism where the inertial and aerodynamic loads keep the blade from operating above its stall angle. Kirke[23,24] and Lazauskas[23,26] performed experiments on passive pitching, both theoretical and in field, and showed the enhanced performance of a passive pitching mechanism. Passive pitch control has shown to enhance peak power generation and greatly enhance the start-up behavior of the VAWT, but rapidly drops in power coefficient past its optimal tip speed ratio.

The performance of any turbine can be generalized through figure 1.1, which defines four distinctive operational regions. In region I the velocity of the freestream is simply too low for the turbine to generate power. Region II is the sub-rated power region of a turbine, between cut-in velocity and rated velocity. While operating in the sub-rated regime, the power coefficient is desired to be as large as possible. At rated velocity the turbine reaches its peak power generation and should not generate more than that. Rated velocity initiates region III, here it is desired to reduce the power coefficient with increasing flow velocity to keep the power generation constant. The available energy in the flow scales with the freestream velocity cubed, so in region III the power coefficient has to be drastically reduced with increasing velocity. The cut-out velocity indicates region IV, where the turbine is shut down to prevent damage to the turbine.[22]

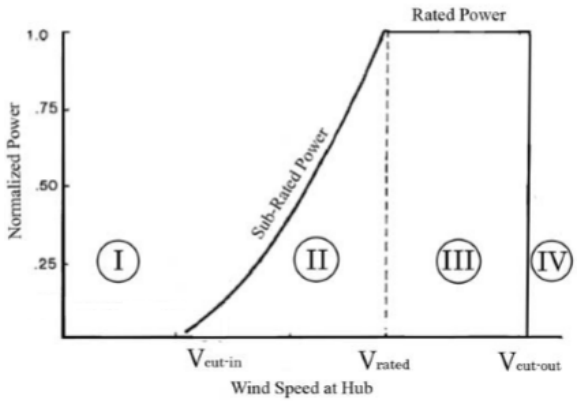

Figure 1.1: Global power curve for wind turbines.[22]

Pitch control has the benefit of being applied to all regions of the global power curve in figure 1.1. Passive pitch control has shown to reduce the cut-in velocity and active pitch control could reduce this value even more, since its actuation is not dictated by circumferential forces. In region II the power coefficient will be raised by reconfiguring the instantaneous loading through pitch actuation. While operating under rated power, the power coefficient has to be reduced to keep the power constant with velocity. Through active pitch control the power coefficient can be reduced efficiently, without inducing dynamic stall or creating unnecessarily large thrust coefficients, which might increase the velocity range of rated power operations. For any velocity larger than the cut-out velocity the turbine will not be operated, but active pitch control can still be applied to ”park” the blades in order to alleviate large aerodynamic loading. These principles have been included in the S4VAWT project by Huijs et al. indicating the potential benefits that could come to the VAWT by the inclusion of active pitch control.[21]

1.1 Research focus:

Active pitch control is selected as the method of load control because it can attain attached flow over nearly a full rotation of the VAWT, as long as there is no limit on the pitch angle. The inability to attain attached flow will occur near the azimuthal areas where the lower pressure side of the blade switches from inboard to outboard and vice versa. The size of the area where flow cannot remain attached is a function of the pitch rate, which is considered a turbine specific parameter and will remain unbound within this work. Pitch control further benefits from having lift and drag polars that are unaffected by actuation, making it a great application to investigate various loading with. Other methods of active circulation control, such as Flap control, plasma actuation and blowing/suction over the blades, alter their polars through actuation and this alteration varies with the intensity of actuation.

The application of active pitch control opens a variety of azimuthal load distributions that are not possible on a fixed pitch turbine. The maximum gross C_P that pitch control can achieve ought to be unique for each turbine representation. For values lesser than maximum it should hold that far more than a single load distribution can achieve the corresponding gross C_P. Therefore, operating below maximum C_P allows one to optimize the azimuthal load distribution in a way that is favorable to the user. This can result in minimizing thrust or adjusting the component of the thrust coefficient normal to the freestream.

Within this thesis focus is applied to the thrust vector and how variations in the thrust vector affect the ability to generate power, for both a VAWT with set design parameters, called PitchVAWT, and for directly applied load distributions that are not restricted by turbine design parameters.
The latter is essentially the method from Madsen,[29] where tangential loading is ignored. This method corresponds to the load idealization calculations, but the term ideal/idealized is considered conflicting in this thesis, since the results that will be presented do not only focus on maximizing the power extraction. The method regarding the idealized calculations within this thesis will be referred to as Pre-

scribed Surface Loading, to distinguish itself from the PitchVAWT analyses, while not presenting the lesser than maximum $C_{P_{ideal}}$ cases as ideal.

1.2 Research questions:

The preceding research focus has been combined into the following research questions:

What is the potential of load control on a VAWT and how does this impact power generation/extraction?

Operation at power coefficients lesser than the maximum, for the specific flow conditions, can be achieved by a variety of instantaneous load forms. This allows one to find an optimum for the integral loading. The optima can be for the minimization of thrust, minimization of streamwise thrust, and the maximization of the thrust component normal to the freestream in either direction. This research question aims to give the relation between the maxima for these optimization cases and establish how the ability to generate power is reduced when adjusting the loads towards these extrema.

How does the distribution of instantaneous loading on the VAWT vary with thrust angle for the Prescribed Surface Loading cases?

The concept of maximizing the power extraction through prescribing surface loading has been worked out by several researchers and resulted in large azimuthal regions of constant loading on both the upwind and downwind halves of the rotor. However, this was only performed under the condition where the integrated load vector was aligned with the freestream and will now be extended for offset angles between these parameters. Both offset angle and thrust will be varied to evaluate the variation of instantaneous loading with thrust vectoring.

How well are the PitchVAWT turbine's integral and instaneous parameters in agreement with the Prescribed Surface Loading cases?

The Prescribed Surface Loading cases create a more global overview of the performance of the VAWT without specifying the turbine's design parameters. The inclusion of turbine parameters and influence of tip speed ratio cause differences between the two representations. This question aims to compare the general turbine representation with a specific turbine in order to justify the method of directly prescribing the surface loading.

1.3 Thesis Layout

The current section provides an overview of the layout of this report. Background information on the theory that is relevant within this thesis is addressed globally in chapter 2.
In chapter 3 the mathematics of the actuator cylinder are presented along with the methodology of the implementation of the PitchVAWT and the prescribed surface loading turbine models and their respective approaches on obtaining results.
The results are presented in chapter 4. The results for the prescribed surface loading cases are presented initially, on integrated parameters and instantaneous parameters, and followed by the PitchVAWT results, which are directly compared to the prescribed surface loading cases. Lastly, the PitchVAWT results of the maximization of the different types of load control are presented.
Finally, in chapter 5 the conclusions from the results are stated, along with recommendations for future work to build upon the foundations set within this work.

1.4 Additional information

Initial work was performed on wind tunnel measurements on a VAWT model, but the test results were not applicable for this thesis. The wind tunnel model is the PitchVAWT by LeBlanc,[27,28] which is seen on the front cover of this report. PitchVAWT is the name for the $2-$bladed, H-Darrieus wind tunnel model with active, individual, preset pitch control at TU Delft. The model is $1.5m$ in diameter, has NACA0021 blades with a length of $1.5m$, with a chord-to-radius ratio and solidity of 0.1 and operates typically at Reynolds numbers of 10^5. Part of this project was wind tunnel testing on this model and performing predictive computations, which makes it apparent that the PitchVAWT's design specifications were applied to compare results with the prescribed surface loading results. No results on the testing or the predictions will be presented in this thesis.

Adjustments were made to the definition of the thrust vector, since the commonly obtained definition in literature mostly focuses on the streamwise component of loading and generally ignores the streamnormal component of loading. The thrust coefficient of VAWTs is defined as the summation of the dimensionless, instantaneous force vector components that are aligned with the freestream. Within this thesis emphasis will be put on the component of the integrated loading that is normal to the freestream and therefore the thrust coefficient will be referred to as the summation of all dimensionless, instantaneous load vectors. This new vector can be decomposed with respect to x and y directions, where x is alligned with the freestream and y is the component normal to the freestream. Thus, C_{T_x} is the thrust component aligned with the freestream and C_{T_y} is the thrust component normal to the freestream. C_{T_x} will be referred to as the streamwise thrust coefficient and the angle that is formed between the thrust vector and the freestream is referred to as the thrust angle, Ψ. Figure 1.2 displays the mentioned vectors and angles, along with the incoming flow and the azimuthal orientation of the turbine,

all in their respective positive orientations. The rotation of the turbine is counter-clockwise or in the same direction as θ, where C_{T_y} and the thrust angle are defined positive when directed towards the windward side of the VAWT.

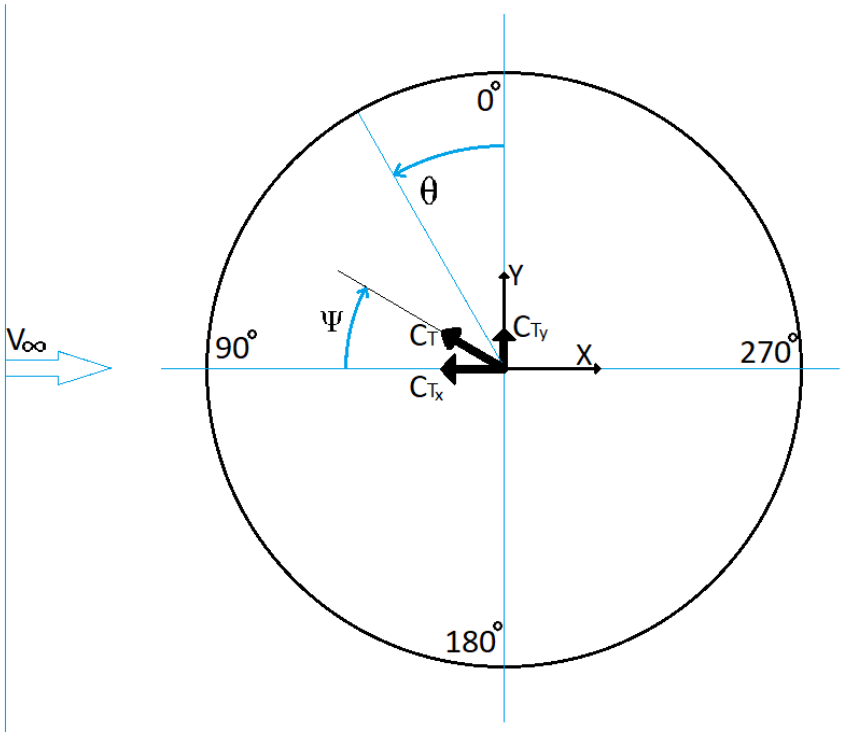

Figure 1.2: Positive direction for loads, freestream, azimuthal angle and thrust angle.

Chapter 2

Research Background

This chapter covers the theoretical basics concerning VAWTs and pitch control. Part of the theoretical background on horizontal and vertical axis turbines and other forms of active and passive circulation control are covered in chapter 1 in the breakdown why VAWTs with active pitch control are investigated. The major developments in VAWT history leading up to the fixed pitch Darrieus turbine are covered in section 2.1. The behavior of HAWTs when their thrust vector is at an offset angle is addressed in section 2.2. Sections 2.3 and 2.4 cover the fixed pitch VAWT's inherent aerodynamic behavior of stall & dynamic stall and flow curvature respectively. The aerodynamic models are reported on in section 2.5, where only the models with low computational costs and the vortex model are discussed. The research performed on both active and passive pitch control is summarized in section 2.6. Finally section 2.7 covers the limitations to power extraction from the flow.

2.1 Brief history of VAWTs

The origin of the vertical axis wind turbine dates back to the Persian empire where the turbine was a drag driven mill through plates that were aligned with the radius of the mill. As this system cannot create torque on its own, it was required to shield approximately half of the mill from the wind to allow for a difference in forces to generate torque.

The (cup) anemometer was invented around 1450. This also was a drag driven device, but based on a difference in drag coefficient between the windward and leeward motion. This was obtained by using thin-walled half spheres. As the windward region experiences larger velocities than the leeward region and aerodynamic forces scale with the velocity squared, it follows that there is a significant difference required in the drag coefficients. The ratio between these values is indicative for the maximum tip speed ratio at which the turbine can operate. It is impossible for any purely drag driven turbine to reach or exceed a tip speed ratio of one.

In 1922 the Savonius rotor was invented as two thin-walled cylinders with a small offset at the axis of rotation that allows air to flow through. This causes the Savonius rotor to be both drag and lift driven. Because of the presence of lift from the unsteady loading through the offset, the Savonius rotor can operate at tip speed ratios slightly above one. The power coefficient of this turbine can reach about 0.3, which is approximately half of the Betz limit.

The Darrieus wind turbine was invented in 1926 and is a purely lift-driven wind turbine, seen in figure 2.1. This allows the Darrieus turbines to operate at tip speed ratios significantly larger than the preceeding drag driven VAWTs. Although all these turbines are VAWTs and many more types are available, from here on the term VAWT refers to the Darrieus wind turbine, specifically the 'H' type .

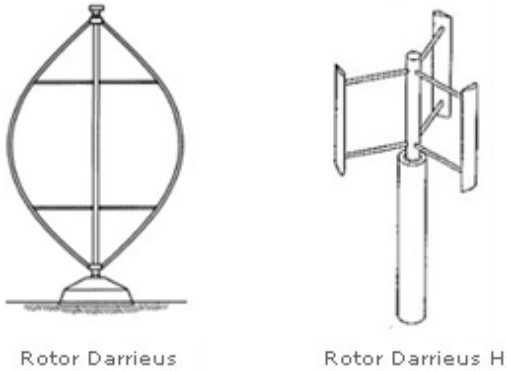

Figure 2.1: Visualization of the standard Darrieus wind turbine and the H-type Darrieus wind turbine.

2.2 Yawed HAWTs

Before going into the background of the inherent characteristics of the VAWT, this section will address the HAWT under yawed conditions. The VAWT will be evaluated in cases where the thrust vector is inclined with the freestream and it will be useful to make a comparison in performance with empirical results from the yawed HAWT. The HAWT has been analyzed under yawed conditions and Dahlberg and Montgomerie[11] developed the relation of power and yaw angle, equation 2.1, based on their measurements. The power drops with the cosine of the yaw angle, ϕ_y, to the power x, where x can vary between 1.88 and 5.14, depending on the operating conditions. Fleming et al.[17] tested tandem HAWTs and the results showed that upwind turbine's power generation scaled closely to equation 2.1 for $x = 1.88$.

$$P = P_0 \ cos(\phi_y)^x \tag{2.1}$$

2.3 Stall & Dynamic stall

The stall angle of attack indicates the angle where under static conditions the flow can no longer remain attached and the airfoil loses performance rapidly with increasing angle of attack. The lift coefficient and angle of attack just prior to stall indicate the limits of an airfoil, but through dynamic stall these performance limits can be exceeded without modifying the airfoil. Dynamic stall is the event where through shed vortex interaction with the airfoil the increasing circulation around the airfoil can briefly be attained, but after the increase, the lift curve plummets and performs during recovery lesser than it would under static conditions.

Stall is characterized by the separation of the boundary layer which leads to a reduction in lift and an increase in drag forces. McCullough & Gault[34] established three distinctive kinds of stall, each inherent to the specific thickness-to-chord ratio of the wing.

The first is trailing-edge stall, where the turbulent boundary layer separates near the trailing edge. With increasing angle of attack, this separation point gradually moves towards the leading edge. This form of stall is characteristic for thickness ratios of approximately 0.15 and larger.

The second type of distinguishable stall is leading-edge separation, a form of stall mostly observed for thickness ratios of about 0.09-0.15. The stalling sequence is initiated with a small laminar separation bubble near the leading edge. The flow separates laminar, but reattaches as the flow becomes turbulent. The bubble has a negligible effect on the integrated loads due to its small size. When the angle of attack is increased further the bubble will burst causing flow separation on the entire upper surface, creating a sudden drop in lift.

The last type of stall is the thin-airfoil stall, characteristic for thickness ratios of 0.09 and less. This type of stall is also caused through a laminar separation bubble, but one that remains at a fixed location with varying angle of attack. For thin-airfoil stall to occur a low Reynolds number is required.[9]

Dynamic stall occurs past the stall angle and requires a continuous increase in angle of attack per unit time in surplus of a critical angle per second. This increasing circulation causes a shedding of vorticity of equal strength and opposite direction, as explained through Kelvin's theory. From Theodorsen's theory[46] it follows that the augmentation in lift due to this circulatory lift increment is gradually added over time.

During dynamic stall a leading edge vortex grows that moves downstream at a little less than half of the free-stream velocity. As this vortex travels downstream, the drag starts to increase, the moment coefficient increases negatively and the lift coefficient increases monotonically past its stall angle. This behavior occurs until the vortex is just past midchord, after that the drag and moment increase exponentially while the lift only makes a small increment. When the vortex is near the trailing edge, lift, drag and moment reach their maximum value, yet not necessarily simultaneously. At this point a counter-vortex is initiated at the trailing edge that reduces the experienced angle of attack. During the growth of this counter-vortex the flow will reattach and the separation point will gradually move backward. During the process of reattachment the lift force is less than it would be at the same angle of attack while under pre-stall conditions.[33]

2.4 Flow curvature

Flow curvature is an aerodynamic side effect of rotational motion. For HAWTs this effect is experienced in spanwise direction, while for a VAWT it is observed along the chord, as is presented in figure 2.2.

The impact of this curvature effect is constant for all azimuthal positions and is mainly dependent of the chord length and the radius to the axis of rotation. Figure 2.2 indicates the chordwise varying rotational velocity experienced by the blade and the chordwise variation of the angle of attack. Migliore et al.[35] developed the idea that the chordwise variations in aerodynamics in curvilinear flow can be projected to a cambered airfoil in rectilinear flow, as is displayed in figure 2.3. The artificial camber and corresponding induced angle of attack are primarily dependent on the chord to radius ratio, c/R. This conclusion was made for a flat plate and therefore did not include the variation of velocity with radial position that an airfoil with finite thickness experiences. This variation in velocity will have a minor effect since the thickness to radius ratio is quite small, but it greatly impacts the rectilinear flow field. This correction by van der Horst et al.[19] is shown in an exaggerated form in figure 2.3.

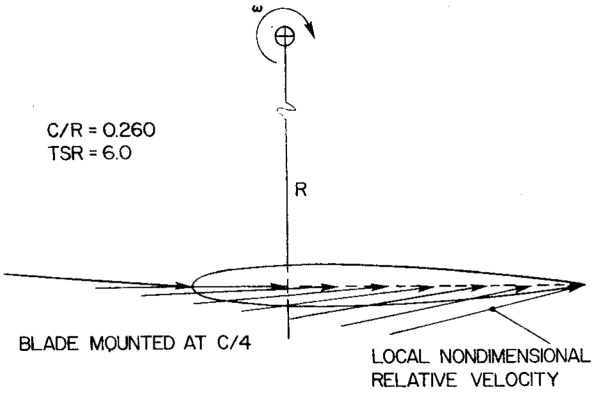

Figure 2.2: Chordwise variation of V_R' and α'.[35]

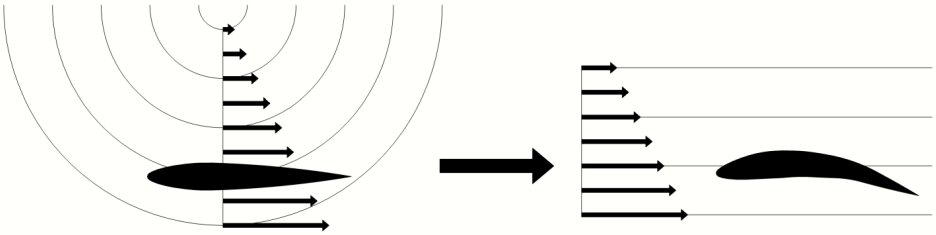

Figure 2.3: Flowfield transformation from curvilinear to rectilinear.[19]

2.5 Basic VAWT engineering models

This section contains a small overview of some of the basic aerodynamic models for VAWTs. The models that are addressed are simplistic enough to produce data rapidly. Their accuracy can be enhanced by incorporating small variations and/or empirical relations. Models such as DNS, RANS and LES are far superior in terms of accuracy, but are computationally extremely expensive. Due to the requirement of little computational time per scenario, DNS, RANS and LES are unsuited for usage in this thesis work and will not be addressed further in this section.

2.5.1 Actuator disk model

The actuator disk model is a blade element momentum model, which combines the discretization method from blade element theory and the conservation of momentum or momentum theory, where the flow is assumed to be steady, inviscid, irrotational, incompressible and has constant internal energy. Blade loading is represented as a body force that acts on an infinitely thin actuation surface. The flow through the actuation plane is considered a single streamtube with uniform flow conditions. The actuator disk model represents the HAWT where the thickness of the rotor is removed, creating a 2D representation. Acknowledging the axisymmetry, this model effectively becomes a 1D actuator strip model, as in figure 2.4

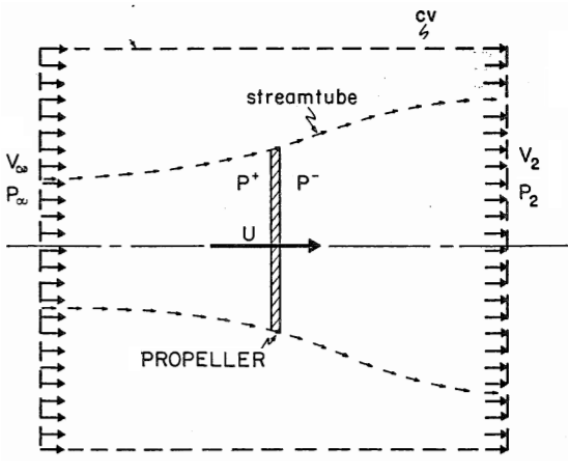

Figure 2.4: Control volume of an actuator disk streamtube.[49]

2.5.2 Multiple streamtube model

The actuator disk model was enhanced by Strickland,[45] who broke down the actuator disk model into a series of parallel streamtubes. For each of these streamtubes the momentum balance is carried out independently. By applying a series of streamtubes, an arbitrary variation of inflow conditions can be attained to more thoroughly compute the flow and loading around the VAWT than a single streamtube can.

2.5.3 Double multiple streamtube model

The actuator disk theory and the multiple streamtube model both apply a single extraction plane per streamtube to compute the flow of the VAWT. Paraschivoiu[37] expanded the multiple streamtube model to model the upstream and downstream conditions separately through the double multiple streamtube model. It is assumed that the flow through the upstream actuator disk fully expands before crossing the downstream actuator disk and therefore there is a reduction in the freestream velocity at the downwind half of the rotor.

2.5.4 Actuator cylinder model

The actuator cylinder model (ACM) was developed by Madsen[29] and models the VAWT loading on a circular path, corresponding the swept area of the blades, as is shown in figure 2.5. The ACM is a $2D$ steady Eulerian model that solves the pressure jump over the actuation surface and the flow field. The model introduces perturbation velocities where the influence of loading at one position affects the flow field over the entire turbine. The influence of the perturbation velocities on the entire rotor is a feature that the streamtube models do not possess. The actuator cylinder model will be described in depth in section 3.2 including the modified-linear solution correction for large induction factors.

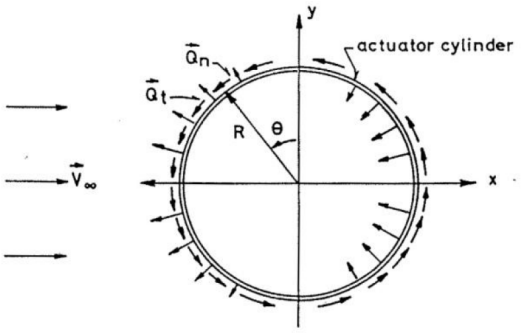

Figure 2.5: Actuator cylinder lay out with actuation of the non-dimensional forces displayed.[31]

2.5.5 Vortex model

The vortex model is based on the theorems of Kelvin[2] and Helmholtz.[4] These respectively state that the time rate of change of circulation in a closed contour is zero and that vortices form a closed path with constant strength along the vortex' length. In 2D this results that for all bound circulation created, there is a counter-rotating vortex shed into the wake. In the 3D case, the bound circulation and the shed vortices from the 2D scenario are connected as a closed path through the trailing vortices, caused by variations of the circulation in spanwise direction.

The vortex model represents the blades as a single (bound) vortex positioned along the chord, commonly at the quarter chord point. The variation in circulation in time causes the shedding of a vortex of equal strength of the variation in circulation, but of opposite direction. All the shed vortices, trailing vortices and the

bound vortex affect the entire flow field as described through the Biot-Savart law[3] from equation 2.2 and through superposition the influence of each vortex can be combined with the free stream to generate the flow field around the cylinder.

$$d\overline{V} = \frac{\Gamma}{4\pi}\frac{d\bar{l} \times \overline{r}}{||\overline{r}||^3} \tag{2.2}$$

The vortex model comes in two distinct forms, free and frozen wake. The free wake is a more accurate representation of the flow where all vortices interact with one another. In frozen wake model the shed vortices travel downstream at a constant velocity. The frozen wake has superior computational performance, but comes with an additional penalty in accuracy compared to the free wake model.

2.6 Past studies on pitch control

The application of pitch control to enhance performance comes in two forms; active and passive. Active pitch control is a more recent application that comes along with the development of large, straight bladed VAWTs. For the application on small scale turbines, active pitch control is currently too complex to be economically viable. Passive pitch control is a viable solution for small scale VAWTs to not only enhance the performance compared to fixed pitch, but it also aids in the turbine's self-starting ability.

2.6.1 Passive pitch control

Passive pitch control comes in two distinct forms; pre-set and self-acting.
The concept of the pre-set pitch sequence was already incorporated by Darrieus himself in 1931 in the original patent. This was executed through the Cycloturbine by Drees.[12] This straight bladed turbine used a central cam that was self-aligned with the flow through a tail vane and applied pushrods to pitch the blades. The downside of such a system is the enhancement of the performance by the cam is only applicable to a small range of TSRs and will negatively effect performance outside this range. Furthermore, the use of pushrods causes a significant drag increase.[40]

The self-acting passive pitching mechanism idea for VAWT applications has been around since the late seventies, but most of these have only been concepts. All of these concepts included pitching of the blade around a pivot point that was not necessarily on the blade, as in figure 2.6, and a method to create a moment to counter the moment caused by the aerodynamic loading. Methods to counter the aerodynamic loading include: an added mass that is subjected to circumferential force as shown in figure 2.6, an intrusive added spring connected to the chord and strut or a combination of spring and balance weight.

The spring system is systematically flawed, as an offset between the periodic oscillations from pitching and the natural frequency of the spring could lead to large performance reductions.[23] The added intrusive mass is the type which contains most variations in design, yet no performance data has been published on these types of pitch control to the author's knowledge. Kirke[23,24] and Lazauskas[23,26] developed a passive pitching mechanism that contains a stabilizing mass that can freely move along the strut, which opposes the aerodynamic moment through centrifugal force, presented in figure 2.7. Computations and field testing have been performed for this method and both show that this passive pitching mechanism has superior self-starting characteristics compared to the fixed pitch, peak C_P is increased and the range of tip speed ratios over which power is generated is increased in comparison to the fixed pitch VAWT.

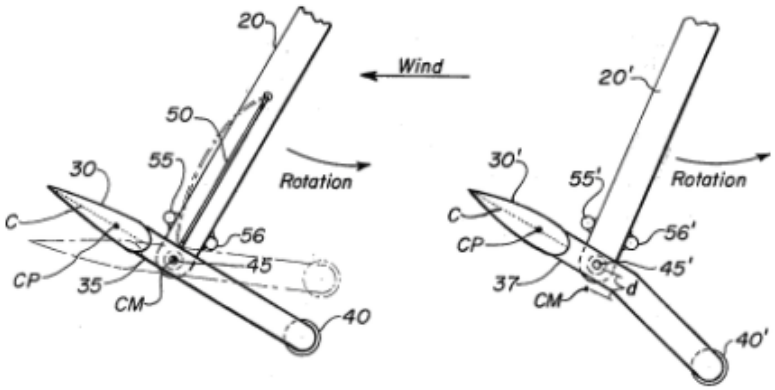

Figure 2.6: Example of an intrusive mass passive pitch mechanism.[6]

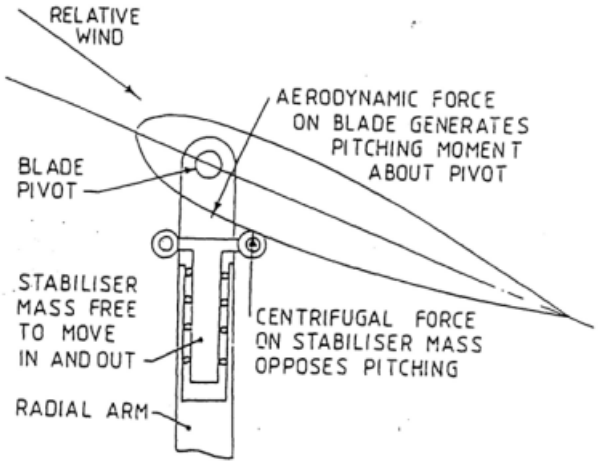

Figure 2.7: Example of passive pitch mechanism positioned in the strut.[23]

2.6.2 Active pitch control

Active pitch control can come in both pre-set and responsive forms, where the latter has not yet been investigated for VAWT applications. Preceding work on active pitch control is mainly focused on maximizing the power extraction by assuming large tip speed ratio, to not be limited by the stall angle, and applying pitch

control to obtain non-varying lift polars with actuation. The corresponding results show that the largest possible power extraction is obtained through separate constant surface loading on the upwind and downwind halves of the rotor.[30] The work of Staelens et al.[44] has shown that at velocities below rated velocity the largest power coefficient is obtained by applying an angle of attack just beneath the stall angle on all azimuthal areas, which typically holds for low solidities. However, it was acknowledged that this is physically impossible to obtain and a continuous pitching scheme was considered more appropriate when taking into account the influences of loading on the structure. Houf et al.[20] demonstrated through the use of active pitch control and smooth pitching schemes with pitch angles up 5° that there is barely an increase peak C_P achievable, but the gain in relative power generation increases when the deviation of the tip speed ratio increases with respect to the TSR corresponding to the maximum power generation.

2.7 Limits to power extraction

The effectiveness of a turbine is defined by the ratio of power that the generator can convert w.r.t. the power available in the wind, C_p. In 1919 the upper limit of C_p was derived, known as the Betz limit, which is at 16/27 or 0.593. The Betz limit was derived using conservation of mass and momentum for a 1-dimensional streamtube, crossing an actuator disc with an infinite number of blades that applies a uniform thrust on the flow over the entire disc area. This theory further assumes a non-rotating wake and an inviscid, incompressible, homogeneous, steady state flow.[5]

The maximum in C_p comes with a limit to the amount of thrust the actuator disk can exert on the flow. The thrust coefficient is related to the pressure jump over the disk, where the pressure of the flow is lower after crossing the disk. As the flow is subsonic, the pressure jump causes a reduction in streamwise velocity of the flow prior to the flow crossing the actuating surface. This relation limits the pressure jump and therefore the maximum thrust, as a too large pressure jump creates a “self-blocking” effect that reduces the generated power below maximum C_p.

Due to the assumptions of momentum theory, no single actuation plane can ever reach or exceed the Betz limit. In $2D$ computations, the VAWT’s actuation surface extends in one dimension further than the actuation plane from the Betz limit and is therefore deemed capable to exceed this limit. The upstream and downstream halves of the VAWT can be considered individual power extractors and can be represented by two actuator disks, which is a gross oversimplification. This tandem set of actuator disks was applied by Newman[36] to determine the upper limit of power extraction, which is at 16/25 or 0.64.

Chapter 3

Methodology

This chapter covers the approach of how the setup for this investigation was established. The global approach on how data points are set to be able to answer the research questions is described in section 3.1. The VAWT's aerodynamic parameters are determined via the actuator cylinder model (ACM) by Madsen,[25,29,30] for which the governing equations are presented in section 3.2, including how the PitchVAWT and Prescribed Surface Loading analyses bypass certain parameters and their respective implications.
The applied optimization function is Matlab's built-in function fmincon. The basics of this function, the settings and how the ability to find a local minimum was implemented to attempt to obtain a global minimum is covered in section 3.3. The procedure of optimizing the results for the set of data points is presented in section 3.4.

3.1 Global approach

This section covers the global approach on how to set data points to possibly establish relations between parameters. The results are generated to be applied over the range of velocities for which the turbine can extract energy. This includes the velocity range between cut-in and rated velocity, where the power coefficient is preferred to be as large as possible and the velocity range past rated velocity and cut out velocity. In the latter the power coefficient is reduced in order to keep the total power generation constant. On all these potential cases thrust vectoring is applied and the performance is maximized.

3.1.1 Prescribed Surface Loading cases

To determine how the prescribed surface loading's instantaneous load distributions vary with thrust angle, a wide variety of thrust vectors is analyzed. The thrust vectors are set over a range of thrust angles from 0° to 75° with 5° intervals. For each thrust angle the maximum power coefficient is determined and with it, the corresponding thrust coefficient. This thrust coefficient is the largest thrust coefficient that is evaluated for each thrust angle, all other thrust vectors are downscaled versions of these maxima.

The prescribed surface loading cases are not bound by turbine specific parameters such as: stall angle, solidity, etc. Due to the lack of design specifications by directly prescribing the surface loading, many load distributions correspond to the same thrust vector. Having multiple potential outcome for a single data point could deny the extracting useful information of the variation of instantaneous load variation with thrust vectoring. To attain a single outcome for each thrust vector, the load analyses are subjected to three optimization procedures.

The first is the maximization of the power coefficient, this maximum value is limited by the thrust coefficient and thus rules out all the inefficient instantaneous load distributions. The second optimization is the minimization of the average load amplitude, which redistributes loading more to regions with efficient power extraction abilities for each thrust vector. The final optimization is the minimization of the azimuthal variation of loading. This third optimization process aims to minimize the shedding of vorticity in the wake.

3.1.2 Maximizing integrated load control on PitchVAWT

The potential that load control can have on the azimuthally integrated loading has been set to four different goals; minimizing thrust, minimizing streamwise thrust and maximizing the thrust component normal to the freestream in both positive and negative directions. Each of these load goals will be assessed how their variation towards their potential maximum affects the VAWT's ability to generate power for the design specification of the PitchVAWT turbine.

These four relations have in common that they include the power coefficient, so a range of power coefficients was set for which the maximizations/minimizations are performed. First the maximization of the power coefficient itself has to be performed. Although this outcome varies between models and settings, for each of them the maximum achievable C_P ought to be unique. Based of the maximum power coefficient, a subset of power coefficients is created, as seen in equation 3.1. Each value of this subset will be evaluated on their respective maximum for each load goal.

$$C_{P,subset} = C_{P,max} \begin{bmatrix} 1 \\ 0.95 \\ 0.9 \\ 0.85 \\ \vdots \\ 0.05 \end{bmatrix} \tag{3.1}$$

3.1.3 Comparing PitchVAWT to directly prescribed load cases

The amount of thrust vectors that are evaluated for the prescribed surface loading cases greatly exceed those that are executed for the maximization of load control on PitchVAWT from section 3.1.2 and do not yet allow for good comparisons between the two models. Similarly to the prescribed surface loading cases, a wide variety of load vectors have to be set for analysis, but the PitchVAWT turbine is limited by its design parameters and might not be able to achieve the same operational range.

The maximum load control evaluations on PitchVAWT, where the thrust component normal to the freestream is maximized, set the span of thrust angles for which computations will be executed. The approach to the PitchVAWT vector range is similar to those with prescribed surface loading from section 3.1.1, where the span of thrust angles is divided into a set of thrust angles with $\sim 5^\circ$ intervals. For each thrust angle the maximum power generation is determined and the corresponding thrust coefficient is the largest thrust coefficient that will be evaluated. This thrust vector forms the basis where all lesser valued thrust coefficients are scaled off.

The design parameters on a turbine limit the amount of instantaneous load distributions that correspond to a single thrust vector. This causes PitchVAWT analyses to differ from those with a prescribed surface loading, since only a single optimization has to be performed on the maximization of the power coefficient to converge to a single possible load distribution per thrust vector.

3.2 ACM setup

This section describes the setup of the actuator cylinder as applied in computations. The equations in this section are the same as presented by Madsen.[25,29,30,31]

The rotor circumference is split evenly into N sections, each with a centered control point. To avoid singularities, each control point's position is slightly scaled up by a factor f where $f = 1.01$.

$$\theta_i = (i - \frac{1}{2})\frac{2\pi}{N}, \quad for\ i = 1, 2, ...N \tag{3.2}$$

$$x_i = f\ R\ sin(\theta_i) \tag{3.3}$$

$$y_i = f\ R\ cos(\theta_i) \tag{3.4}$$

The velocities in cartesian coordinates, V_x and V_y, in cylindrical coordinates tangential and normal to the cylinder, V_t and V_n, respectively and the relative velocity that the blade is subjected to, V_{rel}, are defined as:

$$
\begin{aligned}
V_x &= V_\infty(1 + \lambda \cdot cos(\theta_i) + w_{x,i}) \\
V_y &= V_\infty(\lambda \cdot sin(\theta_i) + w_{y,i}) \\
V_t &= V_{x,i}\, cos(\theta_i) + V_{y,i}\, sin(\theta_i) \\
V_n &= V_{x,i}\, sin(\theta_i) - V_{y,i}\, cos(\theta_i) \\
V_{rel} &= \sqrt{V_{t,i}^2 + V_{n,i}^2}
\end{aligned}
$$

where w_x and w_y are the perturbations velocities in x and y direction respectively. The perturbation velocities are derived to be a function of the distributed loading for the linear solution to the ACM as follows:

$$w_{x,j} = \frac{1}{2\pi} \sum_{i=1}^{i=N} Q_{n,i} R_{wx,i,j} - Q^*_{n,j} + Q^{**}_{n,(N+1-j)} \tag{3.5}$$

$$w_{y,j} = \frac{1}{2\pi} \sum_{i=1}^{i=N} Q_{n,i} R_{wy,i,j} \tag{3.6}$$

The * indicates the term that is added to the flow when it has crossed the cylinder surface and is either within the cylinder or in the wake of the cylinder. The term indicated with ** is added to the flow in the wake of the actuator cylinder only. The influence matrices R_{wx} and R_{wy} relate the influence of every $i'th$ control point on control point j.[25] These influence matrices do not vary with time and are determined as:

$$R_{wx,i,j} = \frac{-\big(x_j + sin(\theta_i)\big) sin(\theta_i) + \big(y_j - cos(\theta_i)\big) cos(\theta_i)}{\big(x_j + sin(\theta_i)\big)^2 + \big(y_j - cos(\theta_i)\big)^2} \tag{3.7}$$

$$R_{wy,i,j} = \frac{-\big(x_j + sin(\theta_i)\big) cos(\theta_i) - \big(y_j - cos(\theta_i)\big) sin(\theta_i)}{\big(x_j + sin(\theta_i)\big)^2 + \big(y_j - cos(\theta_i)\big)^2} \tag{3.8}$$

Aerodynamic properties of the blades are extracted from 2D polars, created through the viscous panel method from Xfoil[13] corresponding to the average Reynolds number over a full rotation. For the prescribed surface loading cases these parameters are bypassed and the normalized cylinder normal, Q_n, load is directly controlled. Based off the flow field, pitch angles and polars, the normalized loadings can be determined.

$$\alpha = tan^{-1}\Big(\frac{V_n}{V_t}\Big) - \theta_p \tag{3.9}$$

$$C_n = C_l\ cos(\varphi) + C_d\ sin(\varphi) \tag{3.10}$$

$$C_t = C_l\ sin(\varphi) - C_d\ cos(\varphi) \tag{3.11}$$

$$F_n = \frac{1}{2}\rho\ c\ V_{rel}^2\ C_n \tag{3.12}$$

$$F_t = \frac{1}{2}\rho\ c\ V_{rel}^2\ C_t \tag{3.13}$$

$$Q_n = \frac{B\ F_n}{2\pi R\ \rho\ V_\infty^2} \tag{3.14}$$

$$Q_t = -\frac{B\ F_t}{2\pi R\ \rho\ V_\infty^2} \tag{3.15}$$

The described set-up contains the linear solutions of the equations and is sufficient for lightly loaded rotors. Including the non-linear equations allows one to more accurately determine heavily loaded rotors, as is often the case in this thesis. The modified linear (mod-lin) solution is implemented instead of the non-linear solution, since the mod-lin solution offers a good improvement on the linear solution without the large computational time penalty imposed by the non-linear case. This mod-lin method applies a correction factor, k_a based on the streamwise thrust coefficient from the linear solution, on to the perturbation velocities.[25] The induction factor, a, is derived from HAWT BEM theory and the Glauert correction, applicable when $a > 0.5$, together result in a polynomial that is only dependent on the streamwise thrust coefficient.

$$k_a = \frac{1}{1-a} \tag{3.16}$$

$$a = 0.0892074\ C_{T_x}^3 + 0.0544955\ C_{T_x}^2 + 0.251163\ C_{T_x} - 0.0017077 \tag{3.17}$$

$$C_{T_x} = \int_0^{2\pi} \big(Q_n(\theta)sin(\theta) + Q_t(\theta)cos(\theta)\big)d\theta \tag{3.18}$$

$$C_{T_y} = \int_0^{2\pi} \big(Q_n(\theta)cos(\theta) - Q_t(\theta)sin(\theta)\big)d\theta \tag{3.19}$$

The forces on the blades are a function of the velocity profile at the cylinder surface and the velocity profile is a function of the blade forces. The two must be iterated until convergence is reached. From the converged solution the power coefficients can be determined as:

$$C_{P_i} = \int_0^{2\pi} Q_n(\theta)\ V_n(\theta)d\theta \tag{3.20}$$

$$C_P = \int_0^{2\pi} -Q_t(\theta)\frac{\omega R}{V_\infty}d\theta \tag{3.21}$$

The computations performed for PitchVAWT were done in this matter, but bypassed the requirements of the pitch angles as input by directly controlling the angle of attack. This had great benefits to the computational time required, but at the cost that very large pitch rates can be obtained.

The computations with prescribed surface loading directly control Q_n and have the tangential loading Q_t set to zero. Therefore, C_n, F_n , α, V_x, V_y and V_{rel} are bypassed and can be dismissed during computations and C_t and F_t are set to zero. The prescribed surface loading cases require only one velocity; the cylinder normal velocity V_n, which is rewritten to:

$$V_n = V_\infty(1 + w_x)\ sin(\theta) - V_\infty\ w_y\ cos(\theta) \tag{3.22}$$

3.3 Optimization function

The optimization is performed through Matlab's built-in function fmincon.[32] The function is a minimization method, or maximization with the inclusion of a minus sign, and with proper constraining can be utilized as an optimization method. The function is applied with the 'interior-point' method to find suitable minima. The interior point method applies inititially Newton's optimization method and if this does not suffice, a conjugate gradient is applied to find a minimum.

Newton's optimization method requires a twice differentiable function in order to find a stationary point, where the first derivative is zero. For a single dimensional problem this would be performed by taking a Taylor series expansion around an initial point and setting the first derivative of the expansion to zero. For equations with higher dimensions the derivative is replaced with the Hessian of the set.

The conjugate gradient method aims to solve the standard equation of $Ax = b$, where both A and b are known for a set of conjugate vectors in x. The method is iterative, where each step the residual is reduced, requiring an amount of n iterations for an $n \times n$ matrix A. Matrix A includes the Hessian of the set of equations and vector b contains a zero vector $\pm$ a numerical tollerance.

When finding a stationary point, either method solves for the first derivative to be (near) all zeros. The Hessian in Newton's optimization method and in the conjugate gradient method varies for every vector of x. This causes a direct correlation between the selection of the method's starting point, x_0 also called initial guess, and the quality of the outcome.

Fmincon finds local optima and not necessarily the global optimum. This demands that the function must be iterated upon with variable inequality constraint(s) in order to obtain/approach the global optimum, even with a good initial guess. Each inequality constraint is set by taking a reference value of the parameter that is being optimized for, where each consequctive optimization has to improve on. Example: on maximizing C_P, where j indicates the number of iterations, then $C_{P_{ref}} - C_{P,j} < 0$ must be satisfied in order to iterate towards the global maximum.

Should an iteration be an improvement upon the reference case, then the outcome becomes the new reference value. By iterating fmincon with this sliding reference value, the function is forced to converge to better output each iteration and has improved chances of being at/near the global maximum.

To avoid negligible improvements on the iterations towards global maximum, the reference value is scaled up by 1.0025. This scaling value is large enough to benefit computational time, yet small enough to not noticeably harm the point of convergence of the output.

Finally, fmincon is capable of converging to stable points where the output is not an improvement on the reference value as demanded. During iterations, the varying parameter x, that corresponds to a successfully converged solution, is entered as x_0 for the next iteration. To prevent the solver from continuously converging to the same stable point, that is no longer an improvement towards the global maximum, the parameter x has to be adjusted before being entered as the new initial value for the subsequent optimization. The adjustment of the varying parameter is forced by a scaling of 3% of its previous value and a random percentage between $0 - 3$% that ensures that the output is uncorrelated to the very first value of x_0.

3.4 Optimization procedures

This section covers the optimization procedures to attain the final 2D results through the use of fmincon as explained in section 3.3. First the optimization procedure for the load control on the prescribed surface loading is described in section 3.4.1. This covers the applied assumptions and methodology that was used to obtain the largest power extraction for the evaluated thrust vectors and simultaneously attempts to minimize the average loading on the turbine and tries to minimize the total shed vorticity. The second optimization procedure is on the PitchVAWT optimizations, which are described in section 3.4.2. This section contains the description of the applied optimization method to find the limits of load control and evaluate a large selection of load vectors to compare results with the prescribed surface loading.

3.4.1 Prescribed surface loading cases

During the optimization for the prescribed surface loading cases, the normalized cylinder normal load, Q_n, is directly varied to observe the relation between power extraction and load on the cylinder. The process evaluates a range of thrust vectors over thrust angles from 0° to 75° in intermediate steps of 5°. For each thrust angle a maximum in power extraction is determined. Based on the thrust vector corresponding to the maximum power extraction, sub-vectors are created for which optimizations are performed. Due to the wider range of instantaneous load distributions from the corresponding assumptions, the maximization of power is followed by optimizations that minimize both the total shed vorticity and the average loading on the turbine to remove variance in outcome and to more consistently converge to a single result for every thrust vector. An overview of the optimization

process can be obtained by the flowchart in figure 3.2.

By directly prescribing the surface loading, a more general representation of the VAWT is obtained that does not include tip speed ratio nor stall angle in its computations. The absence of the tip speed ratio and stall angle in computations removes the difference in maximum achievable load between the windward and leeward sides of the turbine. It is therefore assumed that this VAWT representation can attain the same load profiles in windward and leeward orientation, which makes the analysis of the negative thrust angles redundant. The evaluated thrust angle range from 0° to 75° in intermediate steps of 5°. Further assumptions pose a limit to the streamwise thrust coefficient, which was set a to $C_{T_{x,lim}} = 0.9$, and no direct limitations were applied to thrust coefficient C_T.

The normalized cylinder normal loading, Q_n, is directly varied during optimization by six control points. These are evenly spaced over the circumference of the rotor, rather than being clustered. Clustering the control points allows large areas of constant loading with less control points than for an even distribution and thereby achieve large maximum power coefficients. When using clustered control points, these would be placed at azimuthal positions $\pm 90^\circ$ with respect to the thrust vector for the zero thrust angle case. However, it is unknown if this same relation would hold when the thrust vector is at an offset angle with the freestream and therefore clustered control points distributions are not applied. By applying an even spread in the control points the bias in performance towards certain thrust vectors over others is attempted to be kept minimal. The loading control points are positioned at $0^\circ, 60^\circ, 120^\circ, 180^\circ, 240^\circ$ and 300° azimuth. The values at the control points are interpolated, through a spline interpolation, over three revolutions. This creates a repeatable pattern over the second revolution being both continuous and smooth, including at $0^\circ/360^\circ$ azimuth.

The azimuthal spacing between the load control points impacts the azimuthal range over which the cylinder normal loading switches from cylinder outward to cylinder inward and vice versa. If the azimuthal range over which the loading changes direction with respect to the cylinder decreases, the numerical inaccuracy is expected rise, due to the larger gradient of loading. The amount of load control points that were evaluated range from six up to twenty-four control points.The influence of the amount of control points on the maximum power extraction is shown in figure 3.1a and their respective computational cost in figure 3.1b.

The results of the mesh test show that at fifteen control points the Betz limit is exceeded, but only by a bare minimum that does not noticably improve with the increase of control points. Compared to the applied six control points, a gain in maximum power extraction could be achieved by increasing the amount of control points to nine, but this nearly doubles the computational time. The focus within this thesis is on the relation between the ability to generate power and the thrust vector and not particularly obtaining the largest power extraction. The largest power extraction available at six control points is acceptably close to the Betz limit, where the benefits of the low computational time are used to evaluate more data points to be able to establish more accurately the relation between parameters.

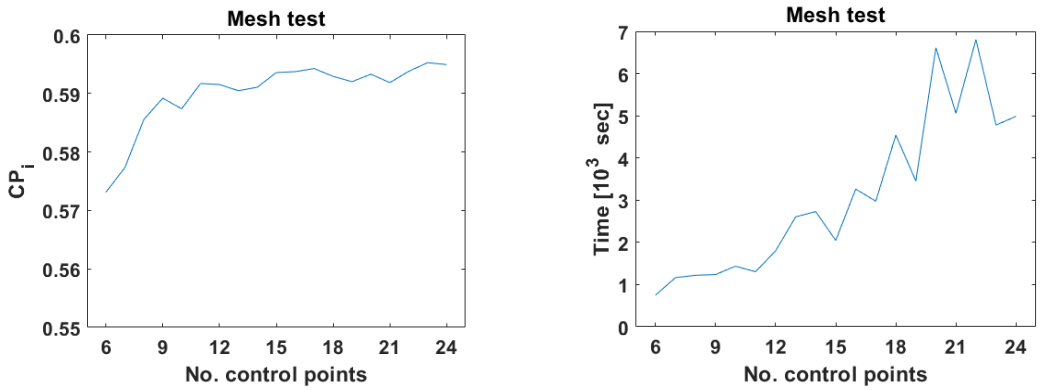

(a) Ability to generate power against number of load control points.

(b) Time required for a full optimization against number of load control points.

Figure 3.1: Influence of the amount of control point to interpolate the azimuthal load distribution over on the performance and computational time.

For every thrust vector the optimization process is executed by three separate optimizations:

The first optimization is the maximization of power extraction. This pushes performance to its limit, but does not apply strong limitations to the instantaneous load distribution. The outcome from just the maximization of power extraction often has load distributions containing several load peaks, where the peak values tend to be unnecessarily large, which can be observed from figure 3.3. Figure 3.3a was only subjected to the maximization of power and experiences large instantaneous loads and a larger total of load gradient than is necessary, while figure 3.3b was also optimized to minimize average load and minimize load gradient. Output as in figure 3.3b impose lesser limitations to the turbine design parameters in being able to achieve the surface loading than those of figure 3.3a would.

The minimization of the average amplitude of the instantaneous load distribution diminishes the peaks in the distribution to have only two remaining. Removing redundant peaks from the load distribution also avoids unnecessary increments in the total load gradient that comes from having multiple peak loads. The minimization of average amplitude does not limit the peak load values, which can still be large and therefore cause large vorticity shedding.

The third and final optimization minimizes the shedding of vorticity into the wake. The shedding of vorticity is not included in the time-averaged ACM, but still has to be taken into account to minimize the error by expanding the computations to non-time-averaged models. The minimization of azimuthal variation of load reduces the peak values of loading and aims to create a more even distribution on both the upwind and downwind halves of the rotor separately, as was applied by others to maximize the extraction of power.

During the maximization of power extraction for the largest vector magnitude on each thrust angle, a limitation was put on Q_n at the control points. This lim-

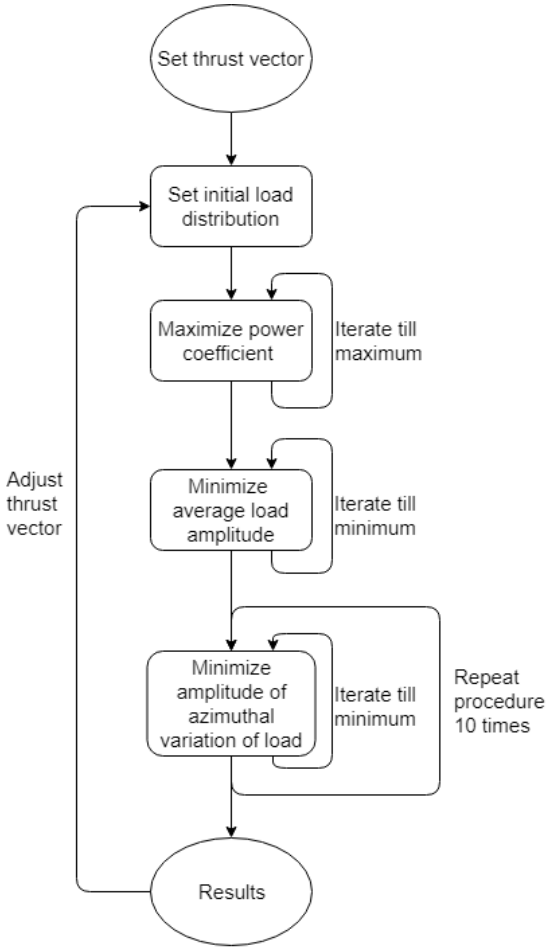

Figure 3.2: Flow chart for load optimization of prescribed surface loading cases.

itation is required to assure convergence of the output within the set amount of computations. The maximization of power extraction was performed for a range of potential $Q_{n_{lim}}$ from 0.1 to 1 in intermediate steps of 0.1. Let j indicate the evaluation number, ranging from 1 to 10, then $Q_{n_{lim}} = Q_{n,j}$ if the corresponding $\frac{C_{P_i,j+1}}{C_{P_i,j}} < 1.01$ for the first time. By setting a limit based of the relative performance rather than a fixed value, the smallest range of top performance is sacrificed for each thrust angle to ensure that load distributions consistently turn out like figure 3.3b and not as in figure 3.3a.

Each of the three optimizations is forced to optimize until it fails to improve upon previous results, 20 times. No limitations were set on the amount successful improvements, since the amplification factor on the reference value, described in section 3.3, ignores negligible improvements that could cause infinite loops. Finally, although fmincon is a fine optimization tool, the amount of potential distributions the solver could convergence to is so large that three sets of at least 20 optimizations attempts each is still no guarantee that output is satisfying. To kill some of the variance in output, the third optimization is performed ten times where only the best result is accepted.

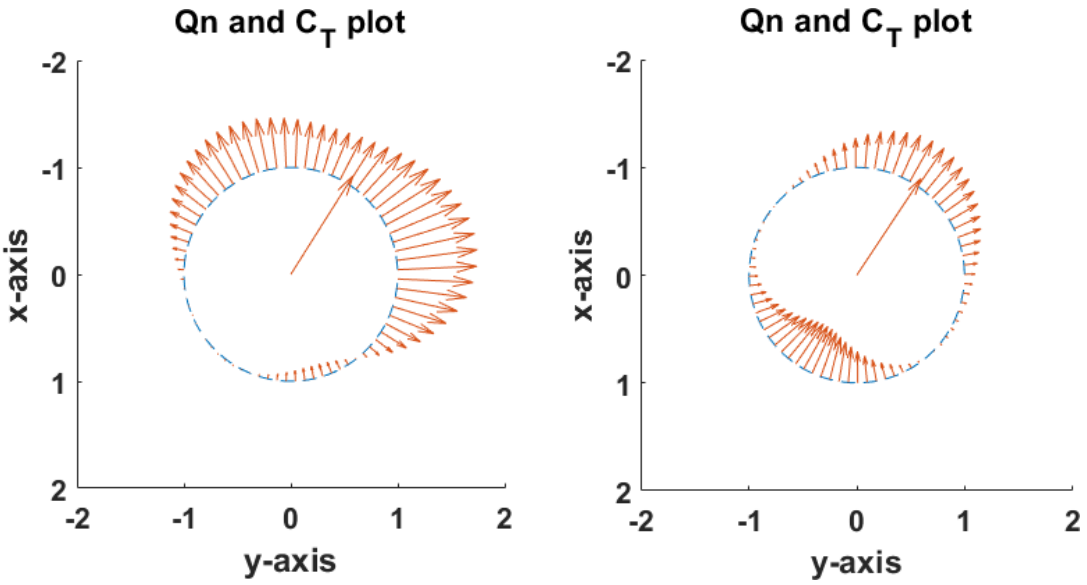

(a) Example of loading with more than two peaks and large average loading.

(b) Example of loading with only two peaks and a small average loading.

Figure 3.3: Examples of bad (a) and good (b) load distributions for thrust angle $\approx 33°$, $C_{T_x} = 0.89$. Freestream in positive x direction, length units in radii, Q_n and C_T values are visualized 1:1 as the load experienced by the flow.

3.4.2 PitchVAWT cases

The optimization procedures for PitchVAWT were performed for two purposes; obtain the relation of power generation with load control for four different cases of integrated load control and to compare the behavior of integrated and instantaneous load to the cases with prescribed surface loading. The maxima of integrated load control are defined as: maximizing the thrust angle for both windward and leeward direction, minimization of streamwise thrust coefficient and minimizing the thrust coefficient.

To establish the relation between power generation and load control, a series of power coefficients is selected for which the respective load control is maximized, which will be elaborated on in section 3.4.2.1. The maxima of the thrust angle in both positive and negative directions span the limits of the thrust angles for which thrust vectors can be generated. Initial computations on the maximization of load control showed that the maximization of thrust angle can also be performed through the maximization of C_{T_y} in the corresponding direction and yielded over 7 decimals the exact same results in every outcome.

Within the range of potential thrust angles, from the maximization of thrust angle, a series of thrust vectors are created for which the instantaneous and integrated loads are compared to those of the prescribed surface loading cases. The optimization procedure for these thrust vectors is similar to those of the maxima of load control and the differences between the methods are highlighted in section 3.4.2.2.

The optimization process for PitchVAWT comes with more numerical challenges than for the prescribed surface loading optimization, since the varying parameter has a wider range of values and the amount of load control points are increased from 6 to 72. Optimization was performed through direct variation of the angle of attack, where an angle of attack limit is imposed that is lesser than the static stall angle. The pitch rate was considered a turbine specific parameter and therefore left unbound. The combination of the increased amount of potential numerical entries and no additional constraint via the pitch rate, raise the need for good initial load distribution, x_0, to let each optimization start from. The absence of direct and indirect constraints on the load distribution causes the outcome to be the upper limit for the $2D$ PitchVAWT design parameters in the absence of (dynamic) stall.

The PitchVAWT design specifications are defined as per table 3.1. Operational average Reynolds number has been selected at $2 \cdot 10^6$.

Table 3.1: PitchVAWT design specifications[27]

Nr. Blades	2
Height	1.5m
Diameter	1.5m
Chord	0.075m
Solidity	0.1
Blade Airfoil	NACA0021

3.4.2.1 Evaluating integrated load control

The relation of load control and power generation is established by creating a series of power coefficient for which the respective form of load control is maximized. A simplified overview of the maximization process can be observed from the flowchart in figure 3.4a. The first step within this process is to establish the maximum power coefficient for the specified operation conditions. From the established maximum value of C_P, power generation can be sacrificed to further maximize integrated load control. For obtaining the maximum power coefficient and all other optimizations it holds that in order to obtain values that are consistently at/near the maximum, the solver must be given a good initial distribution of the angle of attack to start its evaluations from. The initial distribution was referred to, in section 3.3, as x_0, within this section it will be named after the optimization parameter; $\alpha_{x,0}$.

The initial angle of attack distribution, $\alpha_{x,0}$, for obtaining the maximum power generation was created through the principle that the sum of the local maxima cannot be too far off the overall maximum. This principle iterates between the loading and the flow field, where each iteration of equation 3.23 is maximized for every control point. The inflow angle φ is a constant and an interpolation over the lift and drag polars can be applied to obtain the local optimal angle of attack. For the PitchVAWT design parameters, this method obtains power coefficients that only deviate 5% or less from the fully optimized maximum power coefficient up to

tip speed ratio of 3.7. Beyond a TSR of 3.7 the loading starts to negatively affect power generation, but it can still be applied up to a tip speed ratio of 4.

$$C_L \; sin(\varphi) - C_D \; cos(\varphi) \tag{3.23}$$

With the optimization's starting point known, the solver is forced to iterate upon itself to improve until a maximum value is reached for the power coefficient, as is described in section 3.3. Based off the maximum power coefficient, a sub-set of power coefficients, $C_{P,subset}$, is defined for which maximum load control is evaluated. The sub-set of power coefficients that are evaluated on maximum load control are presented in equation 3.1 and computations are executed in that sequence.

Each C_P value of the sub-set requires their own $\alpha_{x,0}$, but these cannot be generated through the same method as was applied for maximum power generation. Instead, each evaluation point of $C_{P,subset}$ uses the final angle of attack distribution from the previous computation, which is adjusted until the power coefficient drops to the required value. The power coefficient is decreased iteratively by applying a weighting function, K, that rates all 72 control points on their contribution to the respective load control via the resultant aerodynamic load vector and the potential power that can be generated and alters the angle of attack of the worst performing control point by 0.1 for the better.

The potential power generation is rated through the inflow angle, since this angle determines how efficient the lift force can contribute to the torque. This is favorable over assessing the local contribution to power generation, since inefficient large loading can have the same power generation as efficient lightly loaded regions.

The resultant aerodynamic load vector is evaluated by its magnitude and the angle between the freestream and the resultant force as experienced by the flow. Due to the four different load optimizations, the influence of the resultant load vector varies per optimization; equation 3.24, K_1, applies to maximizing C_{T_y} for thrust vectoring in windward direction, equation 3.25, K_2, includes a minus sign with respect to K_1 to maximize C_{T_y} for leeward thrust vectoring and equation 3.26, K_3, takes the absolute value of the cosine function for minimization of the (streamwise) thrust coefficient.

The angle between the freestream and the resultant force, as experienced by the flow, is determined by three angles; the azimuthal position, θ, the inflow angle, φ and ε, the angle between lift and the resultant force. The 'C' term within the cosine indicates a correction to the equation, being either 0 or π. From azimuthal angles $180°$ to $360°$ the loading corresponding to positive torque has become cylinder inward, instead of cylinder outward. This requires an additional π within the cosine to keep the mathematics correct. In the case of local power addition to the flow, regardless of azimuthal angle, π must also be added to the cosine term. The angle between lift and resultant force, ε, also experienced varying influence between cylinder outward and cylinder inward loading, but the definition in equation 3.30 ensures the correct sign convention on these regions.

$$K_1 = |\frac{\varphi}{\varphi_{max}}| \cdot cos\Big(\theta - \varphi + \epsilon + C\Big) \cdot \frac{F_{res,w}}{F_{res,w,max}} \tag{3.24}$$

$$K_2 = |\frac{\varphi}{\varphi_{max}}| \cdot -cos\Big(\theta - \varphi + \epsilon + C\Big) \cdot \frac{F_{res,w}}{F_{res,w,max}} \tag{3.25}$$

$$K_3 = |\frac{\varphi}{\varphi_{max}}| \cdot |cos\Big(\theta - \varphi + \epsilon + C\Big)| \cdot \frac{F_{res,w}}{F_{res,w,max}} \tag{3.26}$$

where,

$$K_x = \begin{cases} x = 1, & \text{for maximizing } C_{T_y} \\ x = 2, & \text{for maximizing } -C_{T_y} \\ x = 3, & \text{for minimizing } C_{T_x} \text{ and } C_T \end{cases} \tag{3.27}$$

$$C = \begin{cases} 0, & \text{if} \quad 0^\circ \leqslant \theta \leqslant 180^\circ \text{ and } C_P(\theta) \geqslant 0 \\ \pi, & \text{if} \quad 0^\circ \leqslant \theta \leqslant 180^\circ \text{ and } C_P(\theta) \leqslant 0 \\ \pi, & \text{if } 180^\circ \leqslant \theta \leqslant 360^\circ \text{ and } C_P(\theta) \geqslant 0 \\ 0, & \text{if } 180^\circ \leqslant \theta \leqslant 360^\circ \text{ and } C_P(\theta) \leqslant 0 \end{cases} \tag{3.28}$$

$$F_{res_w} = \sqrt{L^2 + D^2} \tag{3.29}$$

$$\varepsilon = arccos\Big(\frac{L}{L^2 + D^2}\Big) \tag{3.30}$$

$$\tag{3.31}$$

Each of the four load optimizations experiences the same procedure, where the only difference is the parameter that is being optimized. The maximization of the power coefficient and the maximization of load control for all values of $C_{P,subset}$ are performed by means of fmincon from section 3.3. The results corresponding to the first $\alpha_{x,0}$ of each data point become the first reference value that following optimizations have to improve on. Each of the load optimizations is performed where 20 failed optimization attempts must be completed before the solver may proceed to the next data point without limitations to the amount of successful optimizations.

Contrary to the load optimizations of the cases with prescribed surface loading, the PitchVAWT computations frequently do not generate results. Data generation is enhanced by checking the output after 15 failed attempts and should no results be obtained, the reference value is reduced and the optimization procedure restarted. This type of failure is allowed to occur twice, after which no output is recorded. The solver generally requires several successful improvements where the reference value is improved upon in order to be near the global optimum, but these are not always subsequent. The fail-safe check is set at 75% of the required runs to ensure that the required amount successful optimization attempts can be performed, even when the first successful run is obtained after a large amount of failed optimization attempts.

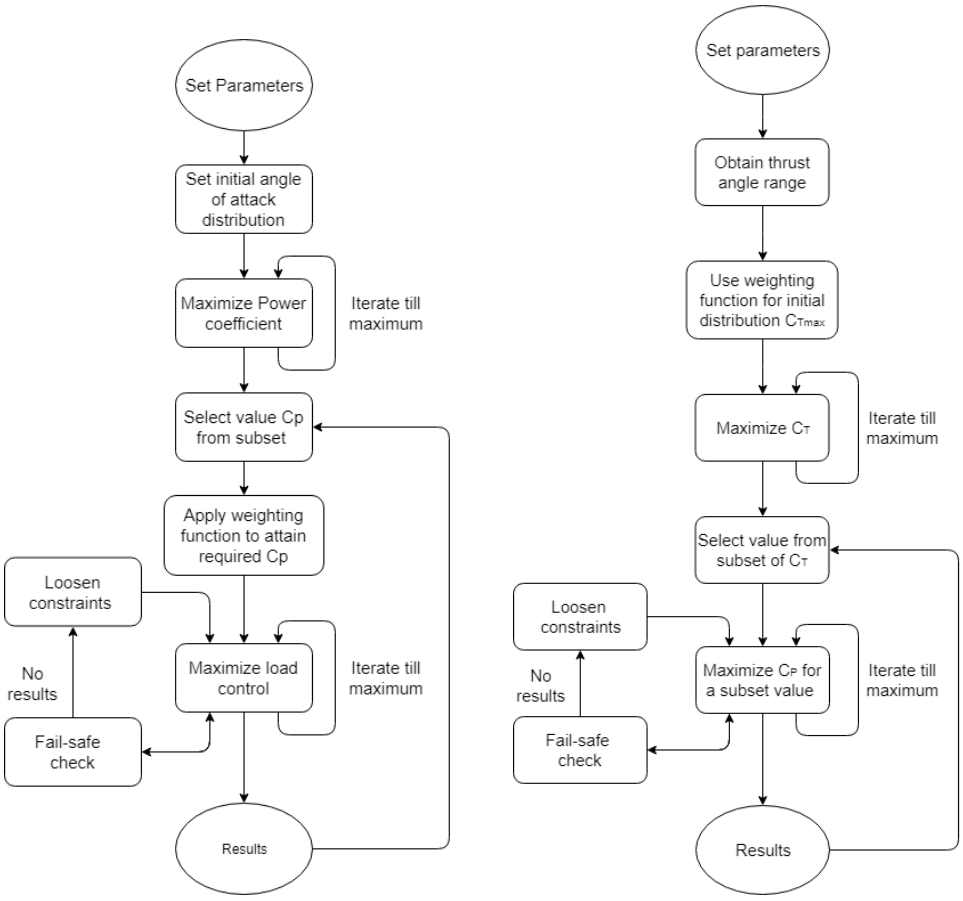

(a) Flow chart for load control maximization for set power coefficients.

(b) Flow chart for load optimization per power coefficient.

Figure 3.4: Flowcharts of the two optimization procedures regarding PitchVAWT

3.4.2.2 Thrust vector evaluations

The thrust vector evaluations were performed to also span the entire range of thrust vectors that are obtainable for the PitchVAWT turbine for several tip speed ratios. The maxima in thrust angle were extracted from the computations on integrated load control evaluations from section 3.4.2.1 and set the span of thrust angles for which thrust vectors were analyzed. Thrust angles were evaluated with 5° spacing between evaluation angles. For each thrust angle the maximum streamwise thrust coefficient was determined. The process for the thrust vector evaluations is quite similar to process of maximizing integrated load control, hence the description on the thrust vector evaluations will not be as elaborate. The flowchart of the thrust vector evaluations can be observed in figure 3.4b.

The computations on the range of thrust vectors are also prone to not create results and an initial entry distribution of $\alpha_{x,0}$ must be carefully selected to enhance the possibility of outcome. Similar to the load control evaluations, a weighting function had to be applied which forces the thrust angle to match the value for which computations are performed. The iterative process between the weighting function, load reduction and performance evaluation starts by setting all angles of

attack at the imposed limit angle, where all loads are directed to extract energy from the flow. The ACM determines the thrust angle based on this initial load function and depending on if the thrust angle needs to increased or reduced to match the thrust angle that is computed, equation 3.24 or equation 3.25 is applied. These weighting functions determine which load control point causes the largest deviation to the current thrust angle and this control point has its angle of attack altered by 0.1 for the better. The new angle of attack distribution is evaluated and altered until its thrust angle corresponds to the value for which computations are intended to be executed. Once the initial angle of attack distribution is obtained, fmincon is applied to find the largest thrust coefficient the turbine can attain.

The data points within a single thrust angle are set by reducing the maximum thrust coefficient by a fixed stepsize until it approaches zero. The $\alpha_{x,0}$ for each of these reduced thrust vectors can be linearly scaled from the final load distribution of the maximum thrust coefficient for the respective thrust angle. For each of the thrust coefficients, that are less than maximum for the respective thrust angle, the power coefficient is maximized by means of fmincon.

The optimizations through fmincon are forced to supply 20 failed attempts at improving on the reference value for either C_T or C_P, depending on which parameter is being maximized. Similar to the load control evaluations the regularly no output can be generated within the set amount of minimum computations, so the same fail-safe mechanism is applied. After 15 failed optimization attempts the output is checked and should no results be obtained, the reference value that must be improved on is reduced and the optimization process for that specific control point is restarted. In the event that the fail-safe mechanism should be applied for the third time, the optimization process is halted for that data point and no output is recorded.

Chapter 4

Results and Discussion

This chapter contains the results to answer the proposed research questions. In section 4.2 the results of the prescribed surface loading cases are presented. Integrated results are presented in section 4.2.1, which focuses on the relation between power extraction against streamwise thrust and the variation of loading with thrust vectoring. In section 4.2.2 the instantaneous loading is evaluated where potential relations with the instantaneous loading with variation in thrust vectors are examined. Section 4.2.2 covers analysis for the PitchVAWT on integrated performance and addresses the variations between the PitchVAWT results and those for the prescribed surface loading cases. Similarly, in section 4.3.2 the instantaneous loading of PitchVAWT is analyzed and compared to the prescribed surface loading cases.

4.1 Preliminary discussion

The results presented in this chapter are generated through the $2D$ time-averaged actuator cylinder model. The VAWT is highly unsteady and applying a steady model representation causes an error in predicting reality.

When computing the $2D$ load distributions in $3D$, the trailing vortices will cause a loss in blade load and therefore also a loss in power extraction compared to the $2D$ results. The trailing vortices are positioned at locations with a spanwise variation in bound vortex strength, which will be mainly at the blade tips. The losses from the trailing vortices are depending on the bound vortex strength, which is apparent when representing the blade by a single horseshoe vortex. For turbines without specified design parameters the streamwise thrust coefficients at maximum power extraction have almost negligible differences between all thrust angles. This means that with increasing thrust angle, the average bound vortex strength increases and therefore the losses caused by trailing vortices increase with increasing thrust angle under constant streamwise thrust.

The linear actuator cylinder model is limited in computing large thrust angles, since the linear model propagates flow speed increments/reductions (the terms that are only added in the wake of the turbine) with the freestream, rather than along the streamlines. Appendix D shows some of the flow fields around the VAWT generated through the linear ACM. In figure D.1a the upwind half of the rotor, 0° to 180° azimuth, only extracts energy, since the load is directed against the wind. Figures D.1b and D.1c have local regions on the upwind half of the rotor where power is added to the flow, since loading is directed along with the wind.

On the downwind half of rotor in the linear wake of the upwind power addition, the streamwise velocity is larger than the freestream velocity. Some of the streamlines that go through this downwind region correspond to locations on the upwind half where power is extracted from the flow. Since the power in the flow scales with the velocity cubed, the linear ACM causes an error in overall power generation that increases with the thrust angle. The linear ACM is expected to be viable in the lower range of the evaluated thrust angles, but it is not yet known which thrust angle value is the upper limit for this statement. Therefore, instantaneous results are only presented for thrust angles up to $45°$.

4.2 Prescribed surface loading

This section contains the results of the cases that only contain prescribed surface loading. All load distributions were created without a representation of a wing, which removes limits imposed through tip speed ratio or solidity, etc. The integrated performance, C_{P_i}, C_{T_x} and such, are presented in section 4.2.1 and the instantaneous results are presented in section 4.2.2 .

4.2.1 Integrated performance

The actuator cylinder model with direct control of the cylinder surface load has been applied over a series of thrust vectors over thrust angles ranging from $0°$ to $75°$. For each thrust angle the power extraction was maximized and the corresponding thrust coefficient was the largest evaluated for that specific thrust angle. Each maximum thrust vector forms the basis for the sub-series of thrust vectors that are analyzed.

The power extraction of all the analyzed thrust vectors is presented against the streamwise thrust coefficient in figure 4.1. The results of the ACM are plotted against the performance of the actuator disk to compare the VAWT's ability to extract energy. The VAWT extracts less energy than the actuator disk, since turbine is modeled by six control point over which loading is interpolated. The influence that the amount of set control points has on the potential maximum of power extraction is presented in section 3.4.1. Increasing the number of control points allows for more complex load distributions and with sufficient control points the VAWT can extract more energy than the actuator disk. The increased computational cost was deemed too much and focus was applied to increasing the data points to more accurately obtain relations between parameters.

The results from figure 4.1 show that, without a limit to the maximum surface loading, the turbine's power extraction is directly related to the streamwise thrust coefficient. There exist deviations to this trend, but those are generally small and are to be expected on computational optimizations. The peak power extraction coefficients for all evaluated thrust angles are highlighted through figure 4.2. The largest power extraction occurs at a $5°$ thrust angle. In absence of a wing representation, the largest possible power extraction is expected to occur at at $0°$ thrust angle. The deviation in angle and the difference in C_{P_i} are not that large and can be considered within the accuracy of the solver.

The difference between power extraction at $5°$ thrust angle and $75°$ thrust angle is only a 1.6% loss of power extraction. Since the variation in power extraction and streamwise thrust with thrust angle are small, the $C_{P_i} - C_{T_x}$ curve is not a suitable method to compare variation in results.

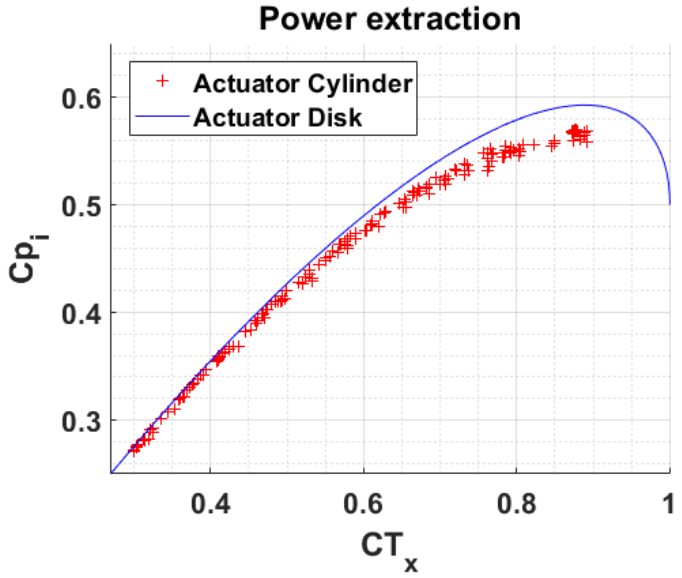

Figure 4.1: Power extraction against streamwise thrust coefficient of the ACM with actuator disk theory as reference.

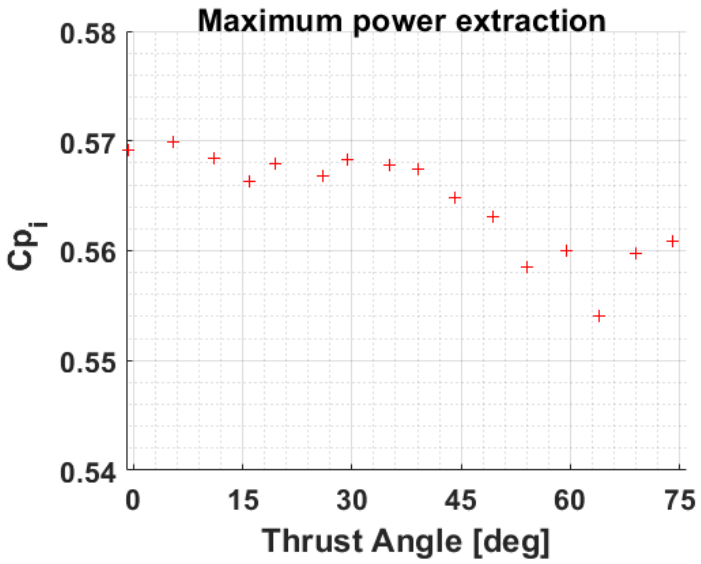

Figure 4.2: Peak power extraction coefficient per thrust angle.

The performance of the turbine, in absence of torque, is no longer evaluated through the streamwise thrust coefficient, but rather through the normalized surface load, Q_n. The normalized surface load is evaluated on peak amplitude and average amplitude, since the ability to execute a load distribution on a real turbine will depend on these two values. Maximum load amplitudes for all thrust vectors are presented in figure 4.3a and show volatile behavior with variations in either thrust angle and power extraction. It was observed that some load distributions were centered around large peak loading combined with regions that were minimally loaded. Some examples of these cases are displayed in figure 4.4c. The evaluation of maximum amplitude of Q_n is important, but the results are fluctuating too much to make a good comparison and indicate that more emphasis should be applied to ensure most loading is on the upwind half of the rotor and the large peak loading is reduced.

The average amplitude of the load distribution from figure 4.3 shows a more even variation with thrust vectoring. On the range of thrust angles from 0° up to 25° the largest power extraction was slightly larger than is achieved at thrust angle 30°. This larger power extraction is only possible by increasing the loading on regions that do not extract energy efficiently. Although the average loading increases with thrust angle for fixed power extraction, the variation of average load amplitude appears nearly invariant near $C_{P_i} \approx 0.57$ due to the slightly larger power extraction on the smaller thrust angles.

At the largest values of power extraction, variation of of the average surface load amplitude is strongly dependent on the value of the power extraction. Evaluating the relations between parameters is executed near $C_{P_i} = 0.5$, since the interpolation between data points at this value of power extraction will be negligibly affected by the results at the largest values of power extraction. From figure 4.3 it can be seen that in the vicinity of $C_{P_i} = 0.5$ the average load amplitude does not vary greatly up to thrust angles of 30° with the exception of the poor results generated at 25° thrust angle.

Tables 4.1 and 4.2 highlight the influence of increasing the thrust angle on the performance in the vicinity of the 30° thrust angle, which appears to be the angle after which performance degrades rapidly under constant average loading, as seen in figure 4.3b. In table 4.1 the average amplitude of the load distribution is kept constant and the loss in power extraction is presented. These results show that the VAWT can extract energy at a 35° thrust angle and only lose 7.6% of its energy extracting potential, compared to the zero thrust angle case for the same average surface load amplitude. According to the power law for HAWTs[11] from equation 2.1 with the most favorable exponent of $x = 1.88$, the loss in power extraction for a HAWT at 35° yaw angle would be 31.3%. However, the losses for the HAWT are computed in $3D$, while the presented loss for the VAWT is in $2D$.

A similar comparison is presented in table 4.2, where the power extraction coefficient is kept constant and the required increment in average amplitude of surface load distribution is evaluated. From this table is observed that at a thrust angle of 30° an increment of only 7.4% in average load amplitude is required. At

a $35°$ thrust angle the required increase in average loading is nearly double the increment required at $30°$ thrust angle. Increasing the thrust angle further than $35°$, the average load amplitude rises more rapidly, indicating that thrust angles up to $30°$ can be obtained with little increased loading, where the turbine design parameters will determine the thrust angle limit that a turbine can achieve.

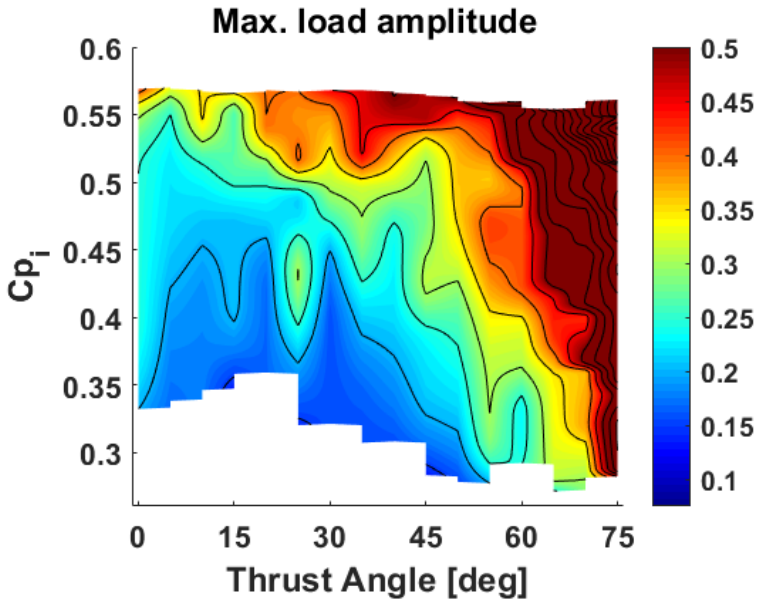

(a) Mapping of the maximum amplitudes of the normalized surface loading Q_n.

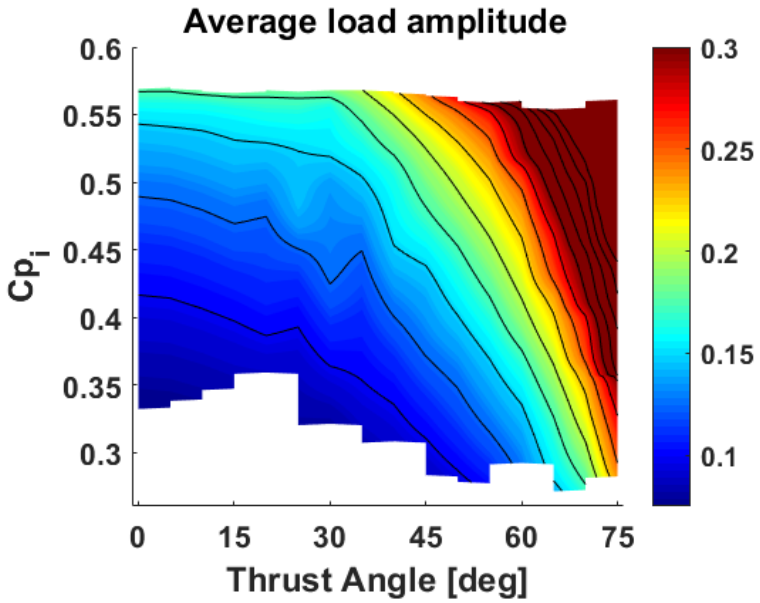

(b) Mapping of average amplitude of the normalized surface loading Q_n.

Figure 4.3: Power extraction against integrated load parameters for all evaluated thrust angles.

Table 4.1: Effect of increasing thrust angle on power extraction under a constant average load amplitude.

Thrust angle	C_{P_i}	Power loss
$0°$	0.500	$-$
$20°$	0.487	2.6%
$30°$	0.470	6.0%
$35°$	0.462	7.6%

Table 4.2: Effect of increasing thrust angle on the average load amplitude under a constant power extraction.

Thrust angle	Average load amplitude	Average load amplitude increase
$0°$	0.130	$-$
$20°$	0.136	4.4%
$30°$	0.140	7.4%
$35°$	0.148	13.9%

4.2.2 Instantaneous performance

This section covers some of the load distributions that are generated and assesses them on the instantaneous scale. The integrated results from section 4.2.1 shown that the model can attain nearly the same $C_P - C_{T_x}$ relation over the full range of thrust angles from $0°$ up to $75°$. The results in this section will only display instantaneous loading for thrust angles up to $45°$, as discussed in section 4.1.

A selection of load distributions are presented in figure 4.4. For readability purpose several load distributions have been left out, as these overlapped too much with others. The full set of load distributions ranging over thrust angles $0°$ to $45°$ can be further examined in appendix A. The vertical lines in these figures represent the locations where on the upwind and downwind halves of the rotor the peak loading is expected to occur. The expected peak loading for the zero thrust angle will be at $90°$ and $270°$ azimuth, since the cylinder normal velocity will naturally be greatest at these azimuthal positions. With the deflection of the thrust vector, the positions of peak loading are expected to deflect with the thrust angle, until a critical thrust angle.

The results for the zero thrust angle in figure 4.4a show for all five load cases close to symmetric loading about their expected peak load azimuthal angle for both the upwind and downwind halves of the rotor. Results further show a good relation between the upwind and downwind load peaks and their expected azimuthal angle of occurance up to a maximum thrust angle of $30°$. For thrust angles above $30°$, peak loading occurs near $60°$ and $240°$ azimuth, e.g. figure 4.4d. Not all distributions abide by these loading guidelines, figure 4.4b shows good examples of such deviations.

The linear actuator cylinder model is capable of adding a ”zero load” to its surface loading, which varies the instantaneous loading, but does not alter the integral parameters. In an attempt to filter out any ”zero loads”, the entire cylinder surface loading was projected onto a single plane. This was executed for a plane that is normal to the freestream and a plane that is normal to the thrust vector. Each plane is positioned through the axis of rotation and is either normal the freestream or normal to the thrust vector. On both planes the positive direction coincides with positive y coordinates when at zero thrust angle.

Projection onto the plane normal to the freestream considered cylinder surface loading positive if the instantaneous load vector has a component directed against the freestream. This projection method results in large fluctuations in peak load location and are highly unsymmetrical, see figure 4.6, with the exception at $0°$, $5°$ and $10°$ thrust angle. No conclusive relation could be established for the load projections on the plane normal to the freestream and therefore no further results on this are presented.

Within figure 4.5 the load cases are displayed where the surface loading is projected on a plane that is positioned normal to the thrust vector. Loading projected onto the plane is considered positive if the instantaneous load vector has a positive interior product with the thrust vector. This is similar to creating a yawed actuator disk, but the presented loading is not the load normal to the plane, but the value that is normal to the cylinder. Overall, the peaks in loading are positioned closely to the center of the disk, with the exception of cases that contain large azimuthal areas of near constant loading, as in figure 4.5c. The results show that the majority of the projected loads appear symmetric around the disk’s center at first glance, but can have distinctive imbalanced loading on either side of the projection surface for a single thrust angle.

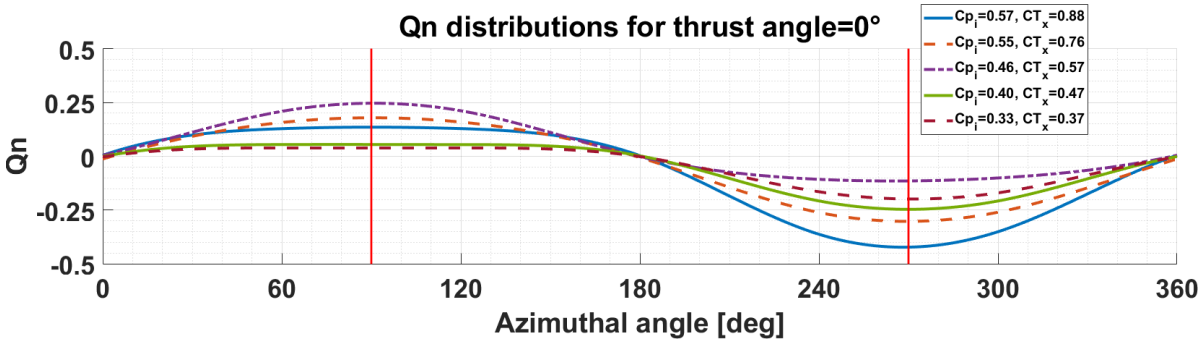

(a)

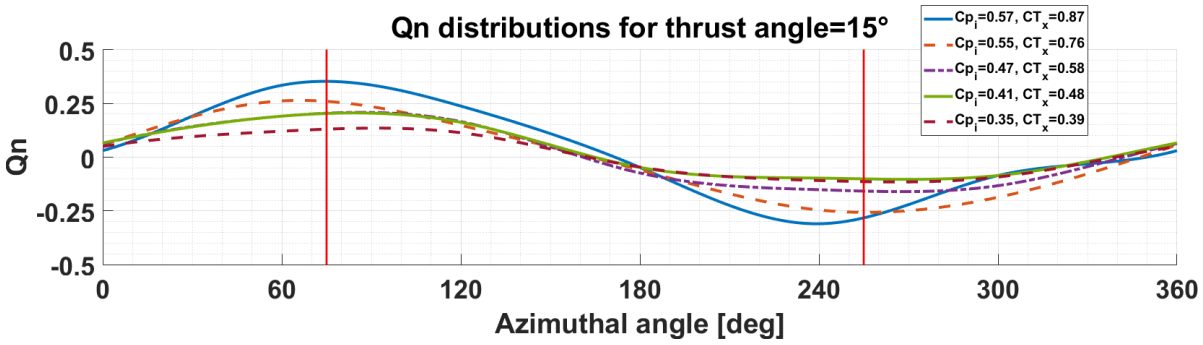

(b)

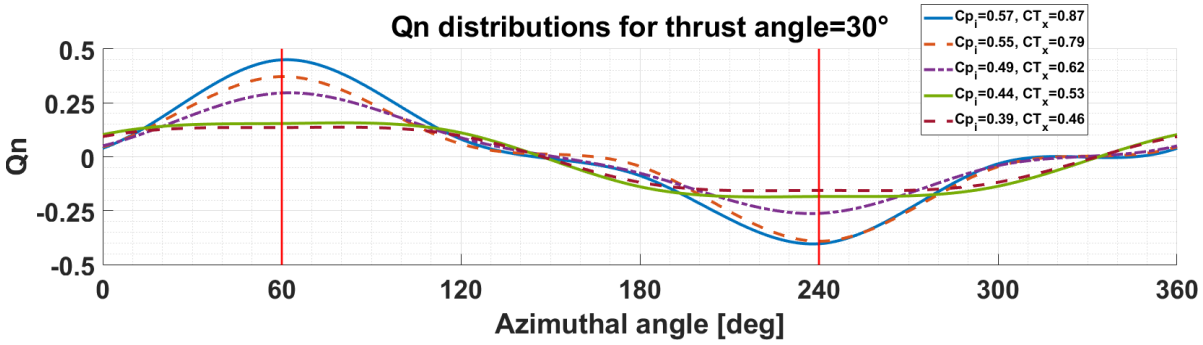

(c)

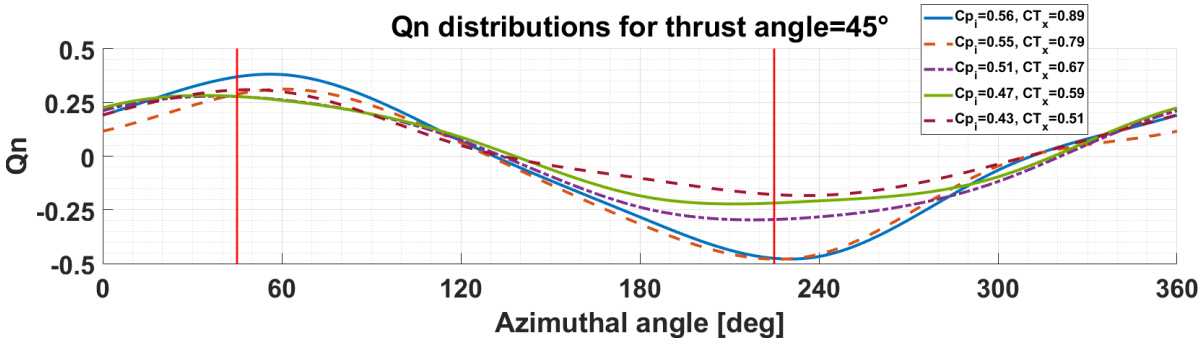

(d)

Figure 4.4: Distributions of the normalized surface load Qn over a full revolution for thrust angles of $0°$ (a), $15°$ (b), $30°$ (c) and $45°$ (d). Vertical line indicates expected peak load location, corrected for thrust vectoring angle.

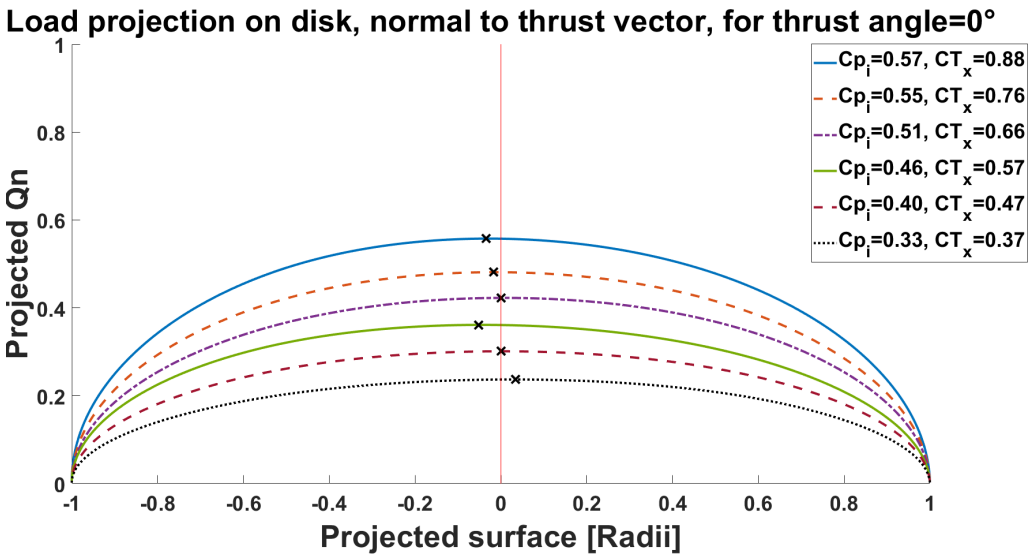
Load projection on disk, normal to thrust vector, for thrust angle=0°
Cpi=0.57, CTx=0.88
Cpi=0.55, CTx=0.76
Cpi=0.51, CTx=0.66
Cpi=0.46, CTx=0.57
Cpi=0.40, CTx=0.47
Cpi=0.33, CTx=0.37
Projected Qn
Projected surface [Radii]

(a)

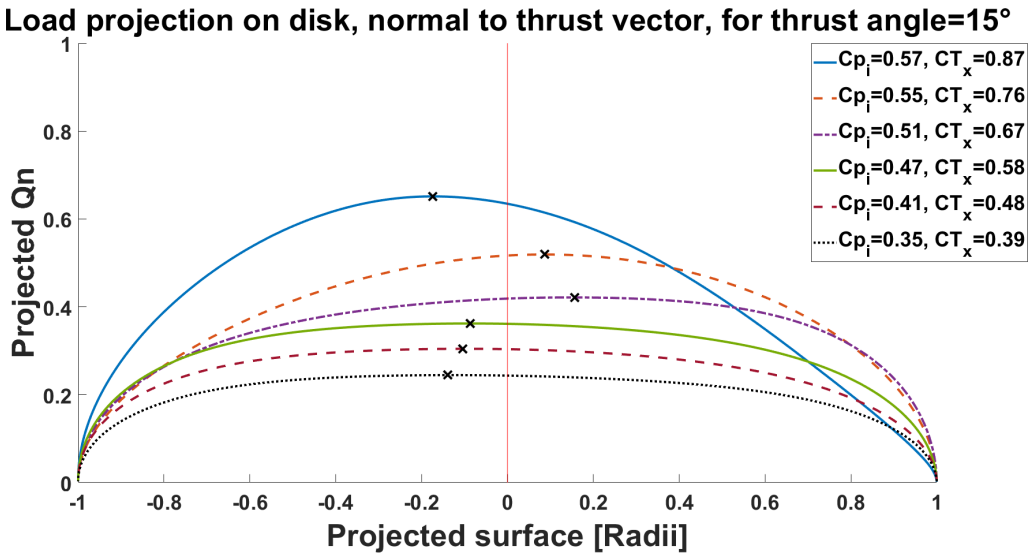
Load projection on disk, normal to thrust vector, for thrust angle=15°
Cpi=0.57, CTx=0.87
Cpi=0.55, CTx=0.76
Cpi=0.51, CTx=0.67
Cpi=0.47, CTx=0.58
Cpi=0.41, CTx=0.48
Cpi=0.35, CTx=0.39
Projected Qn
Projected surface [Radii]

(b)

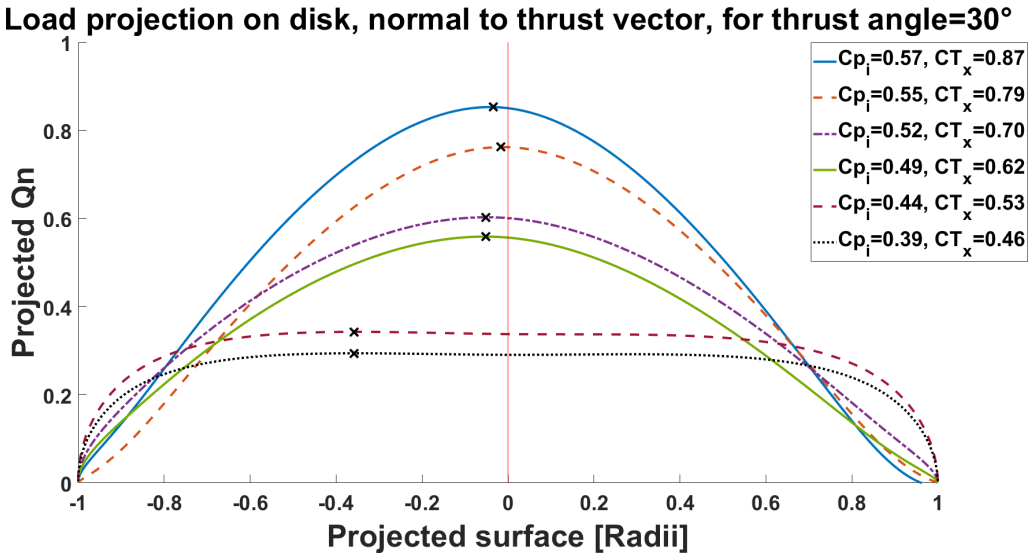
Load projection on disk, normal to thrust vector, for thrust angle=30°
Cpi=0.57, CTx=0.87
Cpi=0.55, CTx=0.79
Cpi=0.52, CTx=0.70
Cpi=0.49, CTx=0.62
Cpi=0.44, CTx=0.53
Cpi=0.39, CTx=0.46
Projected Qn
Projected surface [Radii]

(c)

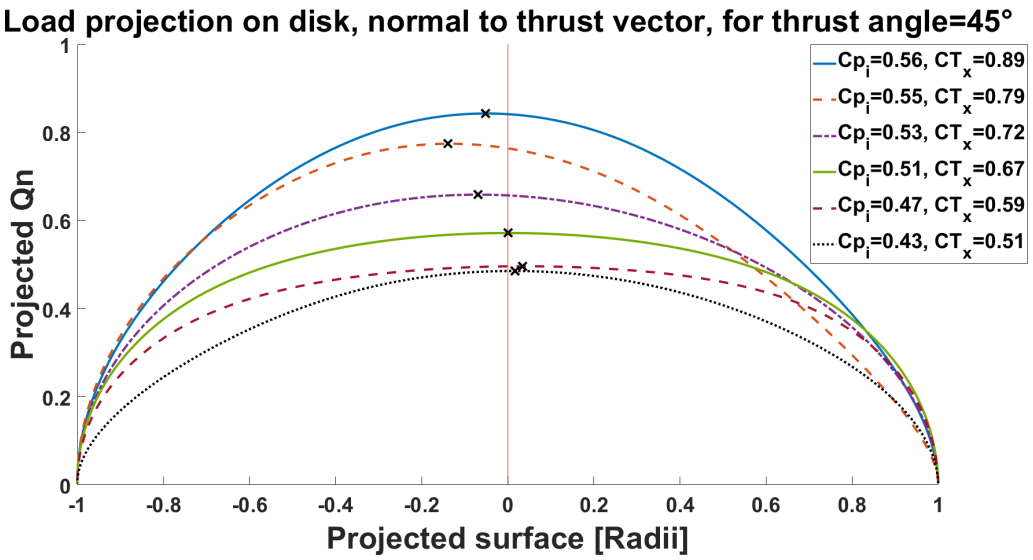

(d)

Figure 4.5: Distributions of the normalized surface load Qn, projected onto a single plane that is normal to the thrust vector, for thrust angles of $0°$ (a), $15°$ (b), $30°$ (c) and $45°$ (d). Vertical line indicates expected peak load location, the black cross indicates the actual peak of loading.

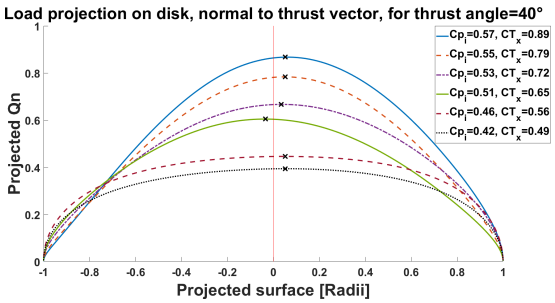

(a) Projection of the normalized surface loading, Q_n, on a plane normal to the thrust vector.

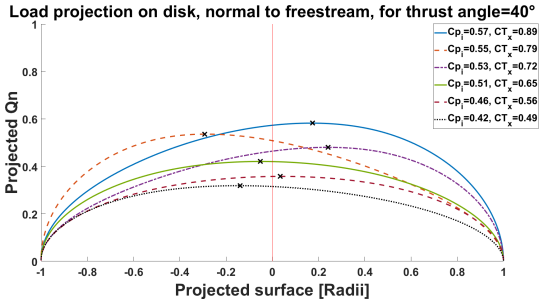

(b) Projection of the normalized surface loading, Q_n, on a plane normal to the freestream.

Figure 4.6: Comparison between two load projection methods to filter out 'zero loads'.

4.3 PitchVAWT

This section covers the results generated for the PitchVAWT turbine, whose design specifications are described in table 3.1. The first comparison between the prescribed surface loading cases and the PitchVAWT results is performed on integrated performance and presented in section 4.3.1, followed by the comparison on instantaneous parameters in section 4.3.2. The PitchVAWT's performance on maximizing load control on the integrated parameters, where the thrust coefficient and streamwise thrust coefficient are minimized and the thrust is maximized in both positive and negative direction for a series of power coefficients is presented in section 4.3.3.

4.3.1 Integrated performance

The integrated power extraction and generation are presented in figure 4.7 against the streamwise thrust coefficient. The power extraction from figure 4.7a shows that the PitchVAWT turbine can exceed the Betz limit, while cases with prescribed surface loading could not. This is a consequence of the selected amount of independent load control points; the prescribed surface loading cases has only six load control points, while the PitchVAWT has 72. The increment in load control points allows more complex load distributions and therefore can capture more power from the flow.

The VAWT can be treated as two energy extraction planes by splitting the cylinder at the locations where loading changes from cylinder inward to cylinder outward and vice versa. Simplyfying this configuration to two tandem actuator disks was proven by Newman[36] to have a limit larger than the Betz limit, but this ignores all loading components normal to the freestream. It is therefore considered that the VAWT can exceed the Betz limit, but by how much remains unknown. The largest power extraction for PitchVAWT was at $C_{P_i} = 0.6087$ which exceeds the Betz limit, but is still closer to the Betz limit than the limit by Newman and is therefore deemed as acceptable in $2D$ computations.

Figure 4.7b shows the power generation and the gap in power generation compared to figure 4.7a due to drag. The peak C_P per streamwise thrust coefficient display a nearly linear shift with respect to the results from figure 4.7a, but the power generation displays a wider spread in results than for power extraction. The wider spreading of results in figure 4.7b over the $C_P - C_{T_x}$ plane indicates the existence of cases with inefficient conversion of power extraction to power generation.

In figure 4.8 the turbine's performance is presented at each thrust angle's largest power extraction obtained. It can be observed that there is a variation in power extraction between windward thrust vectoring and leeward thrust vectoring, but for $-30^\circ \leq \psi \leq 30^\circ$ the relative losses are in the order of 1%. The efficiency of the PitchVAWT shows that thrust vectoring in leeward direction causes a loss in efficiency, which increases almost linearly with increasing leeward thrust angle. Figure 4.8b further shows that applying a thrust angle in windward direction

is more efficient than the zero thrust angle case, while the power extracted from the flow is approximately the same.

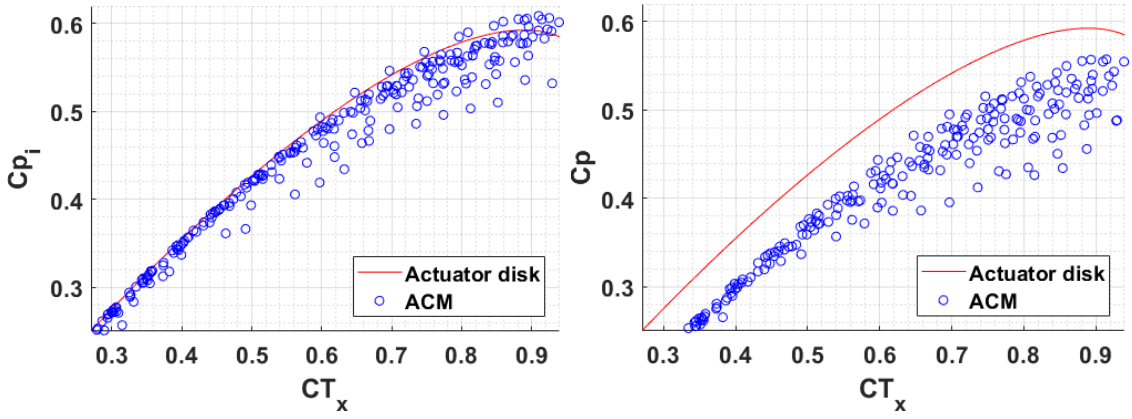

(a) (b)

Figure 4.7: Streamwise thrust coefficient against power extraction (a) and power generation (b) for $TSR = 4$ and thrust angles $-47.5°$ to $47.5°$.

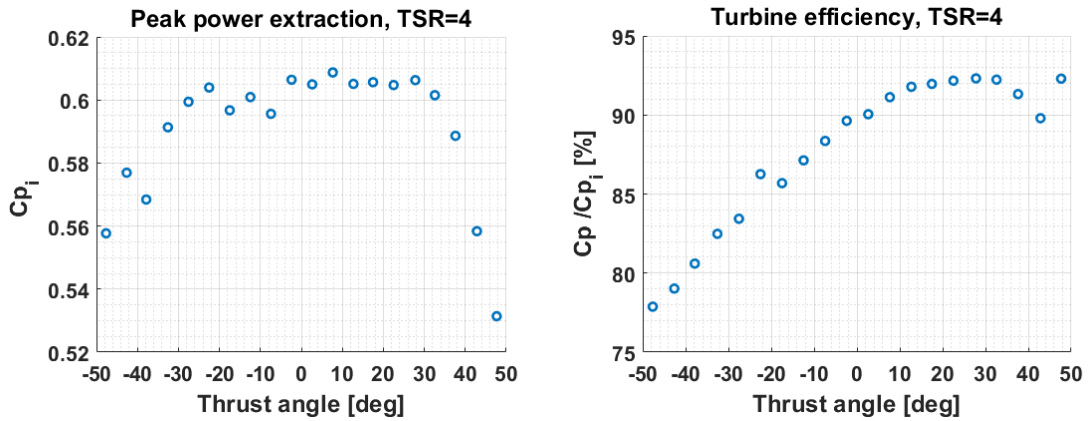

(a) Max. power extraction per thrust angle. (b) Turbine efficiency at peak C_{P_i} .

Figure 4.8: Peak power extraction and respective efficiency of PitchVAWT for $TSR = 4$ and thrust angles $-47.5°$ to $47.5°$.

The computations for PitchVAWT were performed over tip speed ratios from 1.5 to 4 with intermediate step sizes of 0.5, however, the results of TSRs 1.5, 2 and 2.5 were only within the linear region of the $C_P - C_{T_x}$ curve of the prescribed surface loading results and therefore are not presented. The evaluation of load through peak amplitude values and average amplitude are comparable to those of the prescribed surface loading cases in figure 4.9 for peak loads and in figure 4.10 for the average amplitude of loading.

The peak loading for PitchVAWT shows to have a more even variation with varying thrust vectors than the results with prescribed surface loading, however it also shows that peak values of PitchVAWT are clearly larger than the prescribed

surface loading cases. The load distributions show that the applied optimizer to the PitchVAWT model does not generate evenly distributed loadings as in figure 4.4a, but rather concentrates the peak loading near 0° azimuth. At this windward region the largest velocity occurs and through the perturbation velocities the inflow angle is increased to allow for a large power generation. This computational advantage is most clearly visible at thrust angles of 5° near $C_{P_i} = 0.47$ for all tip speed ratios. Unfortunately, due to the large variations per thrust vector of the prescribed surface loading cases, the comparison with PitchVAWT is only qualitative on peak load amplitude.

The average amplitude of the normalized surfacel load, Q_n, is presented in figure 4.10, where only the thrust vectoring in windward direction is presented of the PitchVAWT results. The variation in power extraction between windward and leeward directed thrust vectors is practically negligible and therefore, the leeward power extraction will not be displayed. The three different TSRs show that for a fixed position on the $C_{P_i} - \psi$ plane the average loading amplitude generally increases with increasing tip speed ratio.

A turbine's ability to extract power from the flow is purely dependent on the normalized surface loading and the velocity profile on the turbine, but the variation in results is caused by the influence of the normalized tangential loading. The resultant force vector of all normalized tangential loading has a typical value around 7% of the thrust coefficient, at large power extraction values, but can have an offset angle with the thrust vector over 70° in either direction. The influence of the tangential loading varies per thrust vector and per tip speed ratio, but reduces as the power extraction lessens, down to ~ 2% of the thrust vector around $C_{P_i} = 0.2$.

All results of PitchVAWT from figure 4.10 show steep rise in average load amplitude with thrust vectoring near the largest power extraction values of each thrust angle. In these areas the cylinder surface loading has reached its peak values for the azimuthal angles that can extract power efficiently. The power extraction can then still increase, but only slightly at the cost of relatively large average load increments. This is best observed in figure 4.10c on any thrust angle, where the average amplitude rapidly increases from ≈ 0.17 to ≈ 0.27.

Similar to the results of the cases with prescribed surface loading, the influence of thrust vectoring under either constant power extraction or constant average load are examined. At $TSR = 4$ and $C_{P_i} = 0.5$ the thrust angle can be increased from 0° to 32.5° under constant power extraction and only requires a 6.6% increase in average load amplitude. Performing the evaluation of constant average load amplitude with the same starting condition, the thrust angle can be increased from 0° to 32.5° and the loss in power extraction is only 6.7%. These results are close to the outcome of the prescribed surface loading cases from tables 4.1 and 4.2.

The same analysis for $TSR = 3.5$ yields greater variations. At $TSR = 3.5$ and $C_{P_i} = 0.5$ the increment in average load under constant power extraction is 22.6% when increasing the thrust angle from 0° to 32.5°. Under constant average load

amplitude, starting at $C_{P_i} = 0.5$ the increment in thrust angle from $0°$ to $32.5°$ the loss in power extraction is 15.3%. Results indicate that at $TSR = 4$ the normalized forces can be large enough to have a fair resemblance with the results with prescribed surface loading.

The presented results mainly focus on the power extraction, as this is comparable to the outcome of the results generated through prescribing the surface load. The mapping of power generation has been performed and is displayed in appendix C.

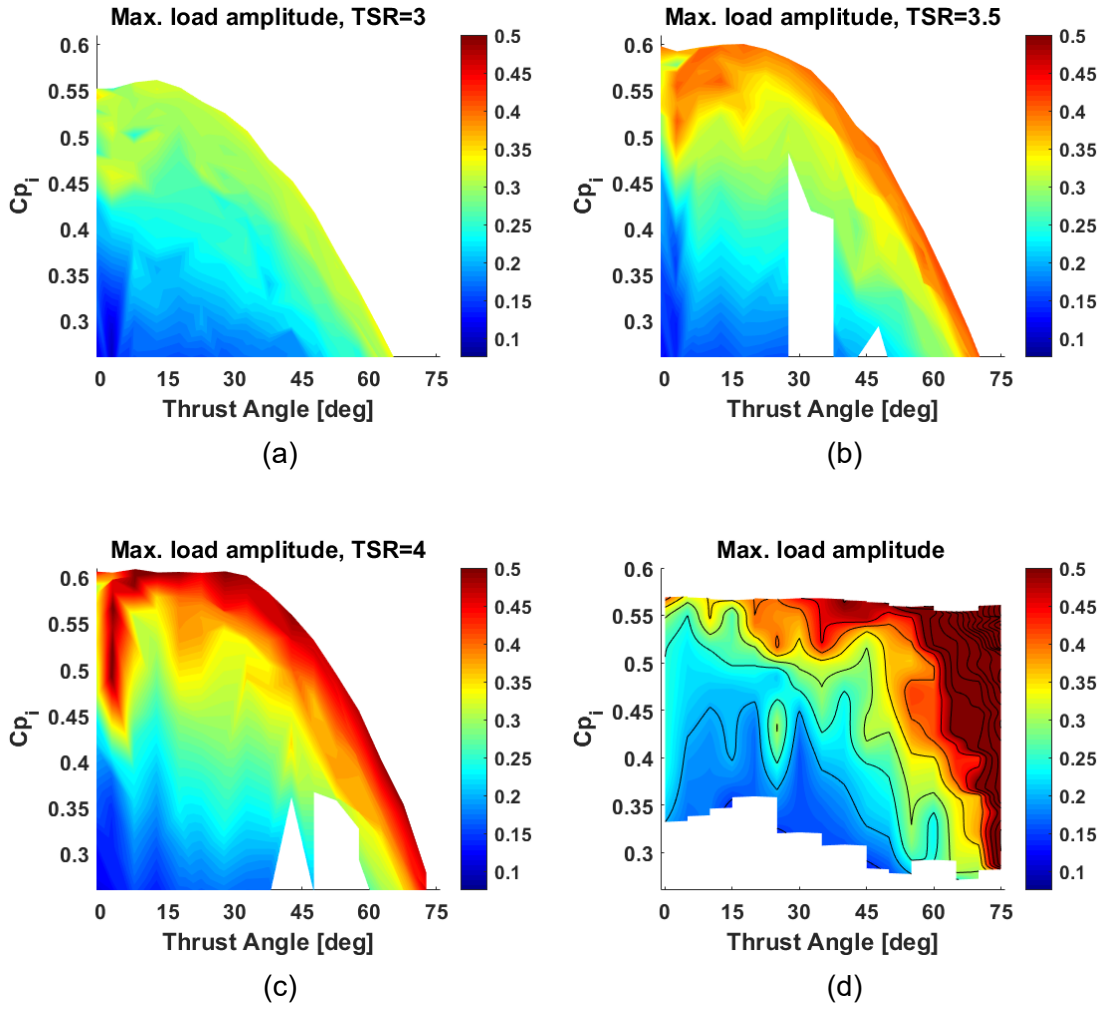

Figure 4.9: Comparison between peak surface load amplitude for the prescribed surface loading (d) and three tips speed ratios on PitchVAWT at an average Re. nr $2 \cdot 10^6$.

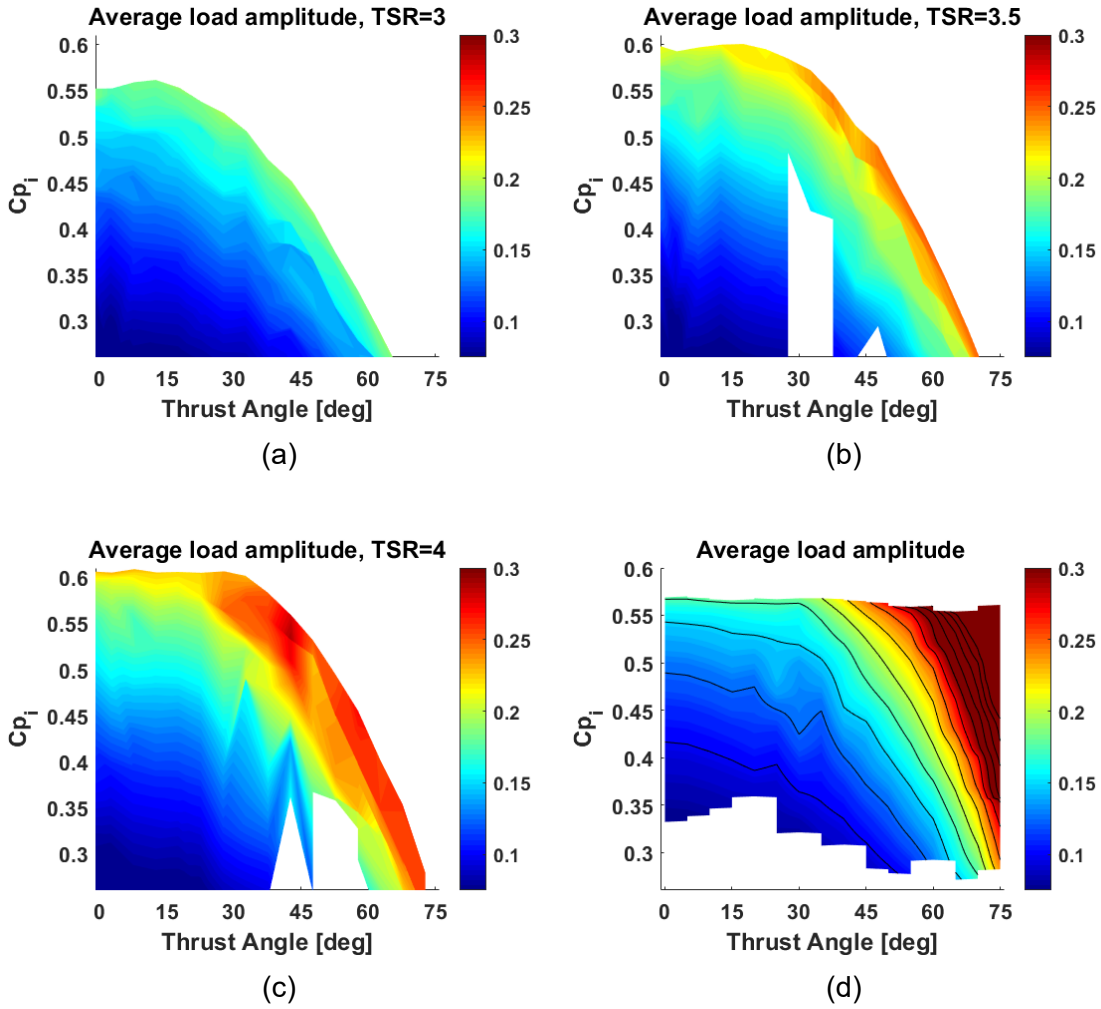

Figure 4.10: Comparison between absolute average surface loading for the prescribed surface loading (d) and three tips speed ratios on PitchVAWT at an average Re. nr $2 \cdot 10^6$.

4.3.2 Instantaneous loading

Results of the integral parameters indicated that at $TSR = 4$ the results are most coherent with the prescribed surface loading results, which is therefore the tip speed ratio that will be examined more thoroughly. The instantaneous loading for comparable thrust angles to the prescribed surface loading results is presented in figure 4.11. The first thing to note is that under zero thrust angle all loading appears to consist of large constant regions on both the upwind and downwind halves of the rotor. The solver systematically obtained small variations over the constant areas to be advantageous over pure constant areas and for the small thrust angles the region near 0° azimuth is highly loaded due to the largest velocity over the blades with non-trivial inflow angle due to the perturbation velocities.

When ignoring load spikes in the region near 0° azimuth, there exists no clear peak in load amplitude for the zero thrust angle case at either half of the rotor for any of the load distributions. This is in line with the results of the prescribed surface load results for power extraction below maximum, but for $C_{P_i} > 0.5$ results of the two methods deviate from another. This is believed to be a consequence of the set amount of load control points for the prescribed surface loading cases. PitchVAWT computations have 72 load control points and can therefore achieve more complex load distributions, which can extract more power from the flow.

The results from the prescribed surface loading cases showed that the load distributions experience a shift in azimuthal angle closely related to the thrust angle. Results for the PitchVAWT turbine show that this shift of the load distribution is not a near linear relation to the thrust angle and the shift in azimuthal angle is performed only for thrust angle above 16°. Smaller thrust angles have their loading mostly altered by varying the upwind half of the rotor, where loading in the windward region is increased and loading in the leeward region is decreased compared to zero thrust angle. On thrust angles larger than 28° the cylinder inward loaded region is altered in the same way; in the windward region the loading is intensified, while in the leeward side the loading is lessened.

The load distributions for the prescribed surface loading could be projected onto a single plane normal to the thrust vector. These projected distributions generally peaked at the center of the plane with roughly symmetrical behavior around the peak value. Performing the same projection for the results of PitchVAWT, see figure 4.12, indicates that the PitchVAWT results do not abide by this relation, aside from the small variations in the load distribution caused by the large amount of load control points. The zero thrust angle shows that the projected loading on the plane is generally constant. The other thrust angles only show that the projected loading increases over the plane up to a critical point.

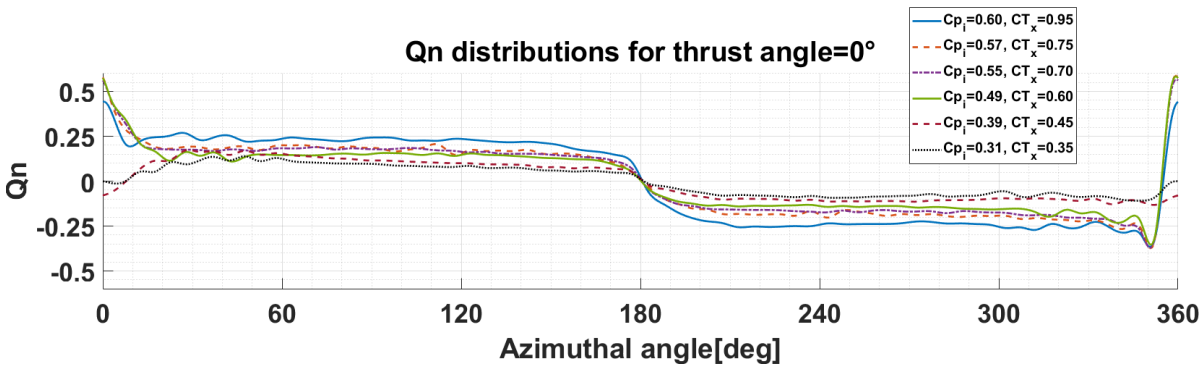

(a)

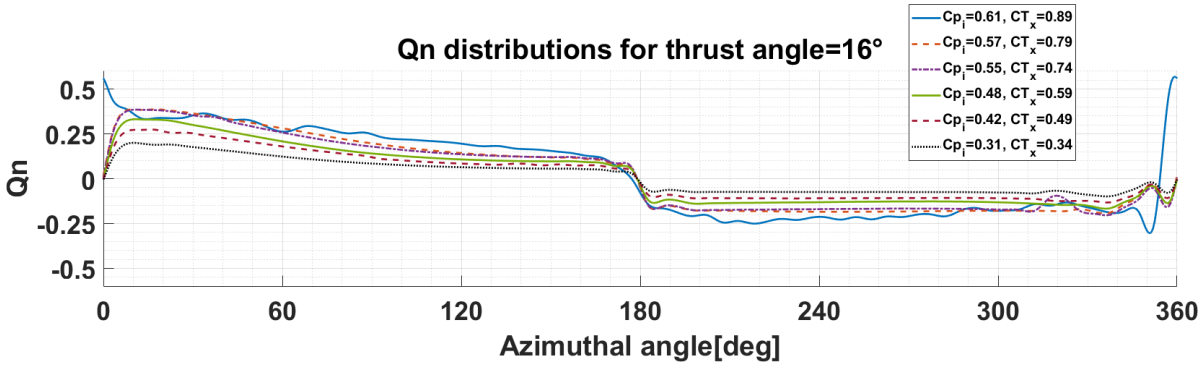

(b)

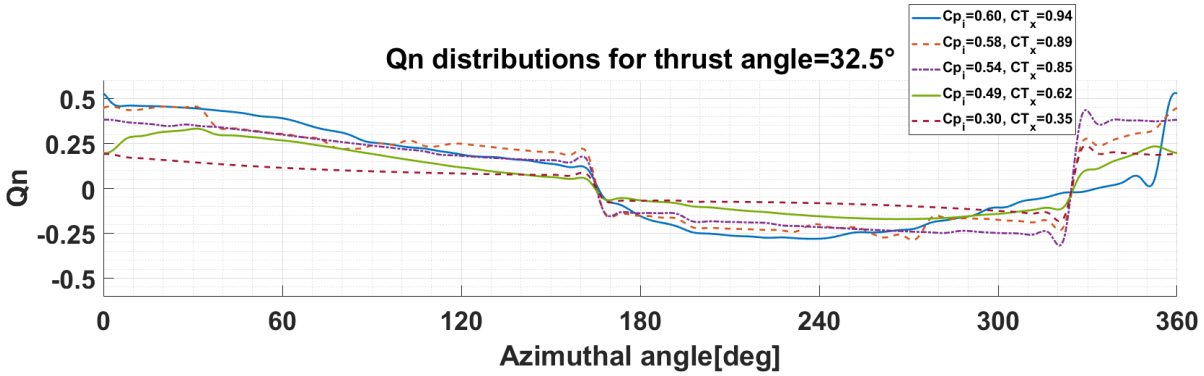

(c)

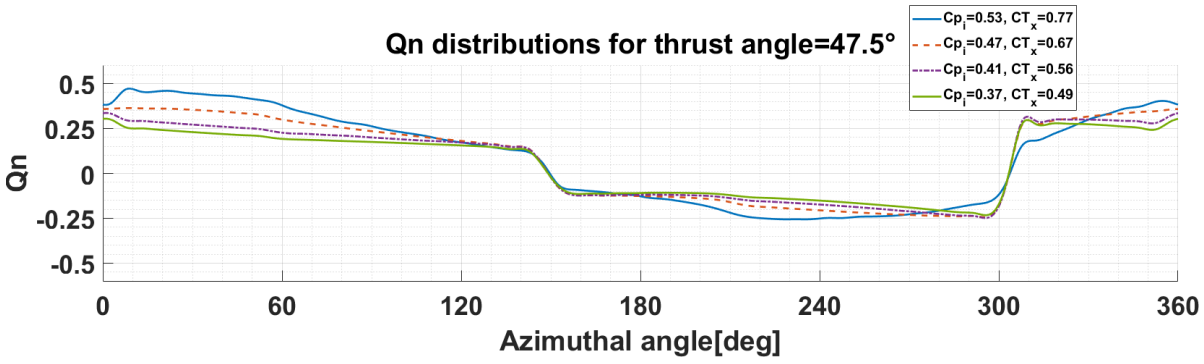

(d)

Figure 4.11: Distributions of the normalized cylinder surface load Qn over a full revolution for thrust angles of $0°$ (a), $15°$ (b), $30°$ (c) and $45°$ (d). $TSR = 4$.

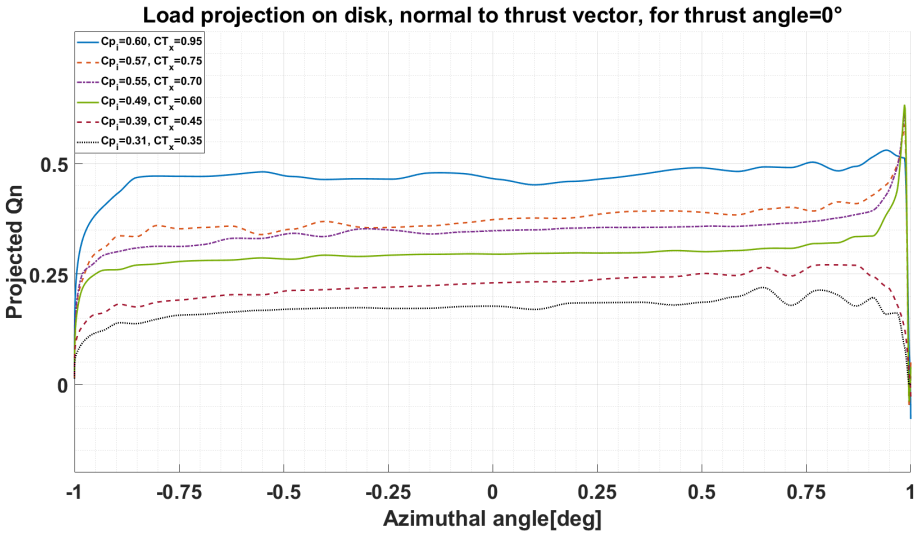
Load projection on disk, normal to thrust vector, for thrust angle=0°
Cp_l=0.60, CT_x=0.95
Cp_l=0.57, CT_x=0.75
Cp_l=0.55, CT_x=0.70
Cp_l=0.49, CT_x=0.60
Cp_l=0.39, CT_x=0.45
Cp_l=0.31, CT_x=0.35
Projected Qn
0.5
0.25
0
-1
-0.75
-0.5
-0.25
0
0.25
0.5
0.75
1
Azimuthal angle[deg]

(a)

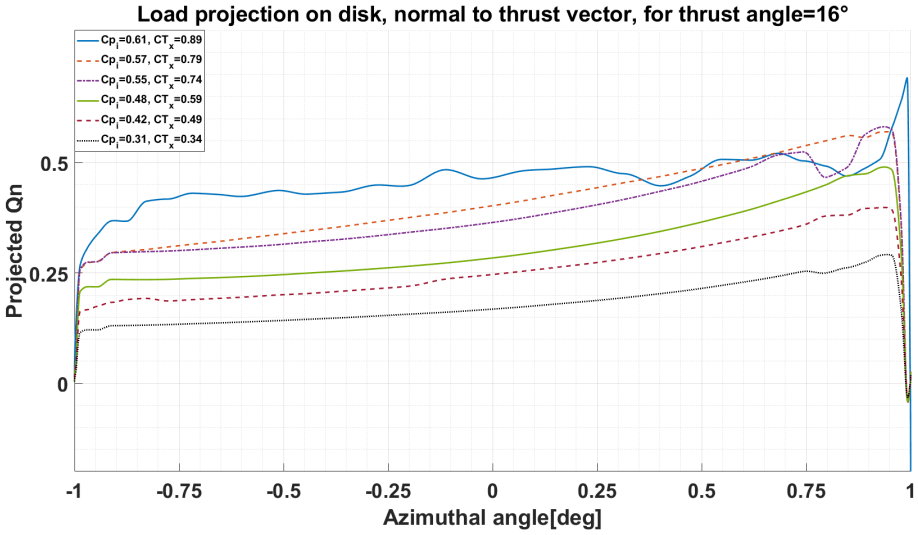
Load projection on disk, normal to thrust vector, for thrust angle=16°
Cp_l=0.61, CT_x=0.89
Cp_l=0.57, CT_x=0.79
Cp_l=0.55, CT_x=0.74
Cp_l=0.48, CT_x=0.59
Cp_l=0.42, CT_x=0.49
Cp_l=0.31, CT_x=0.34
Projected Qn
0.5
0.25
0
-1
-0.75
-0.5
-0.25
0
0.25
0.5
0.75
1
Azimuthal angle[deg]

(b)

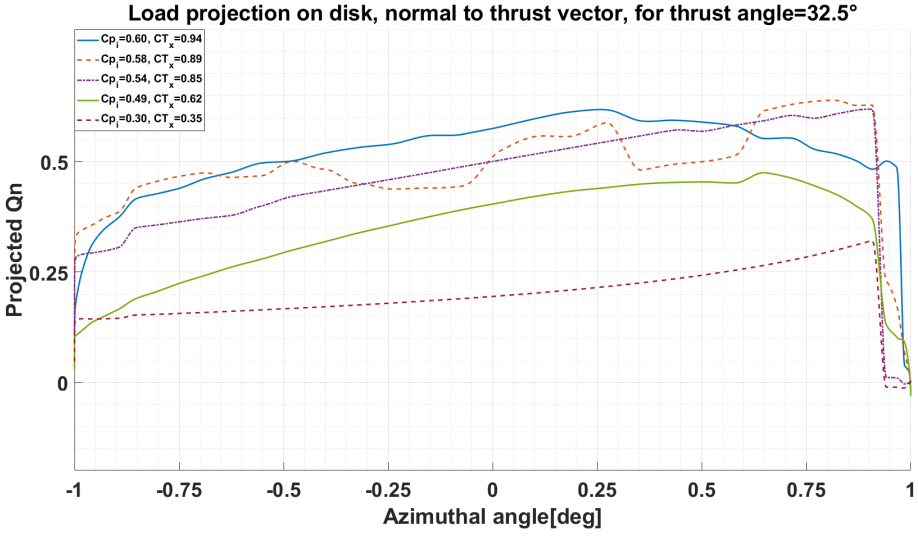
Load projection on disk, normal to thrust vector, for thrust angle=32.5°
Cp_l=0.60, CT_x=0.94
Cp_l=0.58, CT_x=0.89
Cp_l=0.54, CT_x=0.85
Cp_l=0.49, CT_x=0.62
Cp_l=0.30, CT_x=0.35
Projected Qn
0.5
0.25
0
-1
-0.75
-0.5
-0.25
0
0.25
0.5
0.75
1
Azimuthal angle[deg]

(c)

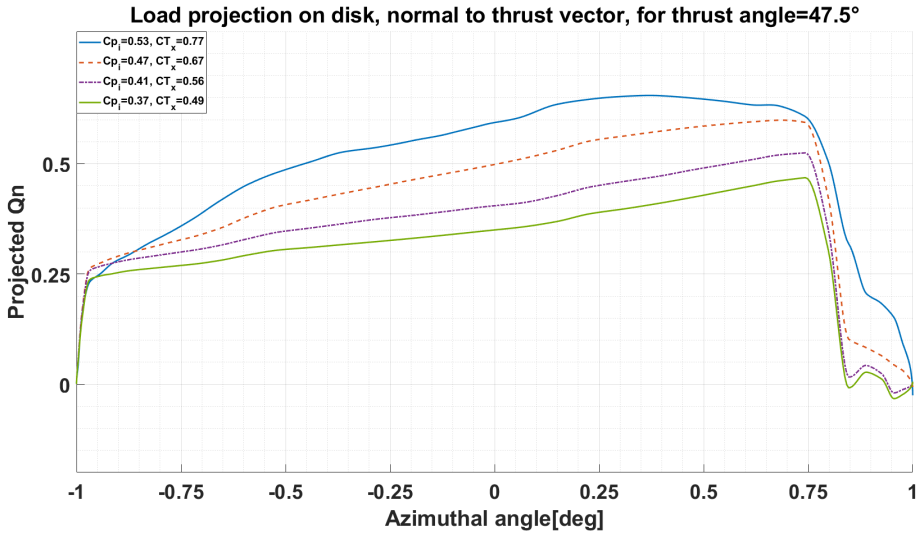

(d)

Figure 4.12: Distributions of the normalized cylinder surface load Qn , projected onto a single plane that is normal to thrust angle for thrust angles of $0°$ (a), $15°$ (b), $30°$ (c) and $45°$ (d). Tip speed ratio $= 4$.

4.3.3 Integrated load control

This section covers the integrated load control on the PitchVAWT. The integrated load control is set on four different loads, each with their respective optimization. Thrust coefficient and streamwise thrust coefficient are both minimized and their relations to power generation are compared. The streamnormal component of the thrust, C_{T_y}, is maximized in both windward and leeward directions over a series of power coefficients to set a relation between the two parameters.

Thrust and streamwise thrust minimization

The minimization of streamwise thrust coefficient and thrust coefficient are applied separately to evaluate the lowest possible loads achievable for specified value of C_P. Both minimizations are presented in figures 4.13 and 4.14. These figures show the results for tip speed ratio values of 3.5 and 4, lower TSRs have the same relation between the parameters as the larger ones and are therefore not displayed. The minimal values of streamwise thrust coefficient for specific values of power generation are typically the same, regardless if the minimization is applied to C_T or C_{T_x}, apart from a poorly generated data point in figure 4.13a. The power generation is directly related to the applied streamwise thrust coefficient, if performed in an efficient manner, and the corresponding lowest value of streamwise thrust coefficient can be obtained by both minimizations.

The results in figure 4.14 show the power generation against thrust coefficient, which includes the streamwise and streamnormal components. At peak power generation of $TSR = 4$, $C_{T_y} = 0.074$, but C_{T_y} is rapidly reduced to 0 with decreasing thrust coefficient for the minimization of the thrust coefficient. The minimization of streamwise thrust coefficient leaves the streamnormal component of the thrust unbound, which causes the differences in results seen in figures 4.14a and 4.14b. The values for C_{T_y} are typically around 0.1, they did not exceed 0.16 and are attained for all power coefficients for the minimization of streamwise thrust coefficient. As the thrust coefficient becomes smaller, these values of streamnormal force coefficient become more noticeable.

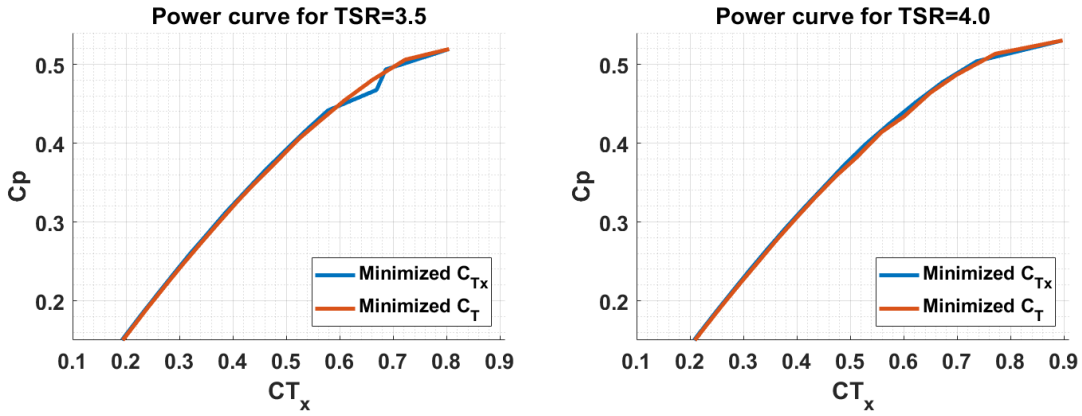

(a) (b)

Figure 4.13: Power coefficient against streamwise thrust coefficient for the minimizations of streamwise thrust coefficient and thrust coefficient.

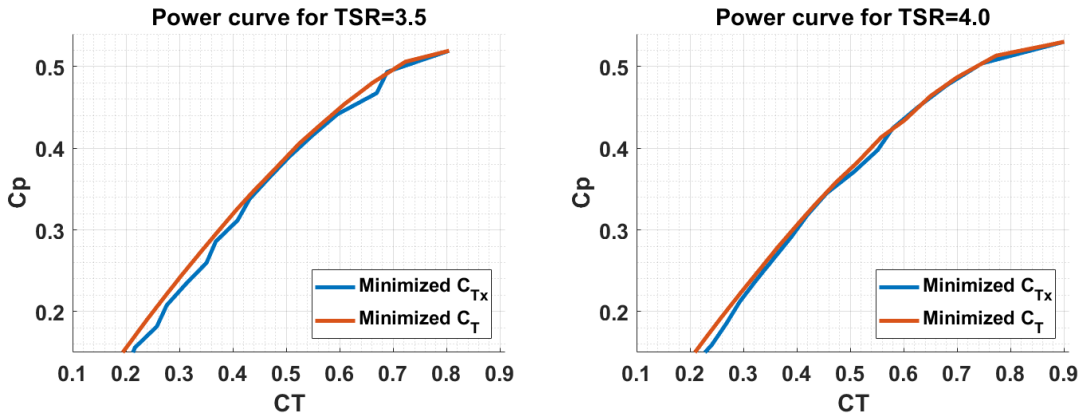

(a) (b)

Figure 4.14: Power coefficient against thrust coefficient for the minimizations of streamwise thrust coefficient and thrust coefficient.

Thrust angle maximization

The results of the maximization of the thrust angle over a range of power coefficients is presented in figure 4.15. Figure 4.15a displays the extrema in power generation and thrust angle deflection. The results show that the peak in power generation is generated within 5° deviation of the zero thrust angle. The mappings found in appendix C show that peak power generation is attained at thrust angles of $\sim 20^\circ$. The difference in thrust angle does not cause large variations in power generation, but does indicate a limitation of applying a local minimum solver on obtaining a global minimum containing many variables.

Table 4.3 highlights the variation in performance and achieved thrust angles for the data points nearest to the peak power generation. As the tip speed ratio increases, the largest attainable thrust angle in either direction increases under constant relative power loss. At $TSR = 4$ and $TSR = 3.5$ the thrust angle can be deflected more than 30° at only a 5% loss in power generation. These results quite closely resemble the relation of power extraction loss for the prescribed surface load results when deflecting the thrust angle 30° under constant average loading. The thrust angle in windward direction can greatly exceed the thrust angle in leeward direction, while achieving the same power generation. At $TSR = 4$ with only a 5% loss in power generation with respect to the maximum the windward thrust angle is over 49°.

The thrust vectors corresponding to the power generation from figure 4.15a are presented in figure 4.15b. Results from figure 4.8 already showed that the turbine is less efficient when thrust vectoring in leeward direction than in windward direction. The results in figure 4.15a show that the PitchVAWT can attain the same power generation values in either direction. However, the corresponding thrust vectors are larger when thrust vectoring in leeward direction than they are for their windward counterparts. All these data points confirm that the VAWT is more efficient when the thrust vector is in windward direction.

Table 4.3: Variation in performance of data points at largest power generation below maximum C_P.

TSR	Power loss [%]	Power loss$[\Delta C_P]$	Min. omnidirectional Ψ angle
1.5	10%	0.019	32°
2.0	7%	0.020	27°
2.5	5%	0.020	25°
3.0	5%	0.025	-
3.5	5%	0.026	31°
4.0	5%	0.026	33°

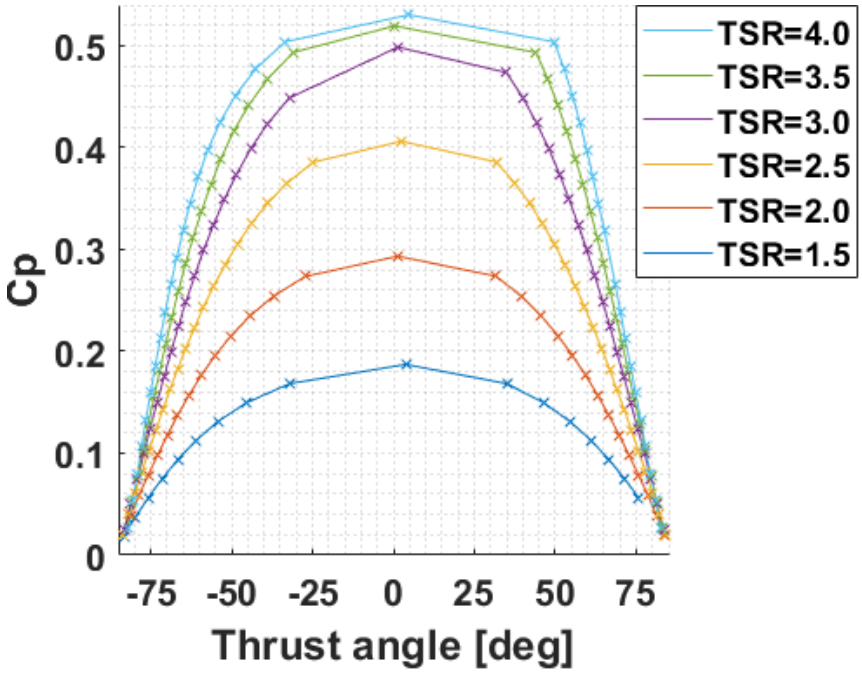

(a) Largest thrust angle deflections in positive and negative direction achievable per C_P.

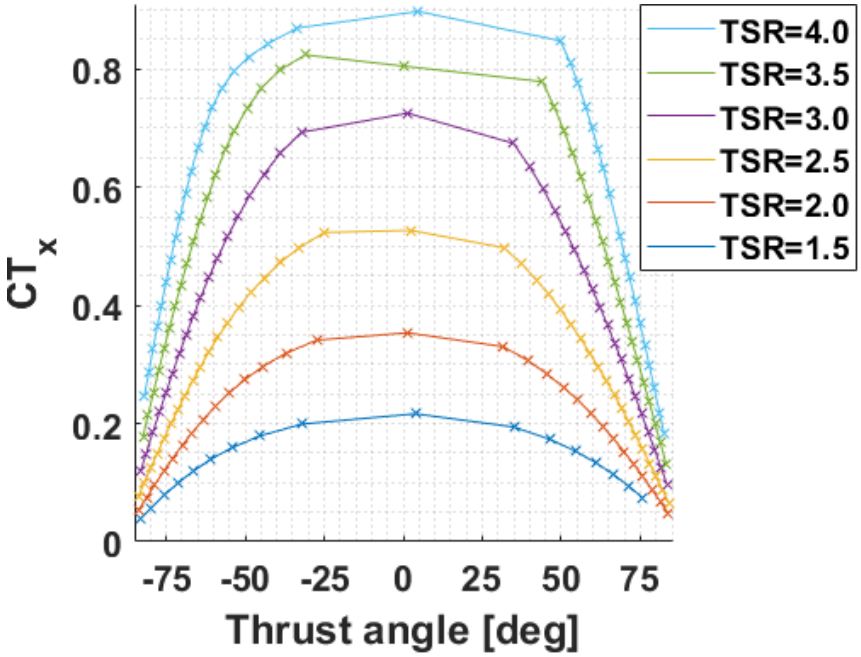

(b) Largest thrust angle deflections in positive and negative direction and their corresponding streamwise thrust coefficient.

Figure 4.15: Maxima in thrust angle deflection in either direction for power coefficients ranging from $C_P \approx 0$ to $C_{P_{max}}$.

Chapter 5

Conclusions and Recommendations

5.1 Conclusions

The VAWT has been analyzed through the linear $2D$ actuator cylinder model with Mod-Lin correction on the VAWT's performance for offset angles of the thrust vector with the freestream for a specific turbine, called PitchVAWT, and the general case where the surface loading is prescribed and no tangential load is imposed.

Test cases with prescribed surface loading have a power extraction against streamwise thrust relation that shows to be nearly invariant with the thrust angle if no limit is applied to the magnitude of the local surface loading. To evaluate the performance of VAWTs in absence of a tangential loading, the integrated parameters have to be compared to the characteristics of the instantaneous load profile on maximum load amplitude and average load amplitude.

The distributions of the instantaneous load profiles for cases with prescribed surface loading generally shifts one-to-one over the azimuth with thrust angle. This shift occurs for the location of peak loading, on both the upwind and downwind halves of the rotor, and the locations where load switches from cylinder inward to cylinder outward or vice versa. The shifting of these locations occurs up to a critical thrust angle, after which the location of instantaneous peak load remains constant for increasing thrust angles.

The comparison between PitchVAWT and the prescribed surface loading shows that as the tip speed ratio of the PitchVAWT increases, the integrated results become more similar. At a tip speed ratio of 4, the variation in performance with thrust vectoring for the two models is close to the same. The instantaneous load profiles of the two VAWT representations are vastly different and no generic trend with thrust vectoring could be established for the PitchVAWT results.

The potential of load control on the ability to extract power has been examined on the PitchVAWT turbine, since there is no significant loss in power extraction when only the surface loading is prescribed. The PitchVAWT model showed that operating at tip speed ratios of 3 or larger, the thrust angle can be over 30° in either windward or leeward direction at only a loss of 5% compared to their respective $C_{P_{max}}$. It could also be concluded that the VAWT can attain notable larger power efficiencies when the thrust vector, as experienced by the flow, is directed in windward direction over leeward directed thrust vectors.

5.2 Recommendations

Turbine modeling where the cylinder surface loading is directly prescribed, inherently lacks the presence of tangential load. It is possible to enhance computations with an imposed tangential loading, but over a range of thrust vectors the imposed tangential load has to alter appropriately. Further investigating the relation between tangential and normal load could lead to empirical relations to enhance computations. The inclusion of empirical tangential loading should lead to more accurate depictions of power extraction/generation without the need to specify all design parameters.

The linear actuator cylinder model with the Mod-Lin correction included has been proven to be a fair tool for determining integrated parameters while operating under zero thrust angle. As the thrust angle increases, regions where power is locally added to the flow, instead of being extracted, start to spread. The perturbation velocities of the linear ACM combine streamtube model wake propagation with the full influence of the pressure field on every position on the rotor. The wake propagating along the freestream, as in streamtube models, causes errors in the velocity field of the downwind half of the rotor. Incorrectly modeling whether an increment or reduction in streamwise velocity should be taken into account on the downwind half of the rotor, gives rise to errors in the prediction of instantaneous loading. The author recommends further investigation of loads with non-zero thrust angles through the non-linear ACM to determine the validity of the linear ACM for non-zero thrust angles.

The $2D$ turbine with prescribed surface loading showed to have only a minor loss in maximum power extraction when a thrust vector is at an angle of 75° compared to the thrust vector at 0°. Peak loading on both the upwind and downwind halves of rotor increase with increasing thrust vector under constant streamwise thrust coefficient. This should lead to an increasing loss in power extraction with increasing thrust angle when performing $3D$ computations. Further investigation on the influence of the thrust angle extended to three dimensional computations is recommended.

Results have shown that there is an innate difference in the relation of streamwise thrust coefficient and the power generation coefficient between thrust angles in windward and leeward directions. Further investigation of this behavior in the turbine's efficiency is recommended and with that methods to enhance to efficiency on leeward directed thrust angles.

Bibliography

[1] H.J. Sutherland, D.E. Berg, T.D. Ashwill. *A retrospective of VAWT technology.* Sandia report: SAND2012-0304, 2012.

[2] J.D. Anderson. *Fundamentals of aerodynamics. 4th edition.* McGraw-Hill, pages 316-319, 2007.

[3] J.D. Anderson. *Fundamentals of aerodynamics. 4th edition.* McGraw-Hill, pages 400-404, 2007.

[4] J.D. Anderson. *Fundamentals of aerodynamics. 4th edition.* McGraw-Hill, pages 403-404, 2007.

[5] A. Betz. *Das maximum der theoretisch möglichen ausnützung des windes durch windmotoren.* Zeitschrift für das gesamte turbinenwesen; 26: pages 307-309, 1920.

[6] B. Brenneman. *Transverse axis fluid turbine* United States Patent 4,415,312. 1983.

[7] V. Chenna *Fatigue-Induced Failure in Horizontal-Axis Wind-Turbine (HAWT) Blades and HAWT Drivetrain Gears* Clemson University paper 1863, 2014.

[8] T. Corke. *Single dielectric barrier discharge plasma enhanced aerodynamics: Physics, modeling and applications* Experiments in Fluids, Jan. 2009.

[9] P. Crimi. *Dynamic stall.* AGARDograph No. 172, 1973.

[10] J.O. Dabiri. *Potential order-of-magnitude enhancement of wind farm power density via counterrotating vertical-axis wind turbine arrays.* Journal of renewable and sustainable energy, 3(4):043104, 2011.

[11] J.A. Dahlberg, B. Montgomerie. *"Research program of the Utgrunden Demonstration Offshore Wind Farm, Final report Part 2, Wake effects and other loads* FOI 2005-02-17, Swedish Defense Research Agency, FOI. 2005.

[12] H. Drees. *The Cycloturbine And Its Potential For Broad Application* In 2nd International Symposium on Wind Energy Systems Oct 3-6 1978, Volume 2, pp. E–7. 1978.

[13] M.Drela, H. Youngren. *XFoil manual v6.9 / xfoil_doc* http://web.mit.edu/drela/Public/web/xfoil/, 2001.

[14] *Europe's onshore and offshore wind energy potential.* EEA (European Environment Agency), 2009.

[15] S. Ertem, C. Simão Ferreira, M. Gaunaa, H.Aa. Madsen. *Aerodynamic Optimization of Vertical Axis Wind Turbine with Trailing Edge Flaps* 34th Wind Energy Symposium, 2016.

[16] N. Fichaux, J Wilkes. *Oceans of Opportunity* EWEA 2009.

[17] P. Fleming, P. Gebraad, S. Lee, J.W. van Wingerden, K. Johnson, M. Churchfield, J. Michalakes, P. Spalart, P. Moriarty. *High-fidelity simulation comparison of wake mitigation control strategies for a two-turbine case* ICOWES2013 Conference, 17-19 June 2013, Lyngby, 2013.

[18] G.W. Gyatt. *Development and Testing of Vortex Generators for Small Horizontal Axis Wind Turbines* Technical Report; NASA CR-179514, 1986.

[19] S. van der Horst, J. van de Wiel, C. Simão Ferreira, N. Ramos García. *Flow curvature effects for VAWT: a review of virtual airfoil transformations and implementation in XFOIL.* Conference paper, 2016.

[20] D.P. Houf, C. Simão Ferreira, M. Gaunaa. *Active pitch control of a vertical axis wind turbine.* European wind energy master- EWEM, 2016.

[21] F. Huijs, E. Vlasveld, M. Gormand, F. Savenije, M. Caboni, B. LeBlanc, C. Simão Ferreira, K. Lindenburg, S. Gueydon, W. Otto, B. Paillard. *Integrated design of a semi-submersible floating vertical axis wind turbine (VAWT) with active blade pitch control* Journal of Physics Conference Series 1104:012022, 2018.

[22] S.J. Johnson, C.P. van Dam, D.E. Berg. *Active load control techniques for wind turbines.* Sandia report: SAND2008-4809, 2008.

[23] B.K. Kirke, L. Lazauskas. *Enhancing the performance of vertical axis wind turbine using a simple variable pitch system.* Wind engineering, Vol. 15, No.4: pages 187-195, 1991.

[24] B.K. Kirke, B. Paillard. *Predicted and measured performance of a vertical axis wind turbine with passive variable pitch compared to fixed pitch.* Wind engineering, Vol. 41, No.1: pages74-90, 2016.

[25] T.J. Larsen, H.Aa. Madsen. *On the way to reliable aeroelastic load simulation on VAWT's.* Proceedings of EWEA 2013, 2013.

[26] L. Lazauskas. *Three pitch control systems for vertical axis wind turbines compared* Wind Engineering, vol. 16, No. 5, pg. 269-283, 1992.

[27] B.P. LeBlanc, C. Simão Ferreira. *Overview and design of pitchvawt: Vertical axis wind turbine with active variable pitch for experimental and numerical comparison.* AIAA SciTech Forum Jan. 2018, 2018 Wind Energy Symposium, 2018.

[28] B.P. LeBlanc, C. Simão Ferreira. *Experimental Determination of Thrust Loading of a 2-Bladed Vertical Axis Wind Turbine* Journal of Physics: Conference Series, Ser. 1037022043, 2018.

[29] H.Aa. Madsen. *The actuator cylinder - A flow model for vertical axis wind turbines.* PhD thesis, Aalborg University, Denmark, 1982.

[30] H.Aa. Madsen, U.S. Paulsen, L. Vitae. *Analysis of VAWT aerodynamics and design using the actuator cylinder flow model.* In Proceedings of Torgue 2012: The science of making torgue from wind, 2012.

[31] H.Aa. Madsen, T.J.Larsen, U.S. Paulsen, L. Vita. *Implementation of the Actuator Cylinder Flow Model in the HAWC2 code for Aeroelastic Simulations on Vertical Axis Wind Turbines* 51st AIAA Aerospace Sciences Meeting including the New Horizons Forum and Aerospace Exposition, 2013.

[32] Mathworks support. https://nl.mathworks.com/help/optim/ug/fmincon.html, 2018

[33] W.J. McCorskey. *The phenomenon of dynamic stall.* NASA Technical Memorandum 81264, 1981.

[34] G.B. McCullough, D.E. Gault. *Examples of three representative types of airfoil-section stall at low speed.* National advisory committee for aeronautics, technical note 2502, 1951.

[35] P.G. Migliore, W.P. Wolfe, J.B. Fanucci. *Flow curvature effects on Darrieus turbine blade aerodynamics.* Journal of Energy, Vol.4 No.2 pages 49-55, 1980.

[36] B.G. Newman. *Actuator-disk theory for vertical-axis wind turbines.* Journal of wind engineering and industrial aerodynamics, Vol.15: pages 347-355. Elsevier science publishers, 1983.

[37] I. Paraschivoiu. *Aerodynamic Loads and Performance of the Darrieus Rotor* Journal of Energy, Vol. 6, No. 6, pages 406-412, 1982.

[38] I. Paraschivoiu. *Wind turbine design - with emphasis on Darrieus concept.* Polytechnic internation press, 2002.

[39] I. Paraschivoiu, O. Trifu, F. Saeed. *H-Darrieus Wind Turbine with Blade Pitch Control* International Journal of Rotating Machinery, Vol. 2009. doi:10.1155/2009/505343, 2009.

[40] N.C.K. Pawsey. *Development and evaluation of passive variable-pitch vertical axis wind turbines.* PhD thesis, The University of New South Wales, 2002.

[41] B. Sasson, D. Greenblatt *Effect of Leading-Edge Slot Blowing on a Vertical Axis Wind Turbine* AIAA journal, September 2011, Vol. 49, No. 9, 2011.

[42] C. Simão Ferreira, H. Aa. Madsen, M. Barone, B. Roscher, P. Deglaire, I. Arduin *Comparison of aerodynamic models for Vertical Axis Wind Turbines.* TORQUE, 2014.

[43] C. Simão Ferreira, F. Scheurich. *Demonstrating that power and instantaneous loads are decoupled in a vertical-axis wind turbine* Wind Energy 2014; Vol 17, pages 385-396, 2014.

[44] Y. Staelens, F. Saeed, I. Paraschivoiu. *A straight-bladed variable-pitch VAWT concept for improved power generation.* ASME 2003 Wind Energy Symposium, Paper No. WIND2003-524, pages 146-154, 2003.

[45] J. H. Strickland. *The Darrieus Turbine: A Performance Prediction Model Using Multiple Stream Tubes* Technical report, Sandia National Laboratories, 1975. SAND75-041, 1975.

[46] T. Theodorsen. *General theory of aerodynamic instability and the mechanism of flutter.* National advisory committee for aeronautics, report No.496, 1949.

[47] W. Tjiu, T. Marnoto, S. Mat, M.H. Ruslan, K. Sopian. *Darrieus vertical axis wind turbine for power generation II: Challenges in HAWT and the opportunity of multi-megawatt Darrieus VAWT development* Renewable Energy March 2015, DOI: 10.1016, 2015.

[48] L. Vita *Offshore Vertical Axis Wind Turbine with Floating and Rotating Foundation.* PhD thesis, Technical University of Denmark, 2011.

[49] R.E. Wilson, P.B.S. Lissaman, S.N. Walker. *Aerodynamic performance of wind turbines.* Oregon State University, 1976.

[50] Q. Xiao, W. Liu, A. Incecik. *Flow control for VATT by fixed and oscillating flap* Renewable Energy Vol.51, pages 141-152, 2013.

Appendices

Appendix A

Prescribed surface loading instantaneous load distributions

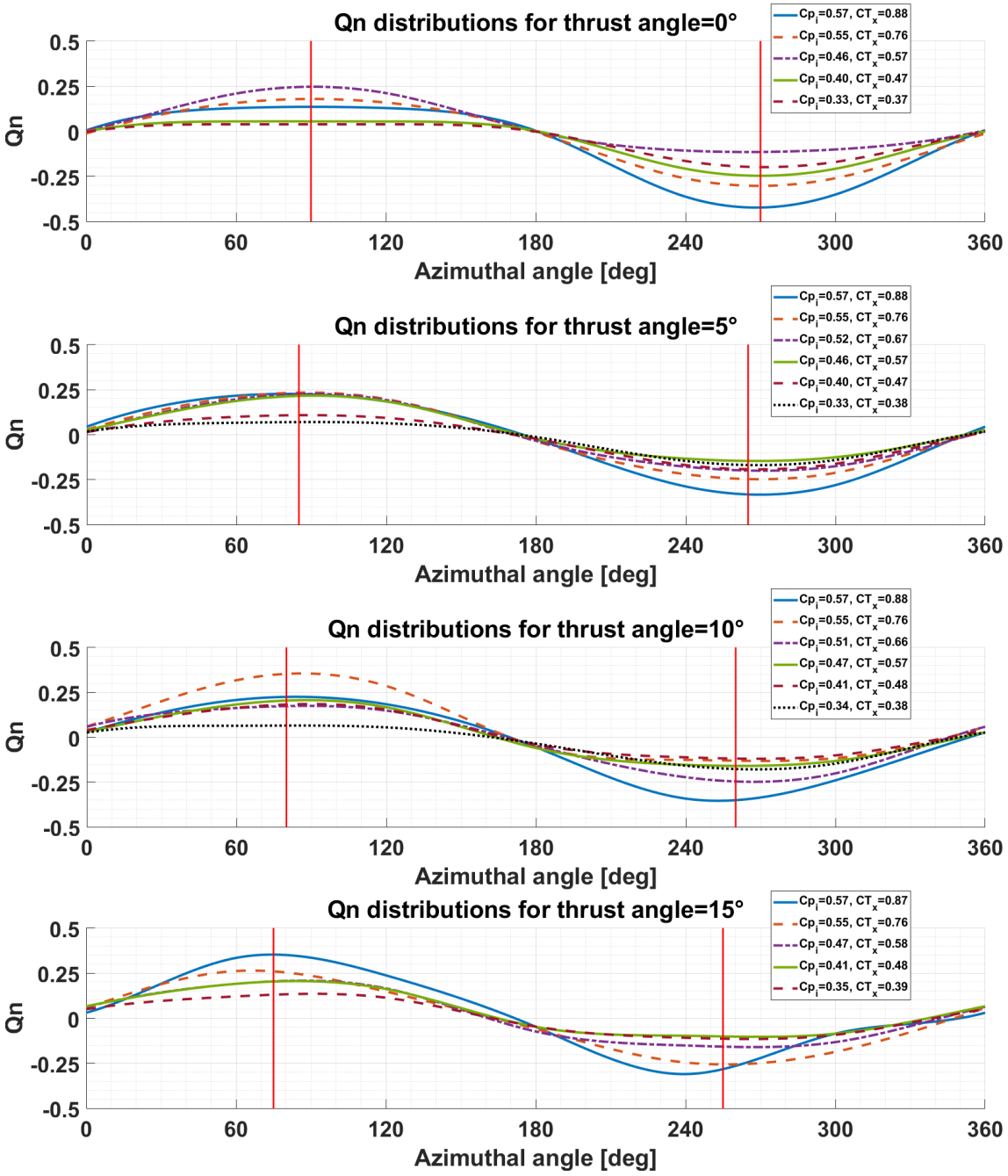

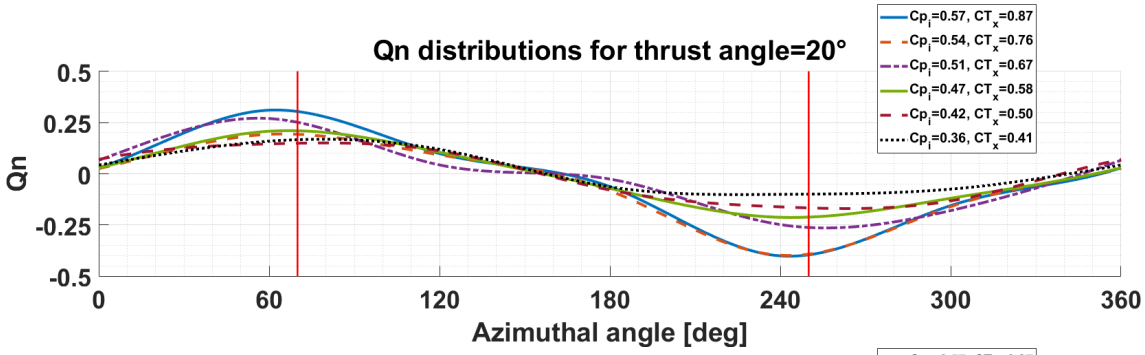
Qn distributions for thrust angle=20°
Cp_i=0.57, CT_x=0.87
Cp_i=0.54, CT_x=0.76
Cp_i=0.51, CT_x=0.67
Cp_i=0.47, CT_x=0.58
Cp_i=0.42, CT_x=0.50
Cp_i=0.36, CT_x=0.41
Qn
Azimuthal angle [deg]

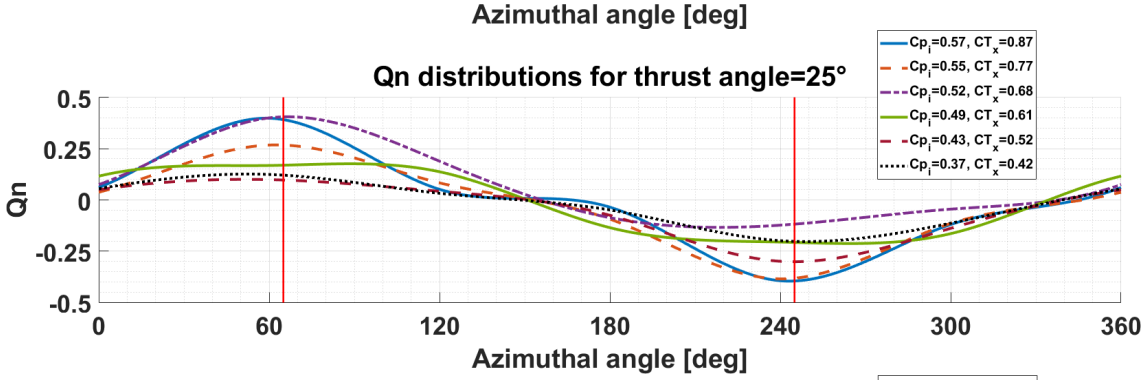
Qn distributions for thrust angle=25°
Cp_i=0.57, CT_x=0.87
Cp_i=0.55, CT_x=0.77
Cp_i=0.52, CT_x=0.68
Cp_i=0.49, CT_x=0.61
Cp_i=0.43, CT_x=0.52
Cp_i=0.37, CT_x=0.42
Qn
Azimuthal angle [deg]

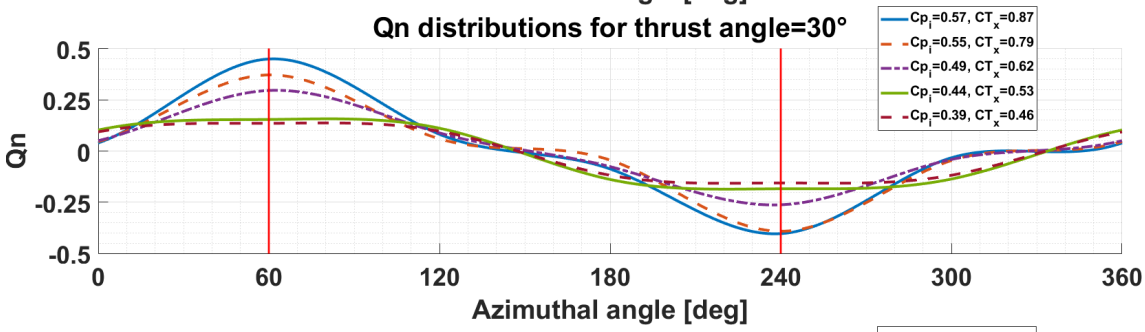
Qn distributions for thrust angle=30°
Cp_i=0.57, CT_x=0.87
Cp_i=0.55, CT_x=0.79
Cp_i=0.49, CT_x=0.62
Cp_i=0.44, CT_x=0.53
Cp_i=0.39, CT_x=0.46
Qn
Azimuthal angle [deg]

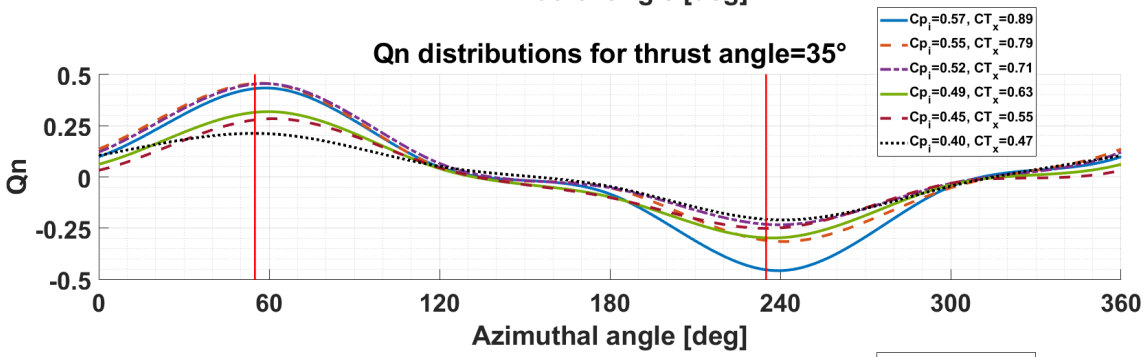
Qn distributions for thrust angle=35°
Cp_i=0.57, CT_x=0.89
Cp_i=0.55, CT_x=0.79
Cp_i=0.52, CT_x=0.71
Cp_i=0.49, CT_x=0.63
Cp_i=0.45, CT_x=0.55
Cp_i=0.40, CT_x=0.47
Qn
Azimuthal angle [deg]

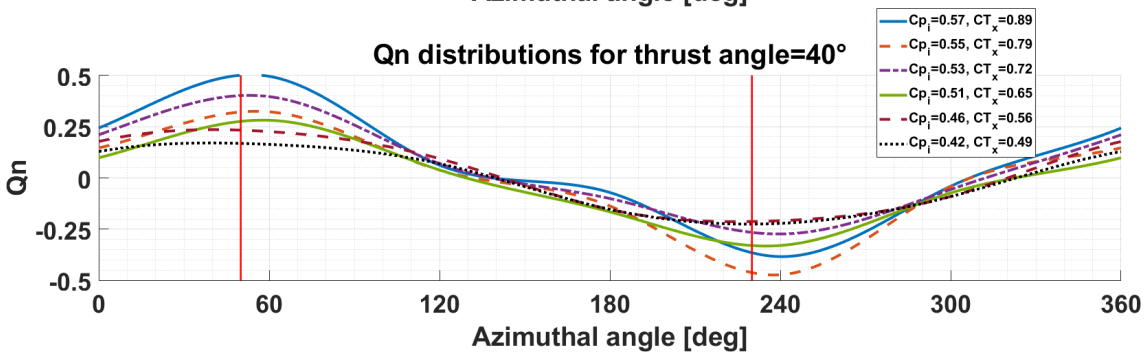
Qn distributions for thrust angle=40°
Cp_i=0.57, CT_x=0.89
Cp_i=0.55, CT_x=0.79
Cp_i=0.53, CT_x=0.72
Cp_i=0.51, CT_x=0.65
Cp_i=0.46, CT_x=0.56
Cp_i=0.42, CT_x=0.49
Qn
Azimuthal angle [deg]

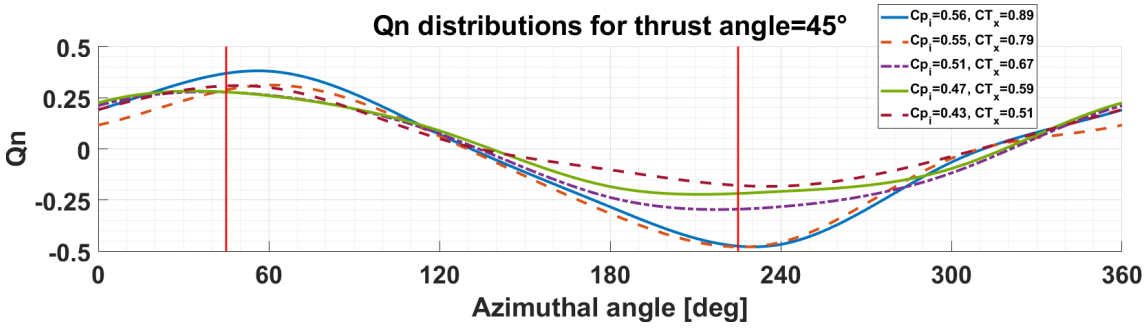

Figure A.1: Instantaneous load profiles for all data points up to a thrust angle of $45°$, for cases with only prescribed surface loading.

Appendix B

Prescribed surface loading projected load distributions

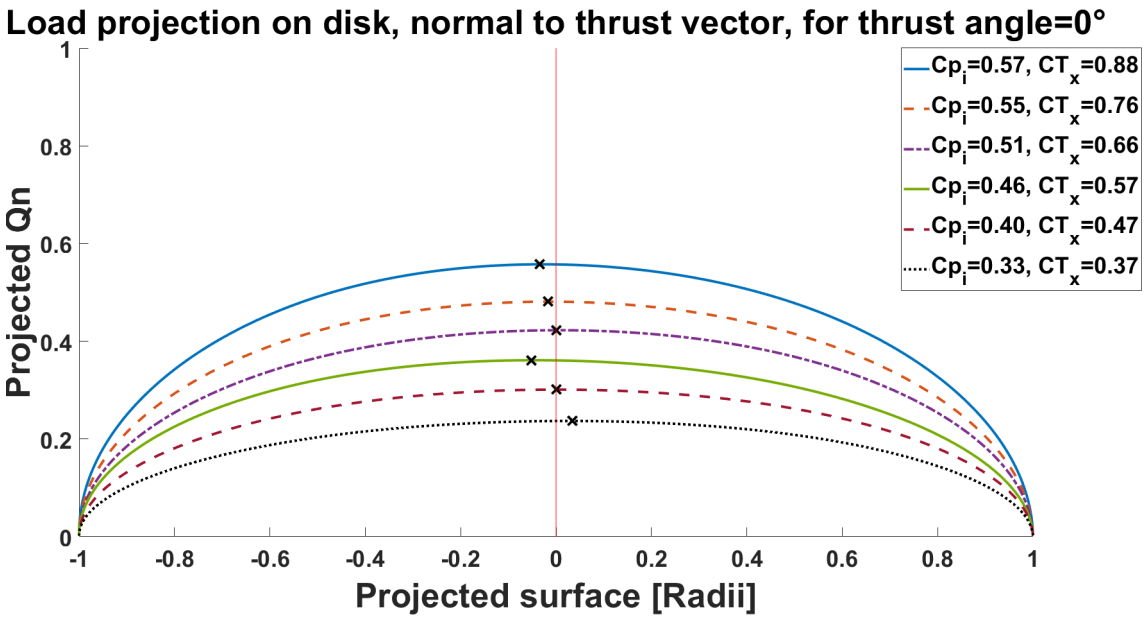

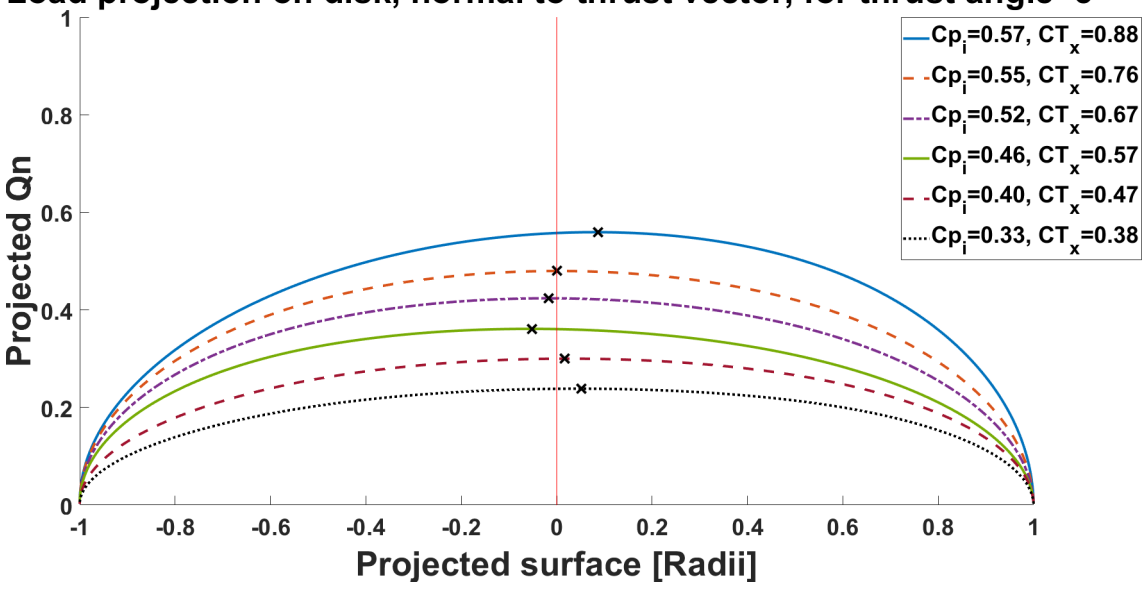

Load projection on disk, normal to thrust vector, for thrust angle=10°

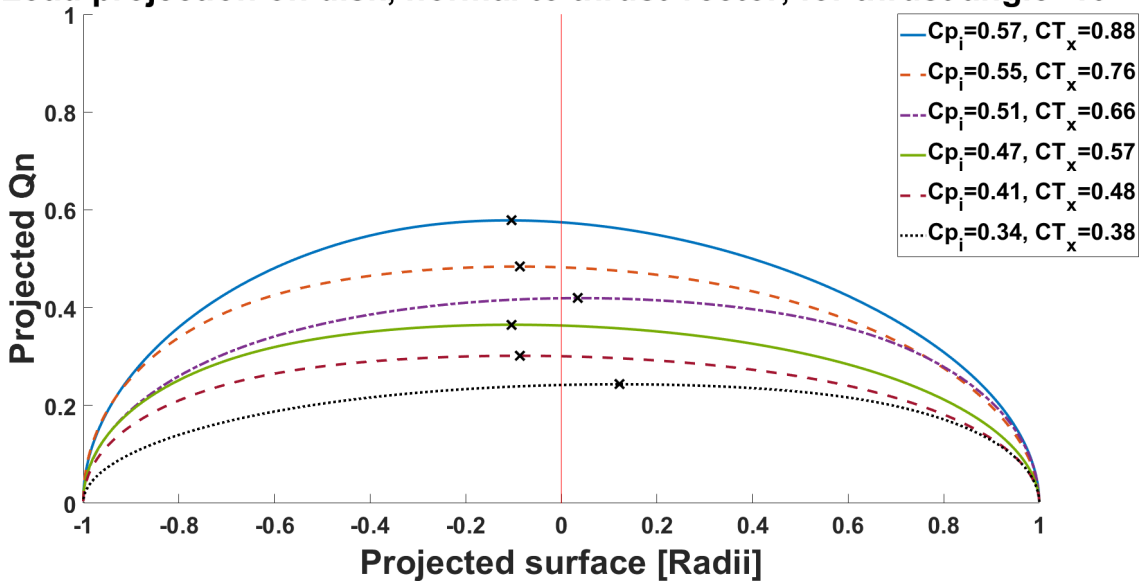

Load projection on disk, normal to thrust vector, for thrust angle=15°

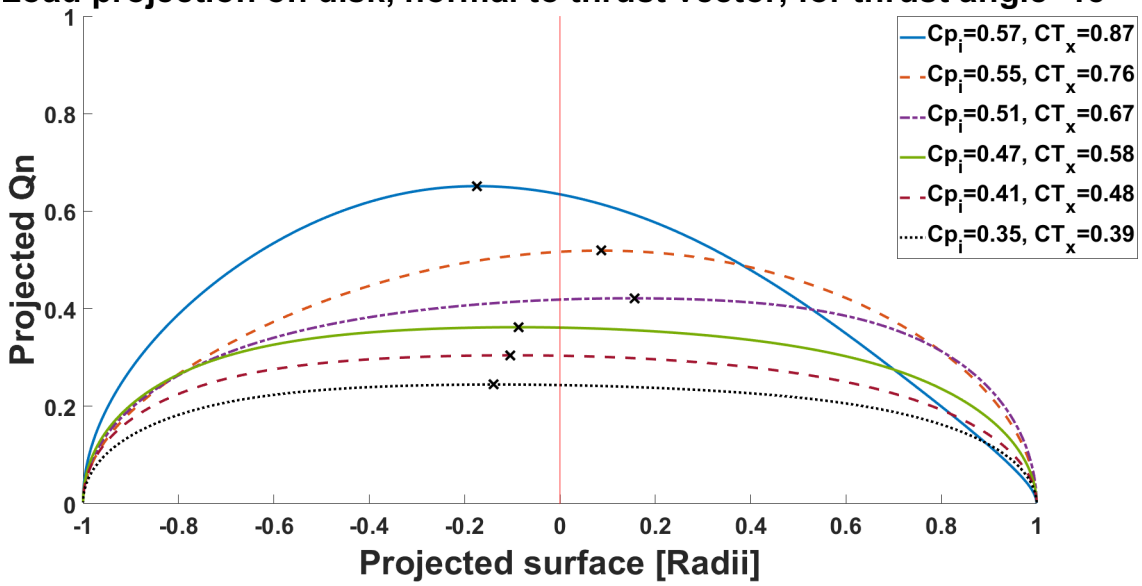

Load projection on disk, normal to thrust vector, for thrust angle=20°

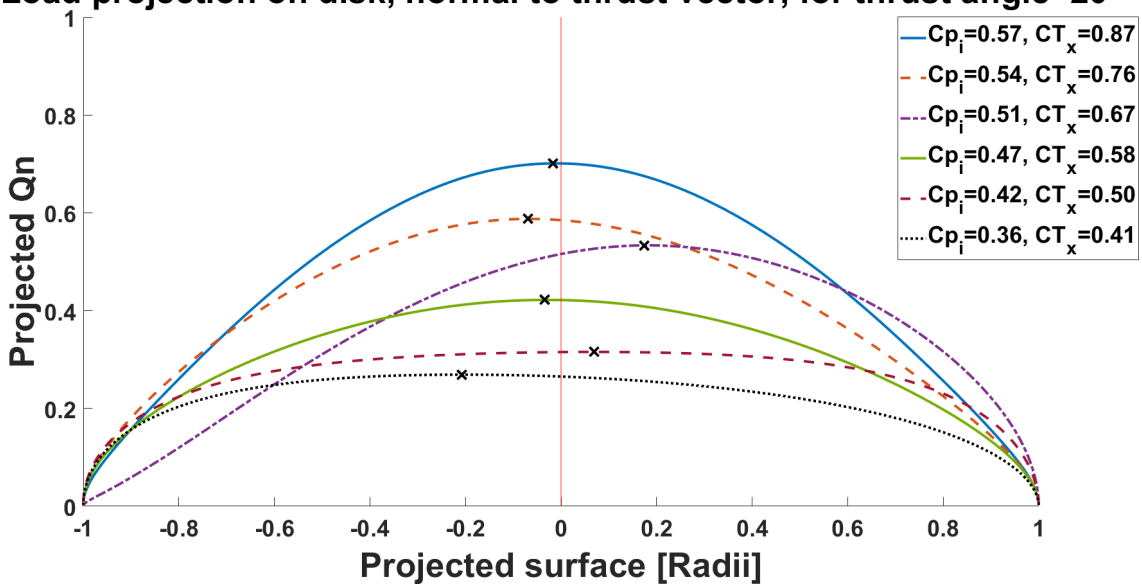

Load projection on disk, normal to thrust vector, for thrust angle=25°

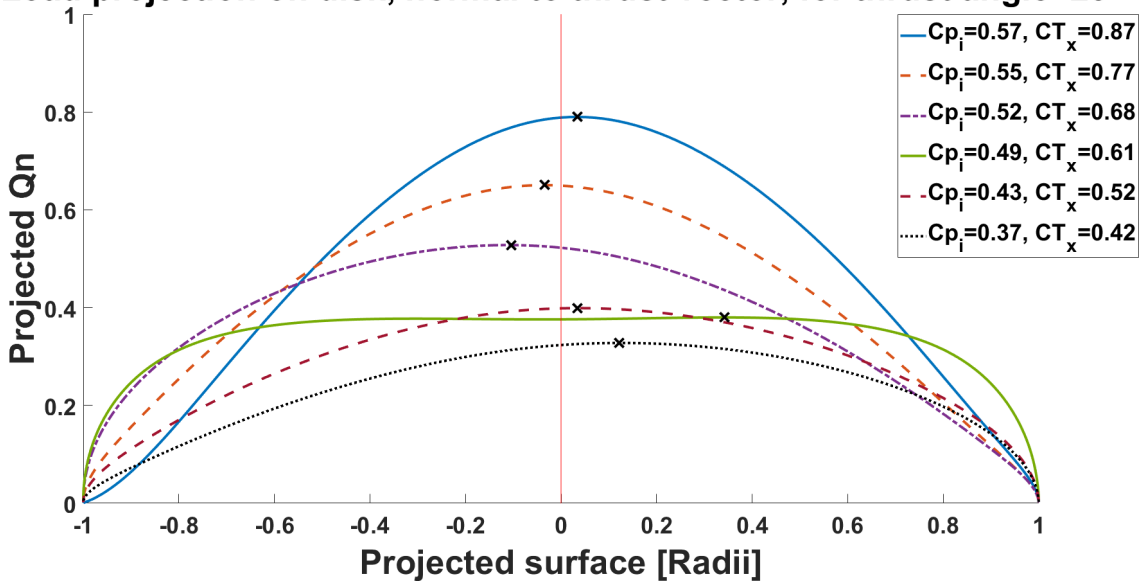

Load projection on disk, normal to thrust vector, for thrust angle=30°

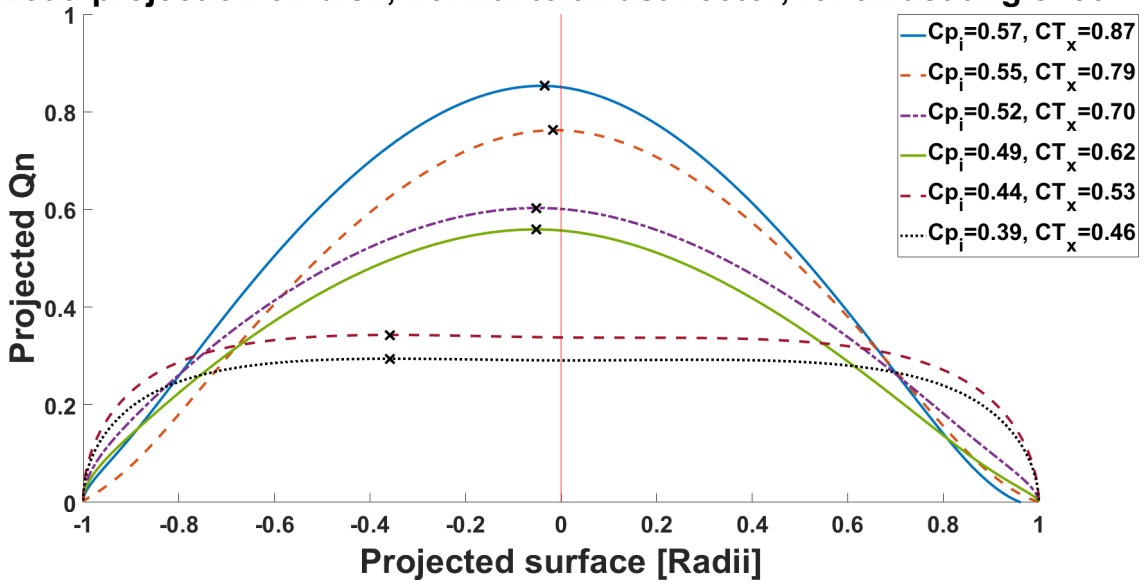

Load projection on disk, normal to thrust vector, for thrust angle=35°

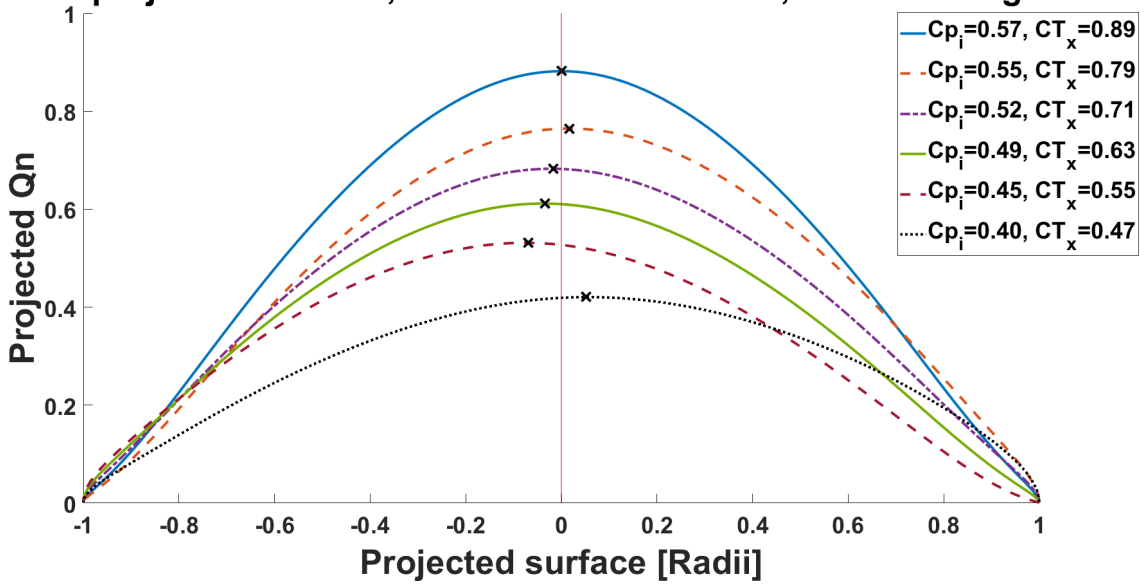

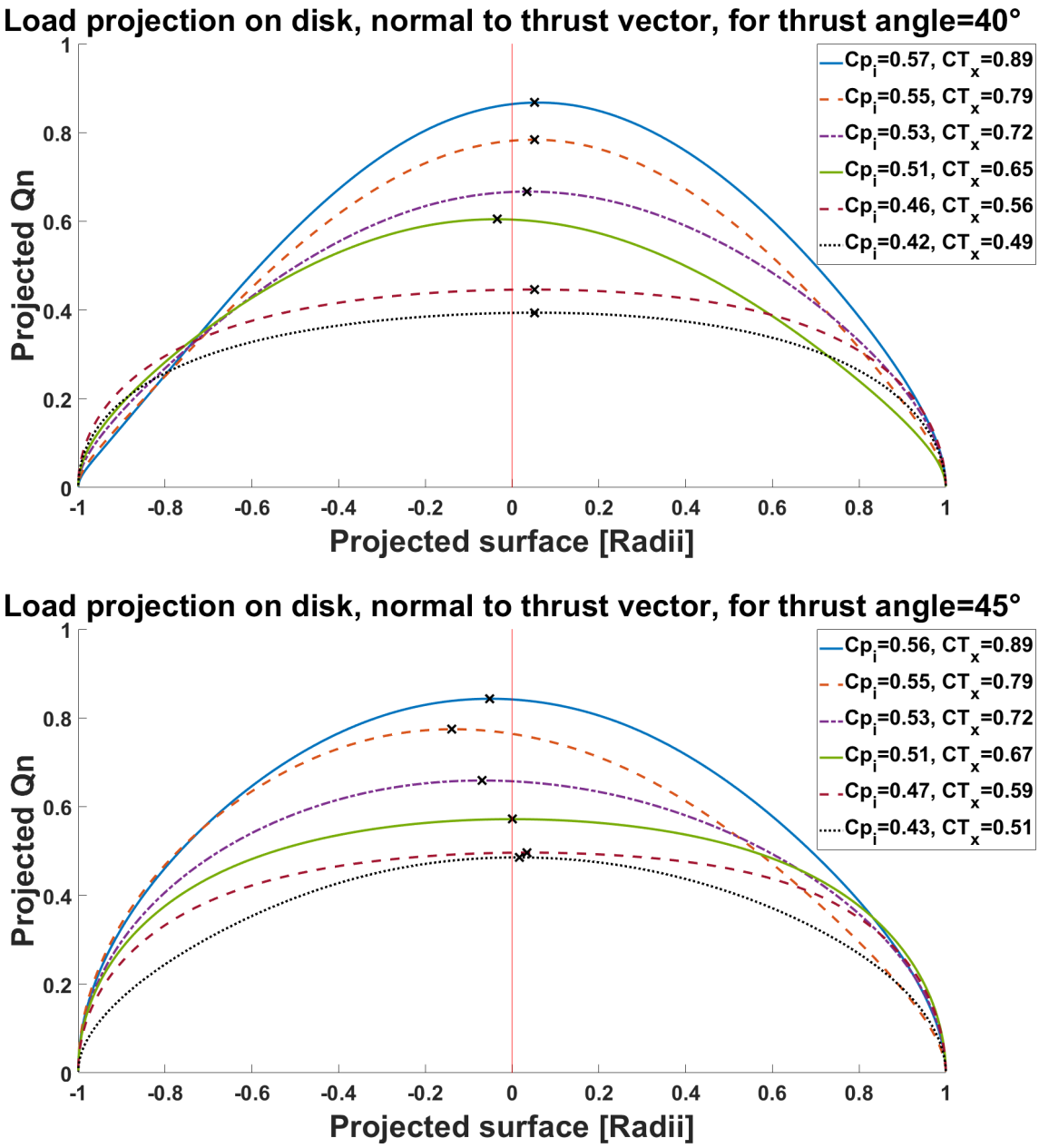

Figure B.1: Projection of surface loading onto a single plane that is normal to the thrust vector for all data points up to a thrust angle of $45°$ for cases with prescribed surface loading.

Appendix C

PitchVAWT: power generation mapped against thrust vectors

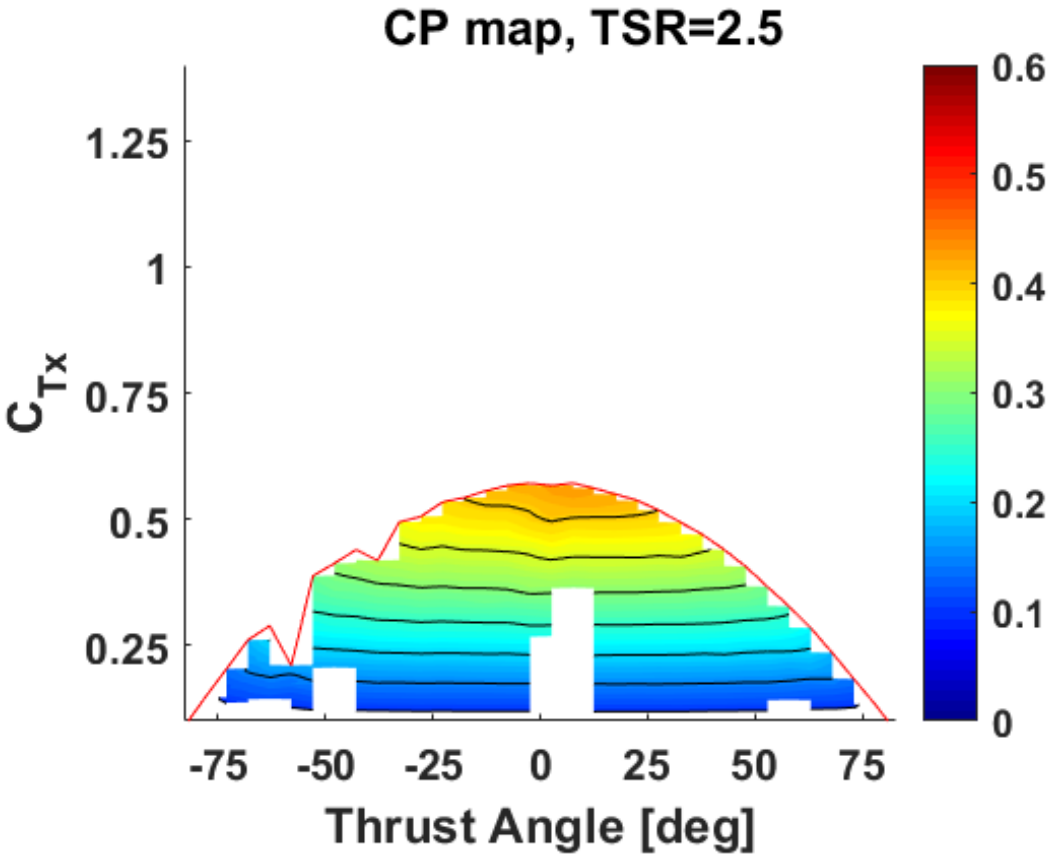

(a)

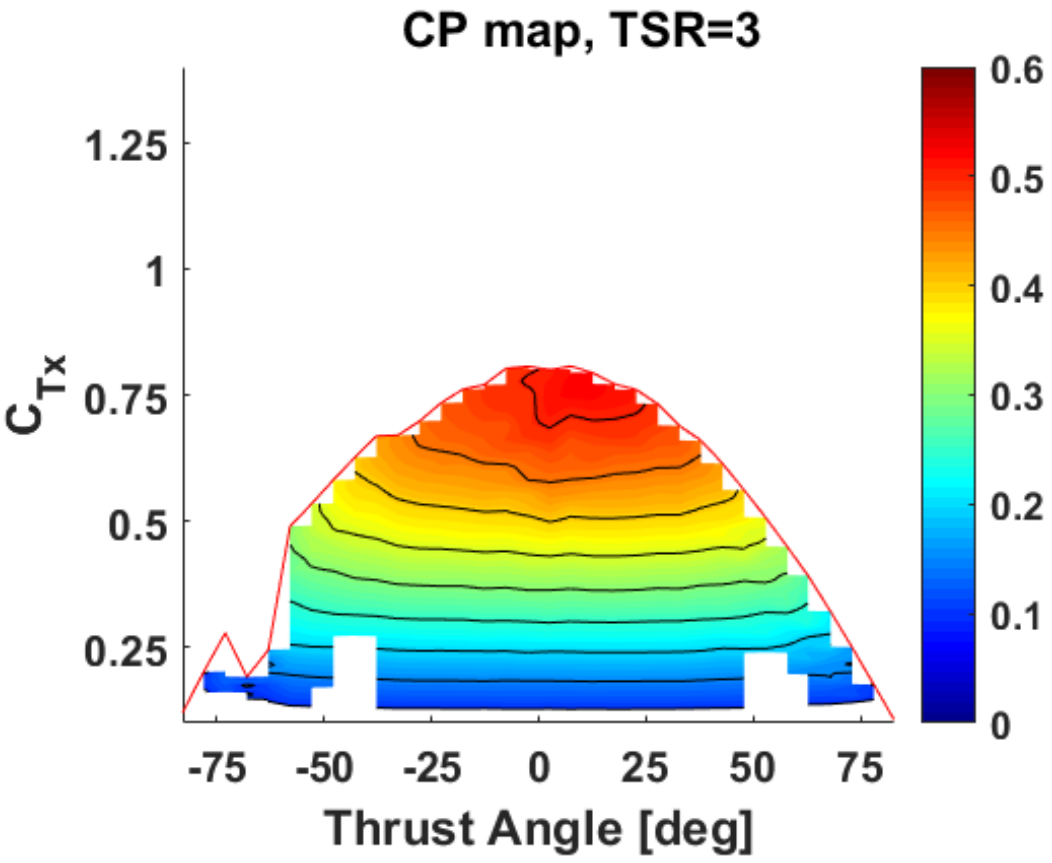
CP map, TSR=3
1.25
1
0.75
0.5
0.25
C_{Tx}
-75
-50
-25
0
25
50
75
Thrust Angle [deg]
0.6
0.5
0.4
0.3
0.2
0.1
0

(b)

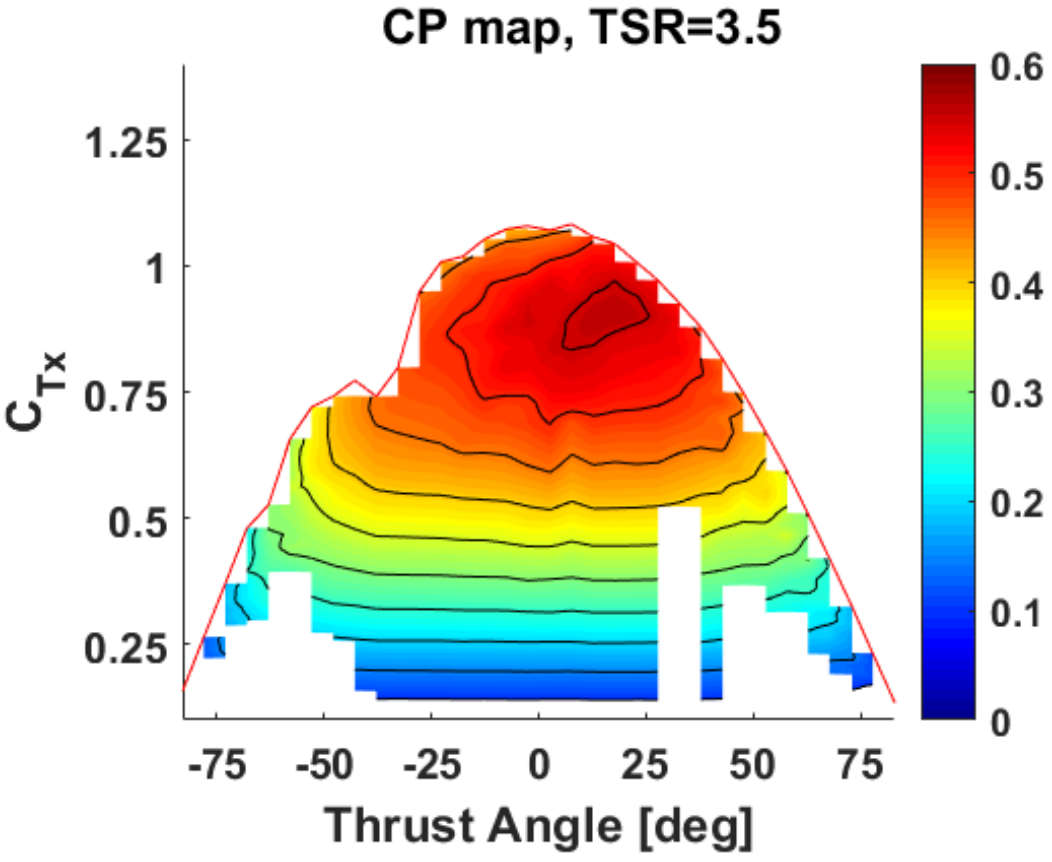
CP map, TSR=3.5
1.25
1
0.75
0.5
0.25
C_{Tx}
-75
-50
-25
0
25
50
75
Thrust Angle [deg]
0.6
0.5
0.4
0.3
0.2
0.1
0

(c)

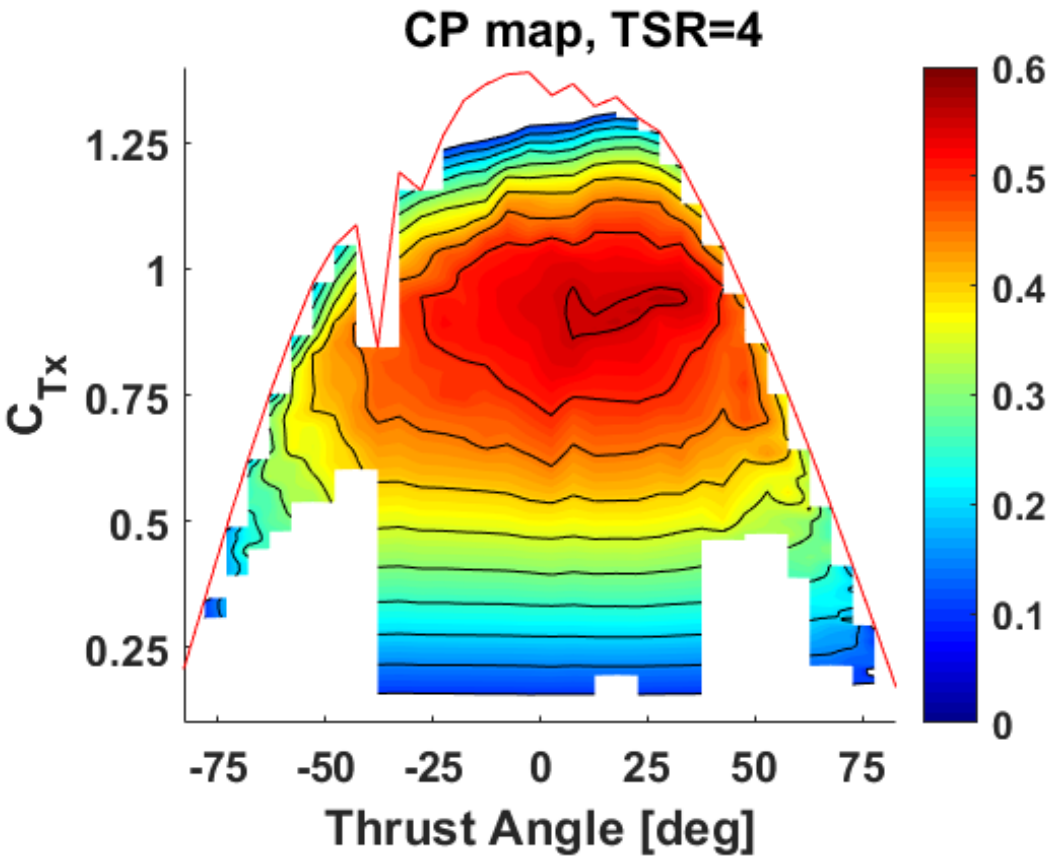

(d)

Figure C.1: Mapping of the power generation of the PitchVAWT turbine model for different TSRs at an average Re. nr $2 \cdot 10^6$. The outline indicates the limit values of the thrust vectors that were able to be obtained on the ACM.

Appendix D

Prescribed surface loading flow fields

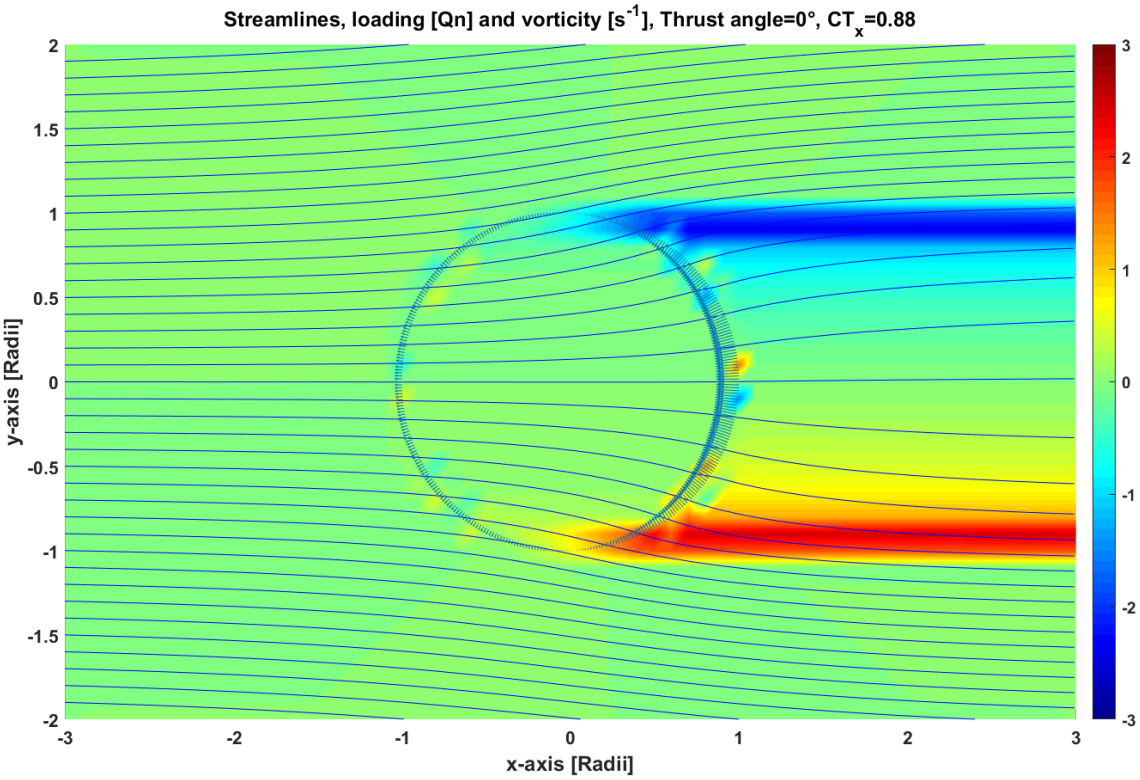

(a)

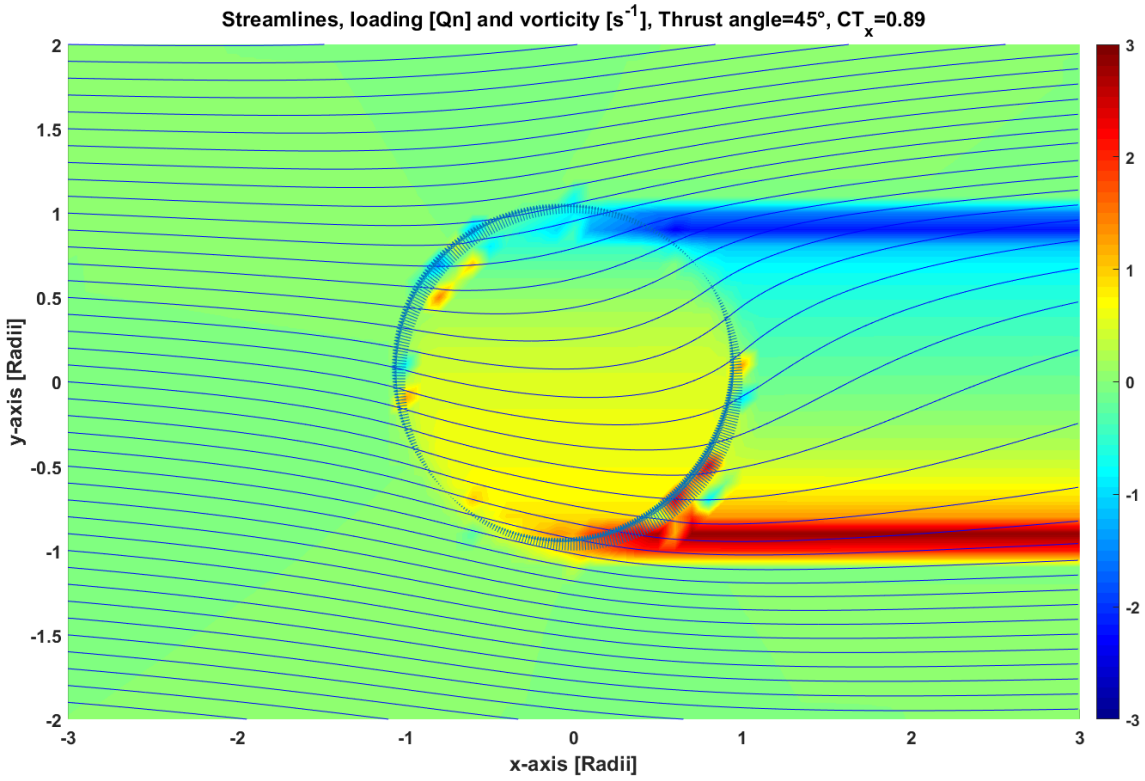

(b)

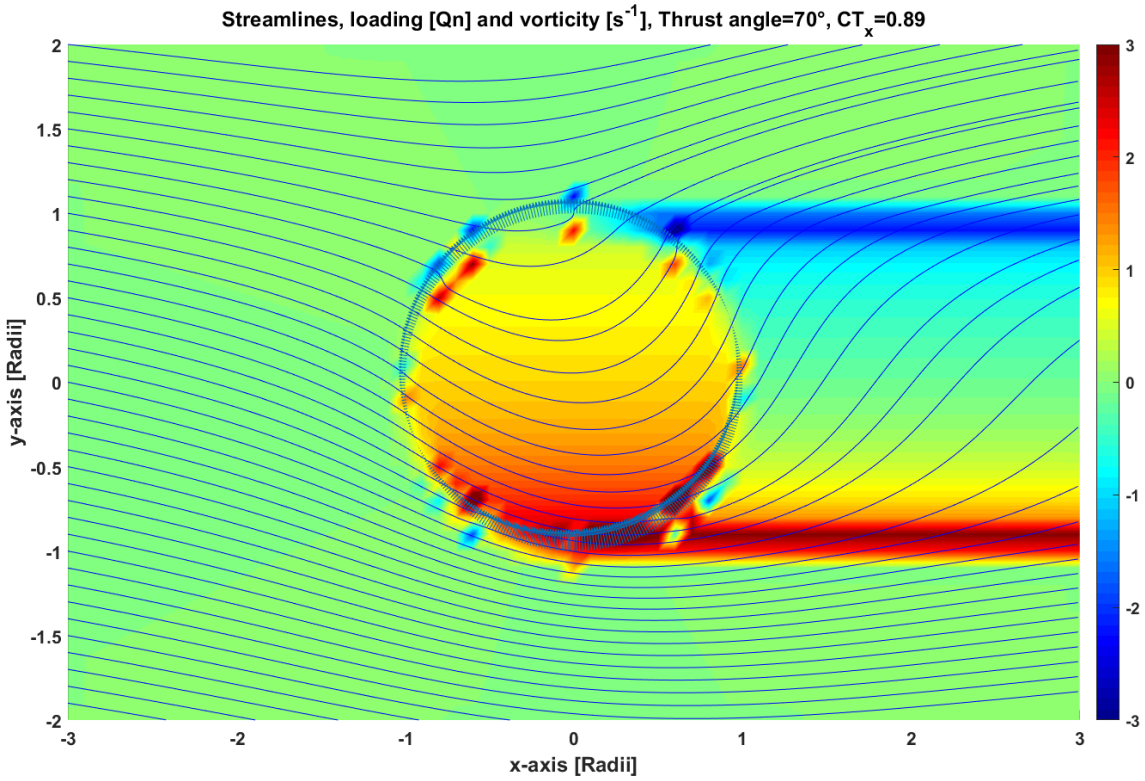

(c)

Figure D.1: Velocity fields through streamlines, including corresponging instantaneous loading and vorticity field by the colored map around the turbine for three different thrust angles at their peak power extraction.